Collective Spin-Cavity Ensembles and the Protection of Higher-dimensional Quantum Information

by

Lane G. Gunderman

A thesis
presented to the University of Waterloo
in fulfillment of the
thesis requirement for the degree of
Doctor of Philosophy
in
Physics (Quantum Information)

Waterloo, Ontario, Canada, 2022

Examining Committee Membership

The following served on the Examining Committee for this thesis. The decision of the Examining Committee is by majority vote.

External Examiner:	Jacob Biamonte Professor, Skolkovo Institute of Science and Technology
Supervisor:	David Cory Professor, Dept. of Chemistry, University of Waterloo
Internal Member:	Dmitry Pushin Associate Professor, Dept. of Physics, University of Waterloo
Internal-External Member:	Jon Yard Associate Professor, Dept. of C&O, University of Waterloo
Other Member:	Michel Gingras Professor, Dept. of Physics, University of Waterloo

Author's Declaration

This thesis consists of material all of which I authored or co-authored: see Statement of Contributions included in the thesis. This is a true copy of the thesis, including any required final revisions, as accepted by my examiners.

I understand that my thesis may be made electronically available to the public.

Statement of Contributions

This thesis is primarily composed of work from a collection of five works for which I was the primary (or sole) contributor. For full clarity I will briefly mention each work and my contributions to them as well as the corresponding chapters in this work.

- Chapters 1 and 2 are based on the work [1] by myself, Andrew Stasiuk, Mohamed El Mandouh, Troy Borneman, and David Cory. In this work, I thought of the approach of using traces and functions of traces to greatly reduce the task of finding meaningful measures on the Lamb shifts. Additionally, I recognized the ability to bound the maximal Lamb shift splittings, as well as finding the so-called region of strong support in the degeneracies of the system, and aided in the degeneracy averaged expression. I worked through the example cases and wrote the bulk of this work.

- Chapter 3 is based off the work [still under internal peer-review] by myself, Troy Borneman, and David Cory. Early stages of this work involved Andrew Stasiuk who noted the temperature regime, as well as Mohamed El Mandouh. The final work was developed by myself and involved discussions with the co-authors to tease out more interesting implications and interpretations.

- Chapter 4 is a chapter constructed solely for this thesis in order to provide a brief introduction to quantum error-correcting codes and permit easier understanding of the chapter which follows.

- Chapter 5 is constructed from a synthesis of my solo works [2, 3] and a work inspired by some observations made with my mentee Arun Moorthy [4]. For the solo works I am the sole researcher and writer, although had helpful discussions with Andrew Jena, David Cory, and Daniel Gottesman about the ideas. For the joint work with Arun Moorthy I proved the results in the work and wrote the work. This chapter is a merging of the works, rewritten to improve flow and clarity, and with a couple of extra examples not shown elsewhere.

Some slight additions have been added in the thesis to ease reading or point out interesting examples which have not been submitted for publication.

This thesis contains two disparate topics with the connection of higher-dimensionality for the treatment of the quantum particles in both cases, however, I would advise reading this work as effectively two separate theses depending on which piece is relevant.

Abstract

The development of devices leveraging their quantum nature to outperform classical analogues has been an ongoing effort for many decades now. In this thesis we investigate two facets related to this effort, albeit at different potential timescales of utility.

First, we discuss our contributions in understanding collective spin ensembles interacting with a resonance cavity. This set up is common in superconducting qubit devices and electron spin-resonance experiments. The traditional model when considering this situation is the Tavis–Cummings model, although many of the methods could be adapted to other mesoscopic systems composed of ensembles of spins and cavities. In particular, we focus on characterizing the shifts in the energies due to dressing states, which are known as Lamb shifts. Before this line of work, most efforts focused on generating difference equations which could be solved iteratively to extract these shifts and dressed states. While this methodology works for systems involving hundreds of spins to thousands of spins, this iterative construction loses utility for larger ensembles due to the time needed to determine the parameters and prevents broad trends from being noted. Through these works we have stated how to determine the moments of the statistical distribution of the Lamb shifts, how to bound the largest of these shifts, and which of the subspaces are most important when finding these shifts. Beyond this, we have found that by including thermal effects we may use the moments of the Lamb shifts to greatly simplify a perturbative expansion to determine values of certain observables in optimal time (in spin ensemble size). These results provide greater insights into this model, provide faster simulation times, and can aide in experimental tests of these devices.

Second, we discuss the contributions made in quantum error-correcting codes. The typical formalism used for quantum error-correcting codes is the stabilizer formalism. In our work we have extended this formalism to no longer directly depend on the local-dimension of the quantum computing device. For instance, most devices being currently designed and built run on qubits, which have local-dimension two, while qutrits have local-dimension of three. By removing this local-dimensional dependency we are able to generate many stabilizer codes, including codes with parameters previously unknown–amongst which are local-dimension-invariant forms, with the same distance parameter value, for the Steane code, the entire quantum analog of the classical Hamming family, and the Toric code. While these codes do not outperform the best known codes, this serves as an interesting pedagogical and extended framework and may provide for improved codes upon sufficient consideration, or aide in other work in fields closely related to stabilizers. Meanwhile, this extended framework permits for the importation of quantum error-correcting codes from lower local-dimension values to devices with higher local-dimension values, which at

least provides some code options if a quantum computer is developed with easily tuned local-dimension value.

These topics should be considered as disjoint, and all variable meanings are reset between the topics.

Acknowledgements

There is a long list of people I would like to thank for various forms of help over the years. I have almost surely forgotten some people. Of course, I must thank my various teachers over my roughly 16 years of school. They motivated, encouraged, and inspired me. Dr. David Derbes put me on this track of being focused on interdisciplinary sciences–although primarily math and physics. Of particular note are the professors who *particularly* piqued my interest in quantum physics and computing: Barton Zwiebach, Seth Lloyd, Isaac Chuang, Aram Harrow, David Cory, John Watrous, Daniel Gottesman, and David Gosset. I particularly would like to thank Aram Harrow for being an encouraging force when I was more lost academically–I may not have gone to graduate school, especially for this topic, without his encouragement.

I got very lucky to have been accepted by David Cory as a student. I spent most college just taking random courses that seemed interesting, which would typically make attending graduate school in a topic more challenging–particularly when you do just "ok" in courses. The research autonomy he gave me allowed me to explore various research projects that interested me over the years, and yet his insights and suggestion to look at the Tavis–Cummings model permitted me to research some actual physics during my physics PhD. I am very grateful to him.

I would also like to thank some of my fellow students over the years. For various helpful discussions and company I would like to thank: Andrew Stasiuk, Mohamed El Mandouh, Shayan-Sean Majidy, Soumik "O(1)" Ghosh, Angus Kan, Supratik Sarkar, Connor Kapahi, and many others that I could list but would like to keep this only rather long and not a thesis itself. My research discussions with Andrew Jena were extremely helpful, helping to dissect interesting and hard problems and generally hanging out and playing games with me online and in person. My mentee Arun Moorthy has helped me grow tremendously in my ability to explain and discuss research, so while he may think that he was only gaining things from our work together, I also gained a lot of skills too.

I would like to thank my pandemic housemates, who were some of the best people to be largely trapped in a house with for multiple years. Vinodh Raj Rajagopal Muthu has provided an open ear, company, and an encouraging voice over these many years–from shortly after meeting him it was clear how great a person he was. Junqiao "Randy" Lin provided countless late night fun discussions about research aspirations, global politics, and reinvigorated my interest in history–so thank you. Tracy Norman, who we just happened to find as a housemate online, has been a wonderful person to talk with about anything and we got truly, exceptionally lucky to have gotten to live with her. Brad van Kasteren

and I spent many afternoons gaming together and working through assignments. Kohdai Kuroiwa provided great conversations over his time, kept me company while drinking, and knows so many things that it has been great talking with him. Turner Garrow has such a sweet heart and was great to talk with. Ian George, who despite having moved out just a few months into the pandemic, has provided so much virtual company and support that I am truly grateful for, as well as providing me a little more insight into other aspects of quantum research that interest me greatly.

Of course, I also must thank my little sister Hazel Martello, my older brother Perry Gunderman, and my grandmother Helinda "Linda" "gramma" Martello. Their support and comfort over the years stopped me from dropping out or quitting.

Dedication

This thesis is dedicated to my grandmother who provided me freedom, time, space, and support to grow as a person into roughly the kind of person I wanted to become. It is also dedicated to Dr. David Derbes who instilled in me a strong desire to explore interdisciplinary research, live life with an incredibly humble approach, and work to communicate challenging things exceptionally clearly. Thank you for your help and guidance during particularly crucial years in high school, and at times since then.

Table of Contents

List of Figures

List of Tables

Part I

Collective Spin-Cavity Ensembles

Collective Spin-Cavity Ensembles Overview

In this part of the thesis we will primarily focus on one particularly prevalent model for collective spin-cavity interactions, known as the Tavis–Cummings model, while some of the results would also apply for similar systems. This model, which can be used to describe hybrid quantum devices, has been studied in a myriad of ways since its conception in the 1960s. Lacking, however, in these analyses has been an ability to even estimate parameters of the dressed energy shifts for larger systems with larger numbers of total excitations in the system. We develop this ability in steps.

In chapter 1 we begin by breaking down the general model for the interaction between spins and cavities into the Tavis–Cummings model, explaining the different assumptions needed for the model to continue to hold. Following this we compute the exact energy level shifts for small systems, in part to explain the breakdown of the model into its irreducible representations but also to illustrate the increasing complexity involved in finding the energy splittings. Generally it requires diagonalizing N matrices with dimensions up to $N \times N$, for N spins, which becomes untenable for larger mesoscopic systems.

In chapter 2 we make use of the observations from the first chapter in order to compute various functions on the set of eigenvalues within each total excitation and angular momentum subspace. Amongst these functions are the average, the variance of these splitting values, all of the odd moments of the splitting values, as well as bounds on the size of the largest splitting within each manifold. While selecting for a particular angular momentum value is generally challenging, this provides some initial expressions which we can further leverage. Beyond this, through analytic continuation of the degeneracy counts in the irreducible representations for the angular momentum subspaces we are able to show that considerations of this model which only include a single subspace, or even a constant number of them, fail to demonstrate the full richness of the system. Together these results provide statements on the spectrum of the energy values in the system, as well as which

manifolds are predominant and which play less significant roles.

In chapter 3 we build on both of the prior chapters to turn these observations from considerations as a function of the total number of excitations in the system into functions of the temperature of the system–making the results more experimentally testable. We begin by noting the particular temperature regime of interest: if the temperature is too low the system can be described rather simply, if the temperature is too high then the rotating-wave approximation will break down; instead we target (and specify) the sweet spot of interest. Following this we demonstrate that the partition function, and many observables, can be considered as expansions in terms of the moments of the energy shifts in the system. Leveraging all of the prior results we are able to show optimal scaling as a function of the system size for simulating parameters preserving particular symmetries–dropping from $O(N^3)$ to $\Theta(\sqrt{N})$. Using this we can obtain some potentially observable signals that have signatures due to the coupling of the spins to the cavity. We then briefly discuss further directions, perturbations to the system, as well as other models that may be able to utilize some of the results shown here. These results allow for better numerical insights into these systems, demonstrates potential signatures due to the interactions between the spins and cavity, and provides a solid theoretical footing for further observations and potential insights.

Chapter 1

Introduction to Collective Spin-Cavity Ensembles

1.1 Introduction

The field of quantum electrodynamics (QED) was initiated by Lamb's discovery that an electron interacts with its own radiation field to split the energies of the $2s_{1/2}$ and $2p_{1/2}$ levels of the Hydrogen atom [7]. This splitting, referred to as the Lamb shift, demonstrates that the electromagnetic field and vacuum can be considered as quantized systems. Cavity QED systems, where two–level quantum systems (such as atoms or spins) are confined in a high quality factor (high Q) cavity, present features analogous to the Lamb shift. The light–matter interaction breaks degeneracies between separable field and atom states with the same number of excitations, k, hybridizing the states with a splitting that scales in magnitude as $\sqrt{k}$. Provided the cavity Q is high enough, and the atomic coherence is long enough, this hybridization may be observed experimentally [8]. Understanding the structure of cavity QED Lamb shifts has become particularly important recently due to their role in the development of large-scale quantum information processors [9, 10, 11, 12] and hybrid quantum devices [13, 14, 15], such as quantum memories for microwave photons [16, 17, 18, 19] and optical photons [20, 21, 22]. Lamb shifts also play a crucial role in radiative ground-state cooling of a spin ensemble interacting with a microwave cavity [23, 24, 25, 26, 27].

In general, experimentally observed splittings in a high–cooperativity spin–cavity system are a complex function of the many Lamb shifts that occur in various collective angular momentum and excitation subspaces. Calculating the full set of Lamb shifts is generally

intractable for mesoscopic systems, leading to a number of approximation methods being utilized to analyze experimental data. The most common approximations are to restrict theoretical treatments to the largest, permutation–invariant, Dicke subspace, or to treat the spin ensemble in the low–excitation regime as a simple quantum harmonic oscillator [28, 29].

Dynamics outside of the Dicke subspace have been shown to be important for nearly all practical laboratory conditions to capture the full picture of the system [30, 31], so we extend the existing techniques to provide descriptive statistics of the Lamb shifts that occur in arbitrary collective angular momentum and excitation subspaces, culminating in a description of these statistics upon averaging over subspace degeneracies. Our analysis provides a tool for compactly describing and analyzing the complex Lamb shifts that occur in spin-cavity systems, with validity over a wide range of temperatures and excitation levels appropriate for experimental mesoscopic quantum devices.

1.2 Hamiltonian Structure

1.2.1 Definitions and Notation

The notion of a Lamb shift in cavity QED may be formally defined using the Jaynes–Cummings Hamiltonian, describing the light–matter interaction of a single two-level quantum system with a quantized single–mode electromagnetic field [32] ($\hbar = 1$ throughout this work):

$$\begin{aligned} \hat{\mathcal{H}}_0 &= \omega_c a^\dagger a + \frac{\omega_s}{2}\sigma_z, \\ \hat{\mathcal{H}}_{\text{int}} &= g_0(a^\dagger \sigma_- + a\sigma_+), \\ \hat{\mathcal{H}}_{JC} &= \hat{\mathcal{H}}_0 + \hat{\mathcal{H}}_{\text{int}}, \end{aligned} \tag{1.1}$$

where H_0 is the Hamiltonian describing the quantization of the two–level system and single–mode field, and H_{int} is the interaction Hamiltonian. The lowering (raising) operators, $\hat{a}$ ($\hat{a}^\dagger$), describe the annihilation (creation) of a photon in the field mode with energy ω_c. The number operator, $\hat{a}^\dagger\hat{a}$, describes the quantization of the field mode in terms of the number of photons, n, occupying the mode, and defines the Fock eigenstates, $|n\rangle$, as $\hat{a}^\dagger\hat{a}\,|n\rangle = n\,|n\rangle$. The corresponding quantization of the two-level system is given by Zeeman eigenstates, $\hat{\sigma}_z\,|\uparrow\rangle = +\,|\uparrow\rangle$ and $\hat{\sigma}_z\,|\downarrow\rangle = -\,|\downarrow\rangle$, with energy splitting ω_s given by the Pauli z spin operator, σ_z. For brevity, we will refer to a general two-level quantum system as a spin and the single–mode electromagnetic field as the cavity.

The spin–cavity interaction Hamiltonian describes a coherent swapping of a single photon between the spin and the cavity mode, where $\hat{\sigma}_+ = \hat{\sigma}_x + i\hat{\sigma}_y$ and $\hat{\sigma}_- = \hat{\sigma}_x - i\hat{\sigma}_y$ correspond, respectively, to the raising and lowering operators of an excitation in the spin system. The strength of the spin–cavity interaction is given by the geometric parameter

$$g_0 = g_e \mu_B \sqrt{\frac{\mu_0 \omega_c}{2V_c}}, \tag{1.2}$$

where g_e is the electron Landau g-factor, μ_B is the Bohr magneton, μ_0 is the permeability of free–space, and V_c is the mode volume of the cavity. We restrict ourselves to the regime $g_0 \ll \omega_c, \omega_s$ such that a rotating–wave approximation (RWA) may be applied to suppress multi-photon processes which do not conserve total excitation count in the system. For simplicity, we will also restrict our argument to the case where the spin system and cavity mode are resonant ($\omega_c = \omega_s = \omega_0$).

We denote the separable k-excitation eigenstates of $\hat{\mathcal{H}}_0$ as $\{|k\rangle|\downarrow\rangle, |k-1\rangle|\uparrow\rangle\}$ and, upon diagonalization under $\hat{\mathcal{H}}_{\text{int}}$, the resulting hybridized spin-cavity eigenstates are:

$$\{\frac{1}{\sqrt{2}}(|k\rangle|\downarrow\rangle + |k-1\rangle|\uparrow\rangle), \frac{1}{\sqrt{2}}(|k\rangle|\downarrow\rangle - |k-1\rangle|\uparrow\rangle)\}, \tag{1.3}$$

with a Lamb shift given by $g_0\sqrt{k}$, and a total splitting due to the Lamb shifts of $2g_0\sqrt{k}$. In the special case of $k = 1$ (the single–excitation manifold), the Lamb shift splitting is commonly referred to as a "normal mode" or "vacuum Rabi" splitting [8]. The non–linearity of the Lamb shift with excitation number has been observed experimentally to verify the "quantum" nature of the spin–cavity interaction [33].

The Jaynes–Cummings model may be generalized to an ensemble of N non–interacting spins independently coupled to a single–mode cavity, with interaction Hamiltonian

$$\hat{\mathcal{H}}_{D,\text{int}} = 2\sum_{i=1}^{N} g_0^i(\hat{a}^\dagger + \hat{a})\hat{\sigma}_x^i. \tag{1.4}$$

Assuming the spin–cavity interaction is homogeneous, such that the spins interact collectively with the cavity mode and the summation may be dropped, yields the Dicke model [34], with interaction Hamiltonian

$$\hat{\mathcal{H}}_{D,\text{int}} = g_0\big(\hat{a}^\dagger + \hat{a}\big)\hat{J}_x. \tag{1.5}$$

Treating an inhomogeneous spin–cavity interaction can become quite complicated and has been treated in the literature using various methods [35, 36, 37]. Upon discarding

the counter–rotating term in a rotating–wave approximation considered in the interaction frame, the system is described by the Tavis–Cummings Hamiltonian [38]:

$$\hat{\mathcal{H}}_{TC} = \omega_0(\hat{a}^\dagger \hat{a} + \hat{J}_z) + g_0(\hat{a}^\dagger \hat{J}_- + \hat{a}\hat{J}_+), \tag{1.6}$$

where the two–level spin operators have been replaced with collective operators that act identically over the ensemble of energetically indistinguishable spins and a RWA has once again been made:

$$\hat{J}_z = \frac{1}{2}\sum_{i=1}^{N} \hat{\sigma}_z^{(i)}, \tag{1.7}$$

$$\hat{J}_\pm = \sum_{i=1}^{N} \hat{\sigma}_\pm^{(i)}. \tag{1.8}$$

The collective operators span the $\mathfrak{sl}(2;\mathbb{C})$ Lie algebra, and thus satisfy the following commutation relations:

$$[\hat{J}_z, \hat{J}_\pm] = \pm\hat{J}_\pm, \tag{1.9}$$

$$[\hat{J}_+, \hat{J}_-] = 2\hat{J}_z. \tag{1.10}$$

The collective operator algebra is a sub-algebra of self–adjoint operators acting on the N-spin system, and conveniently satisfies the same commutation relations as those for a single particle spin operator. By a change of basis, we can identify the transverse spin operators:

$$\hat{J}_x = \frac{1}{2}\big(\hat{J}_+ + \hat{J}_-\big), \tag{1.11}$$

$$\hat{J}_y = \frac{1}{2i}\big(\hat{J}_+ - \hat{J}_-\big). \tag{1.12}$$

The transverse spin operators, along with $\hat{J}_z$, span a collective $\mathfrak{su}(2)$ algebra, which differ from spin-1/2 Pauli operators in that the collective operators are not their own inverses. The representations of the $\mathfrak{sl}(2;\mathbb{C})$ operators can be defined by their action on a state of total angular momentum j with z component m:

$$\hat{J}_z \left|j, m\right\rangle = m \left|j, m\right\rangle \tag{1.13}$$

$$\hat{J}_\pm \left|j, m\right\rangle = \sqrt{j(j+1) - m(m\pm 1)}\left|j, m\pm 1\right\rangle. \tag{1.14}$$

Throughout this work, we focus on two good quantum numbers representing conserved quantities. The first of these is the total angular momentum, j, which determines the eigenvalues of the total angular momentum operator,

$$\hat{\boldsymbol{J}}^2 = \hat{J}_x^2 + \hat{J}_y^2 + \hat{J}_z^2, \tag{1.15}$$

with eigenvalues $j(j+1)$. The second of these conserved quantities is the number of total excitations, k, given as the eigenvalues of the excitation operator,

$$\hat{K} = \hat{a}^\dagger \hat{a} + \hat{J}_z + \frac{N}{2}\mathbb{1}. \tag{1.16}$$

The scaled identity term in the excitation operator ensures excitations are non-negative, as the action of $\hat{J}_z$ on the ground state has eigenvalue $-N/2$.

An important feature of the TC Hamiltonian is that the spin–cavity interaction strength, g_0, is often replaced with an effective interaction strength that is enhanced by $\sqrt{N}$:

$$g_{\text{eff}} = g_0\sqrt{N}. \tag{1.17}$$

This transformation is paired with a $1/\sqrt{N}$ term in the collective angular momentum raising and lowering operators, which we will omit in this work. The ensemble enhancement of the spin–cavity interaction strength has allowed observation of an analogous normal mode splitting (often referred to as "strong coupling") in ensemble spin systems interacting with high quality factor (high Q) cavities [39, 40, 41, 42]. The relative strengths of the parameters necessary to resolve this splitting are formalized by defining the cooperativity:

$$C = \frac{4Ng_0^2 Q T_2}{\omega_0}, \tag{1.18}$$

where Q is the quality factor of the cavity and T_2 is the coherence time of the spin ensemble.

It is common to perform a Holstein–Primakoff transformation on the collective angular momentum operators in order to simplify the underlying algebra [28]. This transformation is valid on a single subspace of angular momentum j, such that

$$\hat{J}_+ \longrightarrow \hat{b}^\dagger\sqrt{2j\mathbb{1} - \hat{b}^\dagger\hat{b}} \tag{1.19}$$

$$\hat{J}_- \longrightarrow \hat{b}\sqrt{2j\mathbb{1} - \hat{b}^\dagger\hat{b}}. \tag{1.20}$$

By requiring that standard angular momentum commutation relations are maintained, the transformation for $\hat{J}_z$ is then fixed:

$$\hat{J}_z \longrightarrow \hat{b}^\dagger\hat{b} - j\mathbb{1}. \tag{1.21}$$

Often j is taken to be the Dicke subspace, such that $j = N/2$, and N is assumed to be large compared to the number of excitations. If the number of excitations approach j, the spin system begins to saturate and the approximation becomes increasingly invalid [43]. In general, thermal population of the Dicke space is negligible at nearly all experimental temperatures [31], so we treat the Hamiltonian in generality across all subspaces and excitation manifolds.

1.2.2 Symmetries of Light–Matter Interaction

When the collective spin–cavity interaction, g_{eff}, is zero, the ground state is $|0\rangle\,|N/2, -N/2\rangle$, which represents a state with zero photons in the cavity and all spins in their ground states–taken in this work to be pointing down. When $g_{\text{eff}} > 0$, the Dicke Hamiltonian is symmetric under the parity operator $\hat{\Pi} = \exp\left[-i\pi\left(\hat{J}_z + \hat{a}^\dagger\hat{a}\right)\right]$, with eigenvalues ± 1. This implies that the Hilbert space of the Dicke model can be decomposed into a direct sum of two spaces labelled by the parity operator's sign: $\mathscr{H} = \mathscr{H}_+ \oplus \mathscr{H}_-$. In this model, excitations are not conserved, and the two parity subspaces are infinite dimensional.

For the case of $N = 1$, this particularization of the Dicke model is known as the Quantum Rabi Model (QRM), which has recently been solved [44, 45], where eigenvalues and eigenstates are given in terms of special functions [46]. The existence of this solution can be seen directly from the symmetry group of the Hamiltonian, as the parity symmetry is sufficient to show that the QRM is integrable [47]. When considering $N > 1$, the parity symmetry is no longer sufficient to show integrability, and it is expected that the Dicke model is not exactly solvable [48]; in other words, there are no explicit solutions in terms of any known functions.

Unlike the Dicke Model, the TC model admits a continuous symmetry, described by the circle group, $U(1)$, in addition to parity symmetry and total angular–momentum symmetry. The generator of the continuous symmetry has infinite eigenvalues, enumerated by $k \in \mathbb{N}$, while the total angular momentum symmetry has eigenvalues $j = N/2, N/2 - 1, \cdots, 1/2\ (0)$, where the last value for j is determined by whether N is odd or even. The additional symmetry is sufficient to make the Tavis–Cummings model integrable and solvable, which is supported by the Bethe ansatz solution provided by Bogoliubov [49, 50].

Given that $\hat{J}_+$ conserves total angular momentum j, the repeated action of $\hat{J}_+$ on the ground state of an N spin ensemble will only populate the $N + 1$ fully symmetric states in the Dicke subspace. Bogoliubov utilized these orbits to verify a Bethe ansatz solution of the Tavis–Cummings model is correct, casting the eigenvalue problem as equivalent to

solving a differential equation [49, 50]. Translating their construction into our notation, the primary expression is

$$|\Phi^{\lambda}_{j,k}\rangle = \sum_{m=0}^{k} A^{\lambda}_{j,k,m} (\hat{a}^{\dagger})^{k-m} \hat{J}_{+}^{m} |0\rangle \, |j, -j\rangle \,, \tag{1.22}$$

for recursively defined scalar coefficients $A^{\lambda}_{j,k,m}$ determined from difference equations, where j indicates the angular momentum space and k indicates the excitation subspace. Eigenvectors within a (j, k) subspace are labeled by the index λ.

The two symmetries of the TC model directly imply that the Hamiltonian admits a two parameter subspace decomposition. This observation will be used throughout the remainder of our analysis. The Holstein–Primakoff approximation largely ignores the angular momentum parameter, j, by focusing on a single value of it, particularly the $j = N/2$ subspace, which is treated as a single harmonic oscillator. The Bogoliubov solution via Bethe ansatz, while correct, is as computationally hard as solving the eigenvalue problem itself. Further work attempting to directly analyze large photon number behavior via a direct diagonalization approach has been performed by restriction to the Dicke subspace and tested experimentally [51].

1.3 Breaking down the model

In this section we discuss the reduction of the Dicke Hamiltonian to the Tavis–Cummings model and its direct sum representation. In particular, we will show that, up to the rotating-wave approximation, we may treat this system in the following way:

$$\omega_0(a^{\dagger}a + J_z) + g_0(a + a^{\dagger})J_x \mapsto \bigoplus_{j,k} (k\omega_0 I + g_0 L(j, k))^{\otimes d_j}, \tag{1.23}$$

for some yet undefined $L(j, k)$ matrices and degeneracies d_j.

1.3.1 Ensembles of spins

Here we consider breaking down an ensemble of N spin-1/2 particles into their eigenstates under the collective spin Hamiltonian $J_z = \sum_i \sigma_z^{(i)}$ and J^2.

For a single spin, the problem is trivial, there is only one basis possible. When there are two spins, we can decompose the space as:

$$\frac{1}{2} \otimes \frac{1}{2} \cong 1 \oplus 0, \tag{1.24}$$

where $\cong$ indicates an isomorphic relation. This means that instead of considering two spin-1/2 particles, we can instead treat the system as the direct sum of a spin-1 particle, with 3 levels, and a spin-0 particle, with a single level. The eigenvectors for J^2 and J_z are given by:

$$\{|\downarrow\downarrow\rangle, \frac{1}{\sqrt{2}}(|\downarrow\uparrow\rangle + |\uparrow\downarrow\rangle), |\uparrow\uparrow\rangle\} \oplus \{\frac{1}{\sqrt{2}}(|\downarrow\uparrow\rangle - |\uparrow\downarrow\rangle)\}. \tag{1.25}$$

These sets of states are known as the triplet and singlet states, respectively.

For three spins the decomposition in terms of single spin states begins to become more complicated. We may summarize the breakdown as:

$$\frac{1}{2} \otimes \frac{1}{2} \otimes \frac{1}{2} \cong \frac{3}{2} \oplus \frac{1}{2} \oplus \frac{1}{2}. \tag{1.26}$$

A valid basis set for this decomposition which are eigenvectors of J^2 and J_z is:

$$\{|\downarrow\downarrow\downarrow\rangle, \frac{1}{\sqrt{3}}(|\downarrow\downarrow\uparrow\rangle + |\downarrow\uparrow\downarrow\rangle + |\uparrow\downarrow\downarrow\rangle) \quad , \quad \frac{1}{\sqrt{3}}(|\downarrow\uparrow\uparrow\rangle + |\uparrow\downarrow\uparrow\rangle + |\uparrow\uparrow\downarrow\rangle), |\uparrow\uparrow\uparrow\rangle\} \tag{1.27}$$

$$\oplus\{\frac{1}{\sqrt{2}}(|\downarrow\uparrow\downarrow\rangle - |\uparrow\downarrow\downarrow\rangle) \quad , \quad \frac{1}{\sqrt{2}}(|\downarrow\uparrow\uparrow\rangle - |\uparrow\downarrow\uparrow\rangle)\} \tag{1.28}$$

$$\oplus\{\frac{1}{\sqrt{6}}(2|\downarrow\downarrow\uparrow\rangle - |\uparrow\downarrow\downarrow\rangle - |\downarrow\uparrow\downarrow\rangle) \quad , \quad \frac{1}{\sqrt{6}}(|\uparrow\downarrow\uparrow\rangle + |\downarrow\uparrow\uparrow\rangle - 2|\uparrow\uparrow\downarrow\rangle)\}. \tag{1.29}$$

When $N = 4$ the decomposition is given by:

$$\frac{1}{2} \otimes \frac{1}{2} \otimes \frac{1}{2} \otimes \frac{1}{2} \cong 2 \oplus 1 \oplus 1 \oplus 1 \oplus 0 \oplus 0. \tag{1.30}$$

To find the representations for these states in terms of single spin values one would use Clebsch-Gordon coefficients, however, the examples worked so far suffices for our purpose. Note that there will be a singly degenerate, totally symmetric subspace that is equivalent to a spin-$N/2$ particle. The general formula for computing the degeneracies of each subspace with collective angular momentum j is given by [52, 53]:

$$d_j = \binom{N}{N/2+j} - \binom{N}{N/2+j+1} \tag{1.31}$$

$$= \frac{2j+1}{N/2+j+1}\binom{N}{N/2+j}. \tag{1.32}$$

With these we may write a collection of N spins in direct sum form preserving J^2 and J_z as:

$$\left(\frac{1}{2}\right)^{\otimes N} \cong \bigoplus_{j=j_{\min}}^{N/2} j^{\otimes d_j}, \tag{1.33}$$

with $j_{\min} = 0$ if N is even, else $j_{\min} = \frac{1}{2}$. This decomposition of an ensemble of spins into collective angular momentum subspaces will form the basis for our analysis upon introducing a coupled cavity to the system.

1.3.2 Rotating-Wave Approximation (RWA)

The on-resonance Dicke Hamiltonian is given by:

$$\omega_0(a^\dagger a + J_z) + g_0(a + a^\dagger)(J_- + J_+) \tag{1.34}$$

Consider the effects of moving into the interaction picture given by $H_I = \omega_0(a^\dagger a + J_z)$:

$$\begin{aligned} U_I H U_I^\dagger - H_I &= e^{it\omega_0(a^\dagger a + J_z)} g_0(a + a^\dagger)(J_- + J_+) e^{-it\omega_0(a^\dagger a + J_z)} && (1.35)\\ &= g_0(e^{it\omega_0 a^\dagger a}(a + a^\dagger)e^{-it\omega_0 a^\dagger a})(e^{it\omega_0 J_z}(J_- + J_+)e^{-it\omega_0 J_z}). && (1.36) \end{aligned}$$

To proceed from here it is easiest to consider the result from applying this Hamiltonian on a test state $|n\rangle|j, m\rangle$:

$$\begin{aligned} &\propto g_0(e^{-i\omega_0 t}a + e^{i\omega_0 t}a^\dagger)(e^{-i\omega_0 t}J_- + e^{i\omega_0 t}J_+) && (1.37)\\ &= g_0(e^{-2i\omega_0 t}aJ_- + e^{2i\omega_0 t}a^\dagger J_+ + aJ_+ + a^\dagger J_-). && (1.38) \end{aligned}$$

Taking the time average of this expression, we drop the first two terms, leaving us only with $g_0(aJ_+ + a^\dagger J_-)$. These prior steps were merely considerations of what would happen were we to move into the interaction picture, however, by making the rotating-wave approximation (dropping the terms which rapidly time average to zero), we reduce the Dicke Hamiltonian to the Tavis-Cummings Hamiltonian:

$$H_{\text{TC}} := \omega_0(a^\dagger a + J_z) + g_0(aJ_+ + a^\dagger J_-), \tag{1.39}$$

which is our primary Hamiltonian of study here. Before closing this section, notice that this time averaging is only a valid approximation when the eigenvalues (or evolution oscillations) of the terms aJ_+ and $a^\dagger J_-$ is a smaller scale than ω_0 since otherwise those terms would oscillate at a similar frequency and dropping the other terms causes as much of a loss of

information. This means that the RWA begins to break down once the eigenvalues of these terms approach ω_0, which is a limitation of this model, however, we focus in this work on the regimes whereby the RWA continues to hold.

We can put both of these reductions together to generate the direct sum decomposition with the $L(j,k)$ matrices determined by acting on the bases with the coupling Hamiltonian divided by the energy scale, $aJ_+ + a^\dagger J_-$. By coupling the two systems we obtain dressed states of collective spin ensembles, with the dressing induced across the number of excitations in the cavity.

1.4 Explicit Calculations for $N = 1, 2, 3$

We now provide explicit calculations of the energy-level structure, state hybridization, and Lamb shifts for small ensembles of $N = 1, 2$, and 3 spins.

1.4.1 N = 1

A single spin coupled to a single–mode electromagnetic field is described by the Jaynes–Cummings Hamiltonian [32]:

$$\hat{\mathcal{H}}_0 + \hat{\mathcal{H}}_{\text{int}} = \omega_0(\hat{a}^\dagger\hat{a} + \hat{\sigma}_z) + g_0\left(\hat{a}^\dagger\sigma_- + \hat{a}\sigma_+\right). \tag{1.40}$$

Since $\hat{\mathcal{H}}_{\text{int}}$ couples spins with equal energy in the unperturbed spectrum, the Hilbert space decouples into blocks of constant total excitation, indexed by the good quantum number k:

$$\bigoplus_k |\psi_k\rangle\Big[\langle\psi_k|\hat{\mathcal{H}}_0 + \hat{\mathcal{H}}_{\text{int}}|\phi_k\rangle\Big]\langle\phi_k|, \text{ with } \hat{\mathcal{H}}_0\phi_k = E_k\phi_k \text{ and } \hat{\mathcal{H}}_0\psi_k = E_k\psi_k. \tag{1.41}$$

The ground state with no excitations ($k = 0$), $|0\rangle|\downarrow\rangle$, is unique and is not hybridized by H_{int}. For the remaining states, hybridization occurs and we utilize conservation of excitation number by H_{int} to calculate the eigenstructure. Consider the two states with finite excitation, $k > 0$, defined by $\{|k\rangle|\downarrow\rangle, |k-1\rangle|\uparrow\rangle\}$. The interaction Hamiltonian represented in this basis is given by the direct sum over all two–dimensional excitation spaces:

$$\hat{\mathcal{H}}_{\text{int}} \cong \bigoplus_k g_0\begin{bmatrix} 0 & \sqrt{k} \\ \sqrt{k} & 0 \end{bmatrix}. \tag{1.42}$$

By direct diagonalization, the energy eigenvalues of H_{int} in the manifold with k excitations are given by

$$E_{k,\pm} = k\omega_0 \pm g_0\sqrt{k}, \tag{1.43}$$

which correspond to hybridized energy eigenstates

$$|\psi_{k,\pm}\rangle = \frac{1}{\sqrt{2}}(|k\rangle|\downarrow\rangle \pm |k-1\rangle|\uparrow\rangle). \tag{1.44}$$

All Lamb shifts that occur for $N = 1$ are summarized in the following table:

Subspace	Excitations	Lamb Shifts	Numerical Values
$j = 1/2$	$k = 1$	g_0	g_0
	$k = 2$	$g_0\sqrt{2}$	$1.41g_0$
	$k = 3$	$g_0\sqrt{3}$	$1.73g_0$
	k	$g_0\sqrt{k}$	

1.4.2 N = 2

Multiple spins coupled to a single–mode electromagnetic field are described by the Tavis-Cummings Hamiltonian [38]:

$$\hat{\mathcal{H}}_{TC} = \omega_0(\hat{a}^\dagger\hat{a} + \hat{J}_z) + g_0(\hat{a}^\dagger\hat{J}_- + \hat{a}\hat{J}_+), \tag{1.45}$$

The case of two spins can be solved in two different ways: one where the full matrix is solved in the Zeeman basis of the spins, and one where the matrix is written in a direct sum representation of a spin-0 space (singlet) and spin-1 (triplet) space. We will solve this case in the Zeeman basis to contrast with the direct-sum representation used for the $N = 3$ case. Inclusion of a second spin leads to a richer energy-level structure than for $N = 1$: Similar to the $N = 1$ case, the ground state with no excitations ($k = 0$), $|0\rangle|\downarrow\downarrow\rangle$, remains unperturbed by H_{int}:

$$|1, 0 : \alpha\rangle = |0\rangle|1, -1\rangle = |0\rangle|\downarrow\downarrow\downarrow\rangle \tag{1.46}$$

The single–excitation manifold ($k = 1$) undergoes hybridization, determined by the coupling matrix $L(1, 1)$:

$$\begin{bmatrix} 0 & 1 & 1 \\ 1 & 0 & 0 \\ 1 & 0 & 0 \end{bmatrix} \tag{1.47}$$

Through direct diagonalization, the hybridized cavity–dressed states and perturbed energies are

$$|1,1:\beta\rangle = \frac{1}{\sqrt{2}}[|1\rangle|1;-1\rangle + |0\rangle|1;0\rangle] = \frac{1}{2}[\sqrt{2}|1\rangle|\downarrow\downarrow\rangle + |0\rangle|\downarrow\uparrow\rangle + |0\rangle|\uparrow\downarrow\rangle], \quad (1.48)$$

$$E = \omega_0 + g_0\sqrt{2} \quad (1.49)$$

$$|1,1:\alpha\rangle = \frac{1}{\sqrt{2}}[|1\rangle|1;-1\rangle - |0\rangle|1;0\rangle] = \frac{1}{2}[\sqrt{2}|1\rangle|\downarrow\downarrow\rangle - |0\rangle|\downarrow\uparrow\rangle - |0\rangle|\uparrow\downarrow\rangle], \quad (1.50)$$

$$E = \omega_0 - g_0\sqrt{2} \quad (1.51)$$

$$|0,1:\alpha\rangle = |0\rangle|0;0\rangle = \frac{1}{\sqrt{2}}[|0\rangle|\downarrow\uparrow\rangle - |0\rangle|\uparrow\downarrow\rangle], \quad (1.52)$$

$$E = \omega_0 + 0, \quad (1.53)$$

where for collective angular momentum j with secondary quantum number m, we have written $|j;m\rangle$. For our figure, we will call these dressed states $|1,1:\beta\rangle$, $|1,1:\alpha\rangle$, and $|0,1:\alpha\rangle$, respectively, where we have labeled our states with $|j,k:\text{index}\rangle$ with *index* being a Greek letter, alphabetically used in order of increasing energy.

For $k = 2$, we have an interaction Hamiltonian given by:

$$\begin{bmatrix} 0 & \sqrt{2} & \sqrt{2} & 0 \\ \sqrt{2} & 0 & 0 & 1 \\ \sqrt{2} & 0 & 0 & 1 \\ 0 & 1 & 1 & 0 \end{bmatrix}. \quad (1.54)$$

This matrix has eigenvectors (dressed states) and eigenvalues (energies with associated

Lamb shift) of

$$|1,2:\beta\rangle := \frac{1}{\sqrt{3}}[-|2\rangle|1;-1\rangle + \sqrt{2}|0\rangle|1;1\rangle] = \frac{1}{\sqrt{3}}[-|2\rangle|\downarrow\downarrow\rangle + \sqrt{2}|0\rangle|\uparrow\uparrow\rangle], \quad (1.55)$$

$$E = 2\omega_0 + 0 \quad (1.56)$$

$$|0,2:\alpha\rangle := |1\rangle|0;0\rangle = \frac{1}{\sqrt{2}}[|1\rangle|\downarrow\uparrow\rangle - |1\rangle|\uparrow\downarrow\rangle], \quad (1.57)$$

$$E = 2\omega_0 + 0 \quad (1.58)$$

$$|1,2:\gamma\rangle := \frac{1}{\sqrt{6}}[\sqrt{2}|2\rangle|1;-1\rangle + \sqrt{3}|1\rangle|1;0\rangle + |0\rangle|1;1\rangle] \quad (1.59)$$

$$= \frac{1}{2\sqrt{3}}[2|2\rangle|\downarrow\downarrow\rangle + \sqrt{3}|1\rangle|\downarrow\uparrow\rangle + \sqrt{3}|1\rangle|\uparrow\downarrow\rangle + \sqrt{2}|0\rangle|\uparrow\uparrow\rangle], \quad (1.60)$$

$$E = 2\omega_0 + g_0\sqrt{6} \quad (1.61)$$

$$|1,2:\alpha\rangle := \frac{1}{\sqrt{6}}[\sqrt{2}|2\rangle|1;-1\rangle - \sqrt{3}|1\rangle|1;0\rangle + 1|0\rangle|1;1\rangle] \quad (1.62)$$

$$= \frac{1}{2\sqrt{3}}[2|2\rangle|\downarrow\downarrow\rangle - \sqrt{3}|1\rangle|\downarrow\uparrow\rangle - \sqrt{3}|1\rangle|\uparrow\downarrow\rangle + \sqrt{2}|0\rangle|\uparrow\uparrow\rangle], \quad (1.63)$$

$$E = 2\omega_0 - g_0\sqrt{6} \quad (1.64)$$

For higher excitation manifolds, $k \geq 2$, there are always exactly four states that must be diagonalized, determined by the coupling matrix H_{int}/g_0 with exactly k excitations:

$$\begin{bmatrix} 0 & \sqrt{k} & \sqrt{k} & 0 \\ \sqrt{k} & 0 & 0 & \sqrt{k-1} \\ \sqrt{k} & 0 & 0 & \sqrt{k-1} \\ 0 & \sqrt{k-1} & \sqrt{k-1} & 0 \end{bmatrix} \quad (1.65)$$

Again, through direct diagonalization, the hybridized cavity–dressed states and perturbed

energies are:

$$\frac{1}{\sqrt{2k-1}}[-\sqrt{k-1}|k\rangle|1;-1\rangle+\sqrt{k}|k-2\rangle|1;1\rangle] \tag{1.66}$$

$$= \frac{1}{\sqrt{2k-1}}[-\sqrt{k-1}|k\rangle|\downarrow\downarrow\rangle+\sqrt{k}|k-2\rangle|\uparrow\uparrow\rangle],$$

$$E = k\omega_0 + 0 \tag{1.67}$$

$$|k-1\rangle|0;0\rangle \tag{1.68}$$

$$= \frac{1}{\sqrt{2}}[|k-1\rangle|\downarrow\uparrow\rangle-|k-1\rangle|\uparrow\downarrow\rangle],$$

$$E = k\omega_0 + 0 \tag{1.69}$$

$$\frac{1}{\sqrt{2}\sqrt{2k-1}}[\sqrt{k}|k\rangle|1;-1\rangle+\sqrt{2k-1}|k-1\rangle|1;0\rangle+\sqrt{k-1}|k-2\rangle|1;1\rangle] \tag{1.70}$$

$$= \frac{1}{2\sqrt{2k-1}}[\sqrt{2}\sqrt{k}|k\rangle|\downarrow\downarrow\rangle+\sqrt{2k-1}|k-1\rangle(|\downarrow\uparrow\rangle+|\uparrow\downarrow\rangle)+\sqrt{2}\sqrt{k-1}|k-2\rangle|\uparrow\uparrow\rangle],$$

$$E = k\omega_0 + g_0\sqrt{2}\sqrt{2k-1} \tag{1.71}$$

$$\frac{1}{\sqrt{2}\sqrt{2k-1}}[\sqrt{k}|k\rangle|1;-1\rangle-\sqrt{2k-1}|k-1\rangle|1;0\rangle+\sqrt{k-1}|k-2\rangle|1;1\rangle] \tag{1.72}$$

$$= \frac{1}{2\sqrt{2k-1}}[\sqrt{2}\sqrt{k}|k\rangle|\downarrow\downarrow\rangle-\sqrt{2k-1}|k-1\rangle(|\downarrow\uparrow\rangle+|\uparrow\downarrow\rangle)+\sqrt{2}\sqrt{k-1}|k-2\rangle|\uparrow\uparrow\rangle],$$

$$E = k\omega_0 - g_0\sqrt{2}\sqrt{2k-1} \tag{1.73}$$

Notice that within each eigenvector only terms involving a single collective spin value j is used for each term. If the direct sum representation is used instead of the Zeeman representation, such that the basis states are constant total angular momentum states (spin-1 and spin-0), the complexity of the problem is somewhat reduced. In this case, the only difference is replacing $|k\rangle|\uparrow\downarrow\rangle$ and $|k\rangle|\downarrow\uparrow\rangle$ with $|k\rangle(|\uparrow\downarrow\rangle+|\downarrow\uparrow\rangle)$ and $|k\rangle(|\uparrow\downarrow\rangle-|\downarrow\uparrow\rangle)$. In this representation, the singlet state $|\uparrow\downarrow\rangle-|\downarrow\uparrow\rangle$ is annihilated by $J_\pm$ and forms its own space. All Lamb shifts that occur for $N=2$ are summarized in the following table:

Subspace	Excitations	Lamb Shifts	Numerical Values
$j=1$	$k=1$	$g_0\sqrt{2}$	$1.41g_0$
	$k=2$	$g_0\sqrt{6}$	$2.45g_0$
	$k=3$	$g_0\sqrt{10}$	$3.16g_0$
	k	$g_0\sqrt{2}\sqrt{2k-1}$	
$j=0$	k	0	0

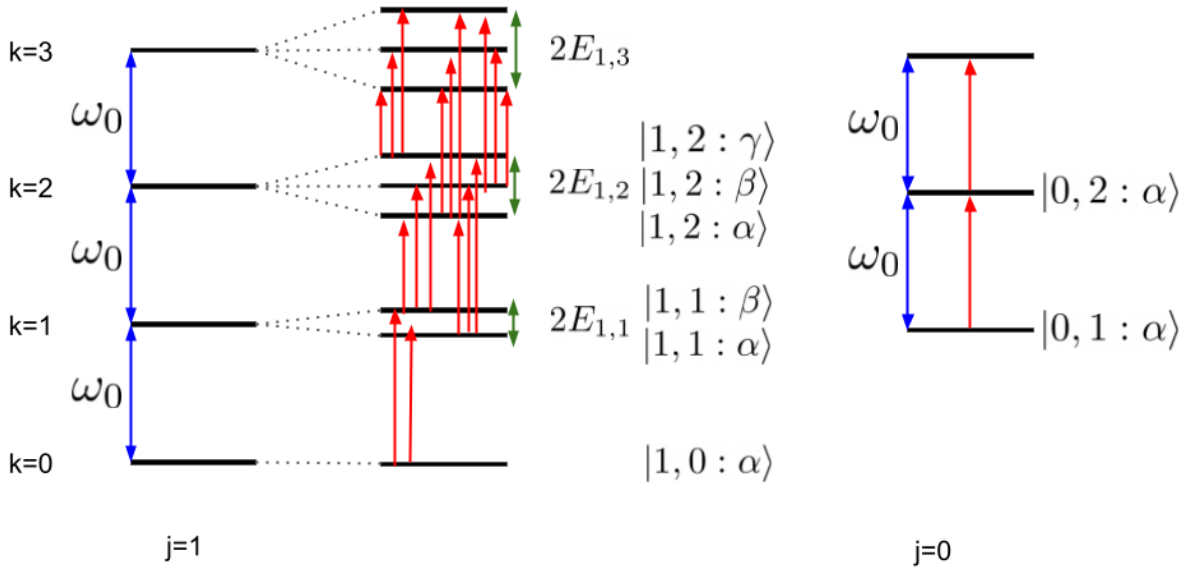

Figure 1.1: Illustration of the resulting hybridization of energy levels in the Tavis–Cummings model for $N = 2$. Vertical single arrow lines (red) indicate transitions mediated by $\hat{J}_+$, meaning that the eigenstates represented by the horizontal bars have a non-zero $\hat{J}_+$ matrix element. Transitions are all–to–all between neighboring excitation subspaces of the same angular momentum. Note that there are no allowed transitions via collective spin or photon operators between distinct angular momentum subspaces, regardless of the value of j. Separation between excitation spaces is a constant ω_0, denoted by bidirectional arrows (blue) between the pre–hybridized angular momentum states. Lamb shift splittings are denoted by bidirectional arrows (green) to the right of the hybridized states. In the $j = 1$ subspace, the Lamb shifts are given by: $E_{1,1} = g_0\sqrt{2} \approx 1.41g_0$, $E_{1,2} = g_0\sqrt{6} \approx 2.45g_0$, and $E_{1,3} = g_0\sqrt{10} \approx 3.16g_0$.

1.4.3 N = 3

The utility of the direct sum representation becomes even more apparent when $N = 3$ and subspace degeneracy first arises (see figure 2.1). As for $N = 1$ and 2, the ground state with no excitations ($k = 0$), $|0\rangle|\downarrow\downarrow\downarrow\rangle$ remains unperturbed by H_{int}. When the number of excitations are such that $k \leq 2$, the number of hybridized states are sub-maximal. For clarity, we divide the analysis into three cases that depend on the total number of excitations present in the joint spin–cavity system: $k = 1$, $k = 2$, and $k \geq 3$.

Case 1: $k = 1$

In the single–excitation manifold there are four basis states, with hybridization determined by the coupling matrix H_{int} for $k = 1$:

$$g_0 \begin{bmatrix} 0 & 1 & 1 & 1 \\ 1 & 0 & 0 & 0 \\ 1 & 0 & 0 & 0 \\ 1 & 0 & 0 & 0 \end{bmatrix} \tag{1.74}$$

Solving this matrix through direct diagonalization gives the hybridized cavity–dressed states and perturbed energies of

$$|3/2, 1 : \beta\rangle := \frac{1}{\sqrt{2}}[|1\rangle|3/2; -3/2\rangle + |0\rangle|3/2; -1/2\rangle] \tag{1.75}$$

$$= \frac{1}{\sqrt{6}}[\sqrt{3}|1\rangle|\downarrow\downarrow\downarrow\rangle + |0\rangle(|\downarrow\downarrow\uparrow\rangle + |\downarrow\uparrow\downarrow\rangle + |\uparrow\downarrow\downarrow\rangle)] \quad , \qquad E = \omega_0 + g_0\sqrt{3} \tag{1.76}$$

$$|3/2, 1 : \alpha\rangle := \frac{1}{\sqrt{2}}[-|1\rangle|3/2; -3/2\rangle + |0\rangle|3/2; -1/2\rangle] \tag{1.77}$$

$$= \frac{1}{\sqrt{6}}[-\sqrt{3}|1\rangle|\downarrow\downarrow\downarrow\rangle + |0\rangle(|\downarrow\downarrow\uparrow\rangle + |\downarrow\uparrow\downarrow\rangle + |\uparrow\downarrow\downarrow\rangle)] \quad , \qquad E = \omega_0 - g_0\sqrt{3} \tag{1.78}$$

$$|1/2, 1 : \alpha\rangle_1 := |0\rangle|1/2; -1/2\rangle_1 \tag{1.79}$$

$$= \frac{1}{\sqrt{2}}|0\rangle(|\uparrow\downarrow\downarrow\rangle - |\downarrow\downarrow\uparrow\rangle) \quad , \qquad E = \omega_0 \tag{1.80}$$

$$|1/2, 1 : \alpha\rangle_2 := |0\rangle|1/2; -1/2\rangle_2 \tag{1.81}$$

$$= \frac{1}{\sqrt{2}}|0\rangle(|\downarrow\uparrow\downarrow\rangle - |\downarrow\downarrow\uparrow\rangle) \quad , \qquad E = \omega_0, \tag{1.82}$$

where the subscript on $|1/2; -1/2\rangle$ indicates the degeneracy number of that subspace.

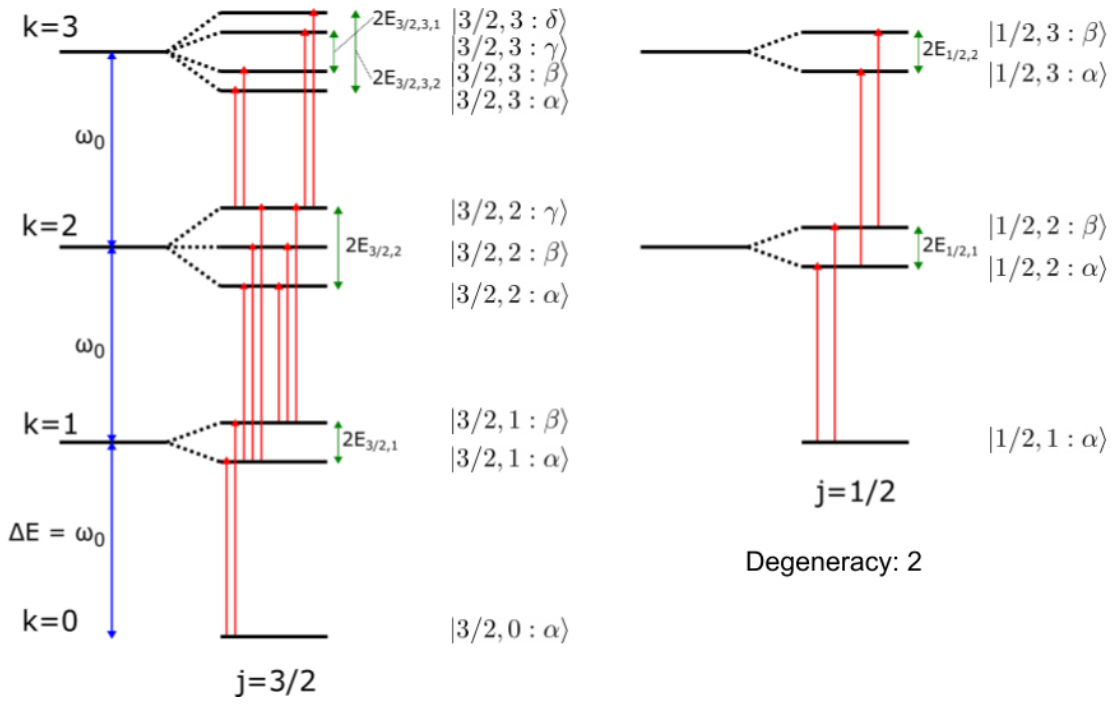

Figure 1.2: Illustration of the resulting hybridization of energy levels in the Tavis–Cummings model for $N = 3$, explicitly on resonance such that $\omega_0 = \omega_s = \omega_c$. Vertical single arrow lines (red) indicate transitions mediated by $\hat{J}_+$, meaning that the eigenstates represented by the horizontal bars have a non-zero $\hat{J}_+$ matrix element. Transitions are all–to–all between neighboring excitation subspaces of the same angular momentum, with some transitions between the $k = 2$ and $k = 3$ subspaces omitted for clarity. Note that there are no allowed transitions via collective spin or photon operators between distinct angular momentum subspaces, regardless of the value of j. Separation between excitation spaces is a constant ω_0, denoted by bidirectional arrows (blue) between the pre–hybridized angular momentum states. Lamb shift splittings are denoted be bidirectional arrows (green) to the right of the hybridized states. In the $j = 1/2$ subspaces, these splittings are given by $E_{1/2,1} = g_0$ and $E_{1/2,2} = g_0\sqrt{2}$. In the $j = 3/2$ subspace, the Lamb shifts are given by: $E_{3/2,1} = g_0\sqrt{3} \approx 1.73g_0$, $E_{3/2,2} = g_0\sqrt{10} \approx 3.16g_0$, $E_{3/2,3,1} = g_0\sqrt{10 - \sqrt{73}} \approx 1.21g_0$, and $E_{3/2,3,2} = g_0\sqrt{10 + \sqrt{73}} \approx 4.31g_0$.

Case 2: $k = 2$

When a second excitation is added to the joint spin–cavity system, the number of basis states increases to seven, with hybridization determined by the coupling matrix $H_{\rm int}/g_0$ for $k = 2$:

$$\begin{bmatrix} 0 & \sqrt{2} & \sqrt{2} & 0 & \sqrt{2} & 0 & 0 \\ \sqrt{2} & 0 & 0 & 1 & 0 & 1 & 0 \\ \sqrt{2} & 0 & 0 & 1 & 0 & 0 & 1 \\ 0 & 1 & 1 & 0 & 0 & 0 & 0 \\ \sqrt{2} & 0 & 0 & 0 & 0 & 1 & 1 \\ 0 & 1 & 0 & 0 & 1 & 0 & 0 \\ 0 & 0 & 1 & 0 & 1 & 0 & 0 \end{bmatrix} \tag{1.83}$$

This matrix may be represented as a direct sum, $H_{\rm int}/g_0 = L(3/2, 2) \oplus L(1/2, 2)_1 \oplus L(1/2, 2)_2$, to yield

$$\begin{bmatrix} 0 & \sqrt{6} & 0 \\ \sqrt{6} & 0 & 2 \\ 0 & 2 & 0 \end{bmatrix} \oplus \begin{bmatrix} 0 & 1 \\ 1 & 0 \end{bmatrix} \oplus \begin{bmatrix} 0 & 1 \\ 1 & 0 \end{bmatrix} \tag{1.84}$$

By direct diagonalization, the first entry in the direct sum gives hybridized cavity–dressed states and perturbed energies of

$$|3/2, 2 : \alpha\rangle := \frac{1}{2}[\sqrt{\frac{1}{2}}|2\rangle|3/2; -3/2\rangle - \sqrt{\frac{5}{2}}|1\rangle|3/2; -1/2\rangle + |0\rangle|3/2; 1/2\rangle] \tag{1.85}$$

$$\frac{1}{2\sqrt{3}}[\sqrt{\frac{3}{2}}|2\rangle|\downarrow\downarrow\downarrow\rangle - \sqrt{\frac{5}{2}}|1\rangle(|\downarrow\downarrow\uparrow\rangle + |\downarrow\uparrow\downarrow\rangle + |\uparrow\downarrow\downarrow\rangle) + |0\rangle(|\downarrow\uparrow\uparrow\rangle + |\uparrow\downarrow\uparrow\rangle + |\uparrow\uparrow\downarrow\rangle)] \tag{1.86}$$

$$E = 2\omega_0 - g_0\sqrt{10} \tag{1.87}$$

$$|3/2, 2 : \gamma\rangle := \frac{1}{2}[\sqrt{\frac{1}{2}}|2\rangle|3/2; -3/2\rangle + \sqrt{\frac{5}{2}}|1\rangle|3/2; -1/2\rangle + |0\rangle|3/2; 1/2\rangle] \tag{1.88}$$

$$\frac{1}{2\sqrt{3}}[\sqrt{\frac{3}{2}}|2\rangle|\downarrow\downarrow\downarrow\rangle + \sqrt{\frac{5}{2}}|1\rangle(|\downarrow\downarrow\uparrow\rangle + |\downarrow\uparrow\downarrow\rangle + |\uparrow\downarrow\downarrow\rangle) + |0\rangle(|\downarrow\uparrow\uparrow\rangle + |\uparrow\downarrow\uparrow\rangle + |\uparrow\uparrow\downarrow\rangle)] \tag{1.89}$$

$$E = 2\omega_0 + g_0\sqrt{10} \tag{1.90}$$

$$|3/2, 2 : \beta\rangle := \frac{1}{\sqrt{11}}[-\sqrt{2}|2\rangle|3/2; -3/2\rangle + 3|0\rangle|3/2; 1/2\rangle] \tag{1.91}$$

$$\sqrt{\frac{3}{11}}[-\sqrt{\frac{2}{3}}|2\rangle|\downarrow\downarrow\downarrow\rangle + |0\rangle(|\downarrow\uparrow\uparrow\rangle + |\uparrow\downarrow\uparrow\rangle + |\uparrow\uparrow\downarrow\rangle)] \tag{1.92}$$

$$E = 2\omega_0 \tag{1.93}$$

Similarly, the second and third entries of the direct sum give

$$\frac{1}{\sqrt{2}}[|0\rangle|1/2;1/2\rangle_1 \pm |1\rangle|1/2;-1/2\rangle_1] \tag{1.94}$$

$$= \frac{1}{2}[|1\rangle[|\downarrow\uparrow\downarrow\rangle - |\uparrow\downarrow\downarrow\rangle] \pm |0\rangle[|\downarrow\uparrow\uparrow\rangle - |\uparrow\downarrow\uparrow\rangle]] \quad , \tag{1.95}$$

$$E = 2\omega_0 \pm g_0 \tag{1.96}$$

$$\frac{1}{\sqrt{2}}[|0\rangle|1/2;1/2\rangle_2 \pm |1\rangle|1/2;-1/2\rangle_2] \tag{1.97}$$

$$= \frac{1}{2\sqrt{3}}[|1\rangle[2|\downarrow\downarrow\uparrow\rangle - |\uparrow\downarrow\downarrow\rangle - |\downarrow\uparrow\downarrow\rangle] \pm |0\rangle[|\uparrow\downarrow\uparrow\rangle + |\downarrow\uparrow\uparrow\rangle - 2|\uparrow\uparrow\downarrow\rangle]] \quad , \tag{1.98}$$

$$E = 2\omega_0 \pm g_0 \tag{1.99}$$

where we define for the figure:

$$|1/2,2:\alpha\rangle_1 := \frac{1}{\sqrt{2}}[|0\rangle|1/2;1/2\rangle_1 - |1\rangle|1/2;-1/2\rangle_1] \quad , \tag{1.100}$$

$$|1/2,2:\beta\rangle_1 := \frac{1}{\sqrt{2}}[|0\rangle|1/2;1/2\rangle_1 + |1\rangle|1/2;-1/2\rangle_1] \tag{1.101}$$

$$|1/2,2:\alpha\rangle_2 := \frac{1}{\sqrt{2}}[|0\rangle|1/2;1/2\rangle_2 - |1\rangle|1/2;-1/2\rangle_2] \quad , \tag{1.102}$$

$$|1/2,2:\beta\rangle_2 := \frac{1}{\sqrt{2}}[|0\rangle|1/2;1/2\rangle_2 + |1\rangle|1/2;-1/2\rangle_2] \tag{1.103}$$

$$\tag{1.104}$$

Case 3: $k = 3$

When $k = 3$, the number of spin states becomes maximal and all $2^3 = 8$ spin states participate in hybridization, determined by the coupling matrix H_{int}/g_0 at $k = 3$:

$$\begin{bmatrix} 0 & \sqrt{3} & \sqrt{3} & 0 & \sqrt{3} & 0 & 0 & 0 \\ \sqrt{3} & 0 & 0 & \sqrt{2} & 0 & \sqrt{2} & 0 & 0 \\ \sqrt{3} & 0 & 0 & \sqrt{2} & 0 & 0 & \sqrt{2} & 0 \\ 0 & \sqrt{2} & \sqrt{2} & 0 & 0 & 0 & 0 & 1 \\ \sqrt{3} & 0 & 0 & 0 & 0 & \sqrt{2} & \sqrt{2} & 0 \\ 0 & \sqrt{2} & 0 & 0 & \sqrt{2} & 0 & 0 & 1 \\ 0 & 0 & \sqrt{2} & 0 & \sqrt{2} & 0 & 0 & 1 \\ 0 & 0 & 0 & 1 & 0 & 1 & 1 & 0 \end{bmatrix}, \tag{1.105}$$

where the ordered basis states for this matrix representation are given by the set $\{|3\rangle|\downarrow\downarrow\downarrow\rangle, |2\rangle|\downarrow\downarrow\uparrow\rangle, \ldots |0\rangle|\uparrow\uparrow\uparrow\rangle\}$. This matrix admits a direct sum representation with coupling matrices $L(3/2,3) \oplus L(1/2,3) \oplus L(1/2,3)$, given by:

$$\begin{bmatrix} 0 & 3 & 0 & 0 \\ 3 & 0 & 2\sqrt{2} & 0 \\ 0 & 2\sqrt{2} & 0 & \sqrt{3} \\ 0 & 0 & \sqrt{3} & 0 \end{bmatrix} \oplus \begin{bmatrix} 0 & \sqrt{2} \\ \sqrt{2} & 0 \end{bmatrix} \oplus \begin{bmatrix} 0 & \sqrt{2} \\ \sqrt{2} & 0 \end{bmatrix}. \tag{1.106}$$

The first matrix is written in the Dicke (fully symmetric) basis (normalized versions of $|k-m\rangle \hat{J}_+^m |\downarrow\downarrow\downarrow\rangle$ with $m \in \{0,1,2,3\}$), while the second and third are written in terms of the composite spin–1/2 bases, given by

$$\frac{1}{\sqrt{2}}|2\rangle(|\downarrow\uparrow\downarrow\rangle - |\uparrow\downarrow\downarrow\rangle) \quad , \qquad \frac{1}{\sqrt{2}}|1\rangle(|\downarrow\uparrow\uparrow\rangle - |\uparrow\downarrow\uparrow\rangle) \tag{1.107}$$

$$\frac{1}{\sqrt{6}}|2\rangle(2|\downarrow\downarrow\uparrow\rangle - |\uparrow\downarrow\downarrow\rangle - |\downarrow\uparrow\downarrow\rangle) \quad , \qquad \frac{1}{\sqrt{6}}|1\rangle(|\uparrow\downarrow\uparrow\rangle + |\downarrow\uparrow\uparrow\rangle - 2|\uparrow\uparrow\downarrow\rangle). \tag{1.108}$$

The matrix representations for the degenerate spin-1/2 subspaces are identical, and thus indistinguishable under a collective operation or measurement. There is freedom in the choices of bases for the degenerate subspaces; the states provided are the standard basis states for these subspaces, as computed via a Clebsch–Gordon table [54].

We diagonalize each block individually, starting with the matrix representing the $j = 3/2$ subspace, and find the resulting (non-normalized) Lamb-shifted dressed states are given by the following superpositions:

$$\begin{aligned} |3/2,3;\pm_1,\pm_2\rangle \;:=\; & \pm_1\sqrt{10 \mp_2 \sqrt{73}}(1 \pm_2 \sqrt{73})|3\rangle|3/2;-3/2\rangle + 3(7 \mp_2 \sqrt{73})|2\rangle|3/2;-1/2\rangle \\ & \mp_1 6\sqrt{10 \mp_2 \sqrt{73}}\sqrt{2}|1\rangle|3/2;1/2\rangle + 6\sqrt{6}|0\rangle|3/2;3/2\rangle \qquad (1.109) \\ =\; & \pm_1\sqrt{10 \mp_2 \sqrt{73}}(1 \pm_2 \sqrt{73})|3\rangle|\downarrow\downarrow\downarrow\rangle \\ & +(7 \mp_2 \sqrt{73})3|2\rangle\frac{1}{\sqrt{3}}(|\downarrow\downarrow\uparrow\rangle + |\downarrow\uparrow\downarrow\rangle + |\uparrow\downarrow\downarrow\rangle) \qquad (1.110) \\ & \mp_1 6\sqrt{10 \mp_2 \sqrt{73}}\sqrt{2}|1\rangle\frac{1}{\sqrt{3}}(|\downarrow\uparrow\uparrow\rangle + |\uparrow\downarrow\uparrow\rangle + |\uparrow\uparrow\downarrow\rangle) \qquad (1.111) \\ & +6\sqrt{6}|0\rangle|\uparrow\uparrow\uparrow\rangle, \qquad (1.112) \end{aligned}$$

each with associated energy

$$E_{3;\pm_1\pm_2} = 3\omega_0 \mp_1 g_0\sqrt{10 \mp_2 \sqrt{73}}. \tag{1.113}$$

We have introduced a shorthand notation via a subscript on the $\pm$ sign, such that $\pm_1, \pm_2$ are a pair of sign choices (and $\mp_1$ indicates that the opposite sign as $\pm_1$ is used, and likewise for $\mp_2$) which allows for a more compact expression for all four dressed states. The four perturbed energy values are not equally spaced, though they still come in oppositely signed pairs of equal magnitude. In terms of the Greek letter notation we have the following equivalences:

$$|3/2, 3 : \alpha\rangle := |3/2, 3; +, -\rangle \quad , \qquad |3/2, 3 : \beta\rangle := |3/2, 3; +, +\rangle, \tag{1.114}$$

$$|3/2, 3 : \gamma\rangle := |3/2, 3; -, +\rangle \quad , \qquad |3/2, 3 : \delta\rangle := |3/2, 3; -, -\rangle. \tag{1.115}$$

For the remaining two matrices with $j = \frac{1}{2}$ in the direct sum decomposition, these systems are algebraically equivalent to the single spin model. This equivalence allows us to immediately write down the diagonalized states and perturbed energies:

$$\begin{aligned}
|1/2, 3; \pm\rangle_1 &:= \frac{1}{2}[|2\rangle[|\downarrow\uparrow\downarrow\rangle - |\uparrow\downarrow\downarrow\rangle] \pm |1\rangle[|\downarrow\uparrow\uparrow\rangle - |\uparrow\downarrow\uparrow\rangle]], \\
E_{3;\pm} &= 3\omega_0 \pm g_0\sqrt{2} \\
|1/2, \pm\rangle_2 &:= \frac{1}{2\sqrt{3}}[|2\rangle[2|\downarrow\downarrow\uparrow\rangle - |\uparrow\downarrow\downarrow\rangle - |\downarrow\uparrow\downarrow\rangle] \pm |1\rangle[|\uparrow\downarrow\uparrow\rangle + |\downarrow\uparrow\uparrow\rangle - 2|\uparrow\uparrow\downarrow\rangle]], \\
E_{3;\pm} &= 3\omega_0 \pm g_0\sqrt{2}.
\end{aligned}$$

The subscript on the kets in the above equations indicate the arbitrarily chosen degeneracy label of that subspace.

Case 4: $k \geq 3$

While the above considered $k = 3$, we can solve this case as well as all higher cases at once. In the general case of $k \geq 3$, the number of manifold states become maximal (see figure 2.1) and all $2^3 = 8$ spin states participate in hybridization, determined by the coupling matrix $L(3/2, k)$:

$$L(k) = \begin{bmatrix} 0 & \sqrt{k} & \sqrt{k} & 0 & \sqrt{k} & 0 & 0 & 0 \\ \sqrt{k} & 0 & 0 & \sqrt{k-1} & 0 & \sqrt{k-1} & 0 & 0 \\ \sqrt{k} & 0 & 0 & \sqrt{k-1} & 0 & 0 & \sqrt{k-1} & 0 \\ 0 & \sqrt{k-1} & \sqrt{k-1} & 0 & 0 & 0 & 0 & \sqrt{k-2} \\ \sqrt{k} & 0 & 0 & 0 & 0 & \sqrt{k-1} & \sqrt{k-1} & 0 \\ 0 & \sqrt{k-1} & 0 & 0 & \sqrt{k-1} & 0 & 0 & \sqrt{k-2} \\ 0 & 0 & \sqrt{k-1} & 0 & \sqrt{k-1} & 0 & 0 & \sqrt{k-2} \\ 0 & 0 & 0 & \sqrt{k-2} & 0 & \sqrt{k-2} & \sqrt{k-2} & 0 \end{bmatrix}, \quad (1.116)$$

where the ordered basis states for this matrix representation are given by the set $\{|k\rangle|\downarrow\downarrow\downarrow\rangle, |k-1\rangle|\downarrow\downarrow\uparrow\rangle, \ldots |k-3\rangle|\uparrow\uparrow\uparrow\rangle\}$. As before, this matrix admits a direct sum representation $(\frac{3}{2} \oplus \frac{1}{2} \oplus \frac{1}{2})$ with coupling matrices $L(3/2,k) \oplus L(1/2,k) \oplus L(1/2,k)$, given by:

$$\begin{bmatrix} 0 & \sqrt{3}\sqrt{k} & 0 & 0 \\ \sqrt{3}\sqrt{k} & 0 & 2\sqrt{k-1} & 0 \\ 0 & 2\sqrt{k-1} & 0 & \sqrt{3}\sqrt{k-2} \\ 0 & 0 & \sqrt{3}\sqrt{k-2} & 0 \end{bmatrix} \oplus \begin{bmatrix} 0 & \sqrt{k-1} \\ \sqrt{k-1} & 0 \end{bmatrix} \oplus \begin{bmatrix} 0 & \sqrt{k-1} \\ \sqrt{k-1} & 0 \end{bmatrix}. \quad (1.117)$$

The first matrix is written in the Dicke (fully symmetric) basis (normalized versions of $|k-m\rangle\hat{J}_+^m|\downarrow\downarrow\downarrow\rangle$ with $m \in \{0,1,2,3\}$), while the second and third are written in terms of the composite spin–1/2 bases, given by

$$\frac{1}{\sqrt{2}}|k-1\rangle(|\downarrow\uparrow\downarrow\rangle - |\uparrow\downarrow\downarrow\rangle) \quad , \quad \frac{1}{\sqrt{2}}|k-2\rangle(|\downarrow\uparrow\uparrow\rangle - |\uparrow\downarrow\uparrow\rangle) \quad (1.118)$$

$$\frac{1}{\sqrt{6}}|k-1\rangle(2|\downarrow\downarrow\uparrow\rangle - |\uparrow\downarrow\downarrow\rangle - |\downarrow\uparrow\downarrow\rangle) \quad , \quad \frac{1}{\sqrt{6}}|k-2\rangle(|\uparrow\downarrow\uparrow\rangle + |\downarrow\uparrow\uparrow\rangle - 2|\uparrow\uparrow\downarrow\rangle) \quad (1.119)$$

The matrix representations for the degenerate spin-1/2 subspaces are identical, and thus indistinguishable under a collective operation or measurement. There is freedom in the choices of bases for the degenerate subspaces; the states provided are the standard basis states for these subspaces, as computed via a Clebsch–Gordon table [54].

We diagonalize each block individually, starting with the matrix representing the $j = 3/2$ subspace, and find the resulting (non-normalized) Lamb-shifted dressed states are given

by the following superpositions for $|3/2, k; \pm_1, \pm_2\rangle$:

$$\begin{aligned}
:= \quad & \pm_1\sqrt{5k-5\mp_2\sqrt{25-32k+16k^2}}(2k-5\pm_2\sqrt{25-32k+16k^2})|k\rangle|3/2;-3/2\rangle \\
& +(1+2k\mp_2\sqrt{25-32k+16k^2})\sqrt{3}\sqrt{k}|k-1\rangle|3/2;-1/2\rangle \\
& \mp_1 2\sqrt{5k-5\mp_2\sqrt{25-32k+16k^2}}\sqrt{3}\sqrt{k-1}\sqrt{k}|k-2\rangle|3/2;1/2\rangle \\
& +6\sqrt{k-2}\sqrt{k-1}\sqrt{k}|k-3\rangle|3/2;3/2\rangle \qquad (1.120) \\
= \quad & \pm_1\sqrt{5k-5\mp_2\sqrt{25-32k+16k^2}}(2k-5\pm_2\sqrt{25-32k+16k^2})|k\rangle|\downarrow\downarrow\downarrow\rangle \\
& +(1+2k\mp_2\sqrt{25-32k+16k^2})\sqrt{3}\sqrt{k}|k-1\rangle\frac{1}{\sqrt{3}}(|\downarrow\downarrow\uparrow\rangle+|\downarrow\uparrow\downarrow\rangle+|\uparrow\downarrow\downarrow\rangle) \\
& \mp_1 2\sqrt{5k-5\mp_2\sqrt{25-32k+16k^2}}\sqrt{3}\sqrt{k-1}\sqrt{k}|k-2\rangle\frac{1}{\sqrt{3}}(|\downarrow\uparrow\uparrow\rangle+|\uparrow\downarrow\uparrow\rangle+|\uparrow\uparrow\downarrow\rangle) \\
& +6\sqrt{k-2}\sqrt{k-1}\sqrt{k}|k-3\rangle|\uparrow\uparrow\uparrow\rangle, \qquad (1.121)
\end{aligned}$$

each with associated energy

$$E_{k;\pm_1\pm_2} = k\omega_0 \mp_1 g_0\sqrt{5(k-1)\mp_2\sqrt{16k^2-32k+25}}. \qquad (1.122)$$

We have introduced a shorthand notation via a subscript on the $\pm$ sign, such that $\pm_1, \pm_2$ are a pair of sign choices (and $\mp_1$ indicates that the opposite sign as $\pm_1$ is used, and likewise for $\mp_2$) which allows for a more compact expression for all four dressed states. The four perturbed energy values are not equally spaced, though they still come in oppositely signed pairs of equal magnitude. In terms of the Greek letter notation we have the following equivalences:

$$|3/2, k:\alpha\rangle := |3/2, k; +, -\rangle \quad , \qquad |3/2, k:\beta\rangle := |3/2, k; +, +\rangle, \qquad (1.123)$$

$$|3/2, k:\gamma\rangle := |3/2, k; -, +\rangle \quad , \qquad |3/2, k:\delta\rangle := |3/2, k; -, -\rangle. \qquad (1.124)$$

For the remaining two matrices with $j = \frac{1}{2}$ in the direct sum decomposition, these systems are algebraically equivalent to the single spin model. This equivalence allows us to immediately write down the diagonalized states and perturbed energies:

$$\begin{aligned}
|1/2, k; \pm\rangle_1 &:= \frac{1}{2}[|k-1\rangle[|\downarrow\uparrow\downarrow\rangle - |\uparrow\downarrow\downarrow\rangle] \pm |k-2\rangle[|\downarrow\uparrow\uparrow\rangle - |\uparrow\downarrow\uparrow\rangle]], \\
E_{k;\pm} &= k\omega_0 \pm g_0\sqrt{k-1} \\
|1/2, \pm\rangle_2 &:= \frac{1}{2\sqrt{3}}[|k-1\rangle[2|\downarrow\downarrow\uparrow\rangle - |\uparrow\downarrow\downarrow\rangle - |\downarrow\uparrow\downarrow\rangle] \pm |k-2\rangle[|\uparrow\downarrow\uparrow\rangle + |\downarrow\uparrow\uparrow\rangle - 2|\uparrow\uparrow\downarrow\rangle]], \\
E_{k;\pm} &= k\omega_0 \pm g_0\sqrt{k-1}.
\end{aligned}$$

The subscript on the kets in the above equations indicate the arbitrarily chosen degeneracy label of that subspace. All Lamb shifts that occur for $N = 3$ are summarized in the following table:

Subspace	Excitations	Lamb Shifts	Numerical Values
$j = 3/2$	$k = 1$	$g_0\sqrt{3}$	$1.73g_0$
	$k = 2$	$g_0\sqrt{10}$	$3.16g_0$
	$k = 3$	$g_0\sqrt{10 \pm \sqrt{73}}$	$1.21g_0, 4.21g_0$
	k	$g_0\sqrt{5(k-1) \pm \sqrt{16k^2 - 32k + 25}}$	
$j = 1/2$	$k = 1$	0	0
	$k = 2$	g_0	g_0
	$k = 3$	$g_0\sqrt{2}$	$1.41g_0$
	k	$g_0\sqrt{k-1}$	
$j = 1/2$	$k = 1$	0	0
	$k = 2$	g_0	g_0
	$k = 3$	$g_0\sqrt{2}$	$1.41g_0$
	k	$g_0\sqrt{k-1}$	

1.4.4 $N > 3$

The following figure illustrates the general decomposition structure into the various angular momentum subspaces:

The case of low excitation count for arbitrary N is discussed in [51], so we stop working through examples now and work toward providing results that hold for larger N and k counts.

This chapter introduced the primary model of interest throughout this part of the thesis. Explicit examples have been worked through, however, general trends have only been touched upon. In the next chapter we discuss how to extract information about the distribution of the Lamb shifts without needing to diagonalize each coupling matrix, which becomes untenable for large values of N and k.

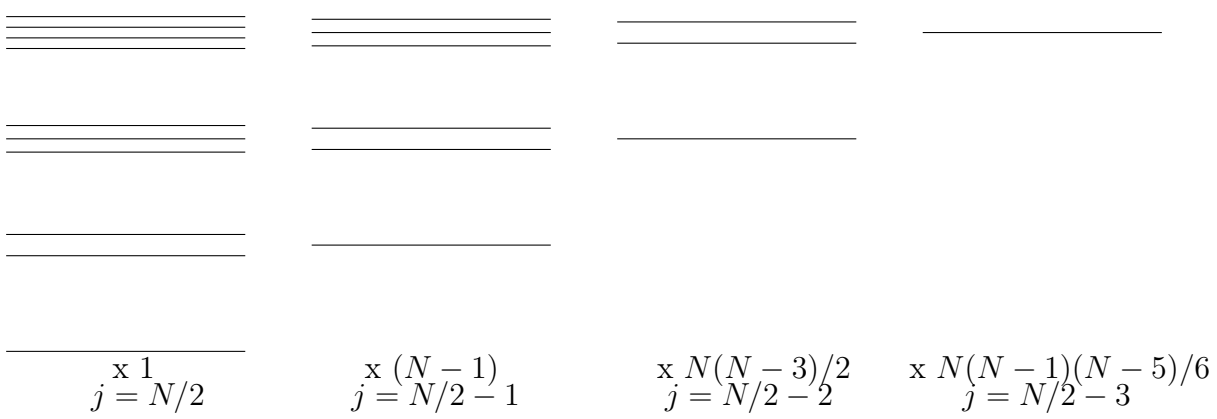

Figure 1.3: Schematic representation of the energy eigenstates of the Tavis-Cummings Hamiltonian with excitations $0 \leq k \leq 3$ along the vertical, and labelled horizontally by the number of degeneracies of each angular momentum subspace.

Chapter 2

The Tavis-Cummings Model's Energy Structure

In this chapter we delve into the Tavis–Cummings model and aim to extract information about the distribution of the Lamb shifts without either solving difference equations nor diagonalizing matrices. Both of these methods become intractable for large excitation numbers and spin-ensembles, so instead we take a trace based approach and put this approach into physical meanings. The chapter following this carries this idea further from making statements about the spectrum of the Lamb shifts to extraction of expected time evolutions for thermalized states.

2.1 Subspace Decomposition of the TC Model

A direct sum decomposition of the TC Hamiltonian was given explicitly in the original 1968 work by Tavis and Cummings [38]. Recast in our notation, the decomposition is

$$\hat{\mathcal{H}} \cong \bigoplus_{j,k} \big(\omega_0 k \mathbb{1}_{j,k} + g_0 L(j,k)\big), \tag{2.1}$$

where $L(j,k)$ are coupling matrix representations of the interaction Hamiltonian defined in equation (2.5). Solving for the structure of the TC model is akin to diagonalizing the Hamiltonian in each subspace under the action of the coupling matrix. As discussed in Section 2.3.1 and calculated explicity for $N = 1, 2, 3$ in the appendix, the numerical and analytical complexity of the eigenstructure problem scales unfavourably with ensemble size,

N, and excitation number, k. Thus, analyzing the TC model according to the statistical behaviour of the Lamb shifts, represented by $L(j,k)$, becomes valuable for mesoscopic ensembles with a moderate level of excitation (Section 2.3).

We define a natural basis for a specific (j,k) subspace with total angular momentum j and k excitations as

$$\mathcal{B}_{j,k} = \{|\alpha_{j,k}\rangle \mid \alpha = 1, \cdots, n_{j,k}, n_{j,k}+1\}, \tag{2.2}$$

using a shorthand ket representation of the tensor product of a spin-cavity state:

$$|\alpha_{j,k}\rangle = |k - \alpha - k_0(j)\rangle\,|j, -j+\alpha\rangle\,. \tag{2.3}$$

The single parameter, α, provides a convenient representation of states within a (j,k) subspace. The value, $n_{j,k} = |\mathcal{B}_{j,k}|-1$, one less than the dimension, is chosen for convenience. We define $k_0(j) = N/2 - j$ as the number of excitations present in the ground state of an angular momentum j subspace within an N spin ensemble. Explicitly, $n_{j,k}$ is given as

$$n_{j,k} = \min\{2j, k - k_0(j)\}. \tag{2.4}$$

If $k < k_0(j)$, then the basis set is empty and there are no states present at this excitation level within the j angular momentum subspace (Figure 1.3 shows this generally, while Figure 2.1 illustrates this for the the case of $N = 3$).

Under unitary evolution generated by collective operators, two subspaces with the same value of j stemming from ensembles of differing N will behave identically, as these subspaces have isomorphic representations. The main functional difference between them is their relative locations within the energy level spectrum of their respective Hamiltonians. Thus, while the evolution or action of a collective operator, J_+ and J_-, can be calculated identically, the resultant contribution of the evolution to aggregate statistics or an observable will be weighted differently.

By applying the interaction term from $\hat{\mathcal{H}}_{TC}$, $g_0(\hat{a}^\dagger \hat{J}_- + \hat{a}\hat{J}_+)$, to the bases defined in Equation (2.2), the Lamb shift coupling matrix for a (j,k) subspace may be written as

$$L(j,k) = \sum_{\alpha=1}^{n_{j,k}} l_\alpha(j,k)\Big(|\alpha_{j,k}\rangle\langle(\alpha+1)_{j,k}| + |(\alpha+1)_{j,k}\rangle\langle\alpha_{j,k}| \Big), \tag{2.5}$$

where the matrix elements are given by

$$\begin{aligned} l_\alpha(j,k) &= \frac{1}{g_0}\left\langle \alpha_{j,k}\right| \hat{\mathcal{H}}_{\text{int}} \left|(\alpha+1)_{j,k}\right\rangle \\ &= \sqrt{\big(2\alpha j - \alpha(\alpha-1)\big)\big(k - k_0(j) - \alpha + 1\big)}. \end{aligned} \tag{2.6}$$

In the above expression subscripts are only included within kets such as $|\alpha_{j,k}\rangle$, while α itself is a scalar.

The index j runs from $N/2$ to 0 (1/2) when N is even (odd). Each angular momentum space is of dimension $2j+1$, such that the total number of spin states accounted for across all values of j is $O(N^2)$, as opposed to 2^N for the full space. The degeneracy of a subspace of total angular momentum j on N spins is given as

$$d_j = \frac{N!(2j+1)}{(N/2-j)!(N/2+j+1)!}. \tag{2.7}$$

There are d_j disjoint angular momentum subspaces with total angular momentum j present in a direct sum decomposition of $\left(\mathbb{C}^2\right)^{\otimes N}$ [31]. By including this degeneracy, we recover the identity that the sum over the dimension of all disjoint subspaces is equal to the dimension of the entire space:

$$\sum_j (2j+1)d_j = 2^N. \tag{2.8}$$

Through Schur–Weyl duality, we can associate total angular momentum symmetry with invariance over permutations (or subgroups of permutations) of the ordering of the underlying spin Hilbert spaces [55]. Within this context, the Dicke subspace ($j = N/2$) is the fully symmetric subspace with every angular momentum state remaining invariant under action of the permutation group of order N, $S(N)$. The remaining subspaces have a more complex structure under the action of a spin-permutation.

Importantly, each degenerate copy of a j subspace can be naturally and uniquely labelled by a Young Tableau. If one wished to consider a perturbation to the TC Hamiltonian which distinguished individual spins, such as a field inhomogeneity, then these Young Tableaux would be required to properly determine the perturbation's action on subspaces with identical total angular momentum j. For clarity, explicit detailed examples for $N = 1, 2, 3$ were worked out in the prior chapter.

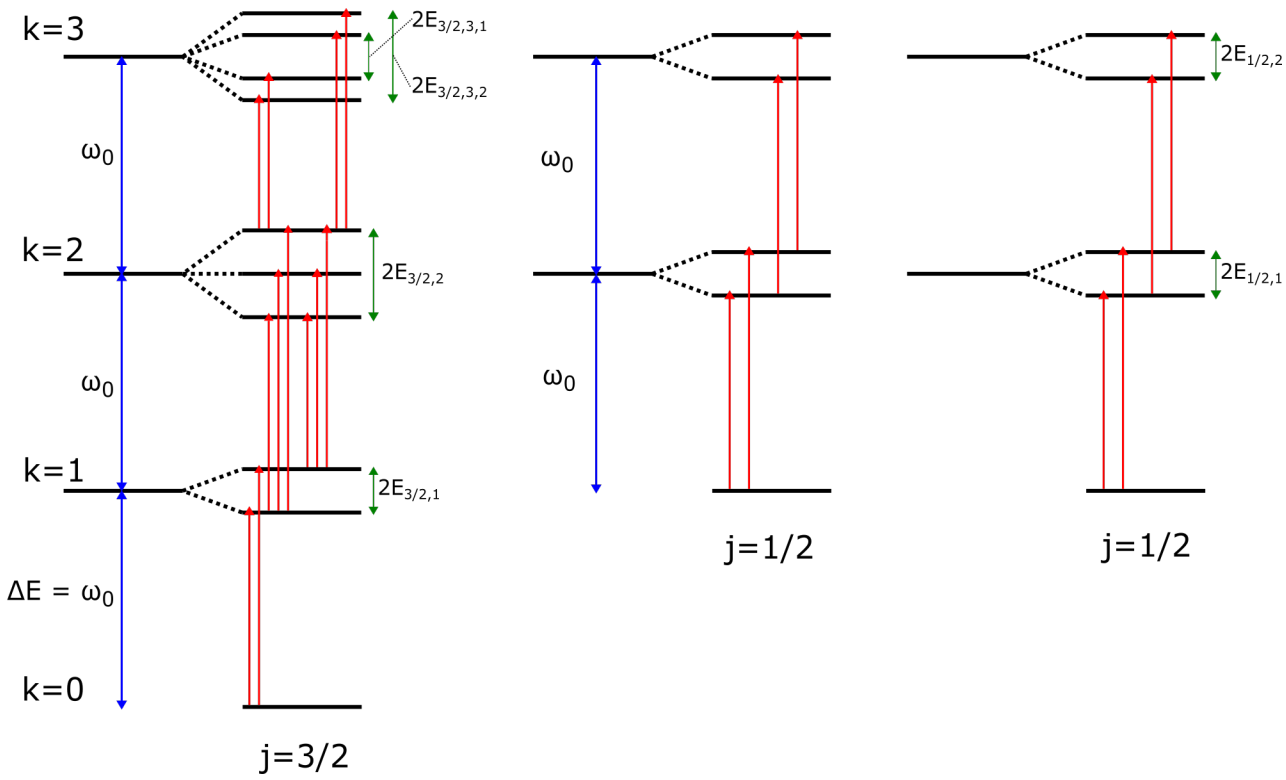

Figure 2.1: Illustration of the resulting hybridization of energy levels in the Tavis–Cummings model for $N = 3$, explicitly on resonance such that $\omega_0 = \omega_s = \omega_c$. Vertical single arrow lines (red) indicate transitions mediated by $\hat{J}_+$, meaning that the eigenstates represented by the horizontal bars have a non-zero $\hat{J}_+$ matrix element. Transitions are all–to–all between neighboring excitation subspaces of the same angular momentum, with some transitions between the $k = 2$ and $k = 3$ subspaces omitted for clarity. Note that there are no allowed transitions via collective spin or photon operators between distinct angular momentum subspaces, regardless of the value of j. Separation between excitation spaces is a constant ω_0, denoted by bidirectional arrows (blue) between the pre–hybridized angular momentum states. Lamb shift splittings are denoted be bidirectional arrows (green) to the right of the hybridized states. In the $j = 1/2$ subspaces, these splittings are given by $E_{1/2,1} = g_0$ and $E_{1/2,2} = g_0\sqrt{2}$. In the $j = 3/2$ subspace, the Lamb shifts are given by: $E_{3/2,1} = g_0\sqrt{3} \approx 1.73g_0$, $E_{3/2,2} = g_0\sqrt{10} \approx 3.16g_0$, $E_{3/2,3,1} = g_0\sqrt{10 - \sqrt{73}} \approx 1.21g_0$, and $E_{3/2,3,2} = g_0\sqrt{10 + \sqrt{73}} \approx 4.31g_0$.

2.2 The Maximally Degenerate Subspace

The maximally degenerate collective angular momentum subspace for N spin–1/2 particles, which we denote as j^*, is given by

$$j^* = \frac{\sqrt{N}}{2} - \frac{1}{2} + \frac{1}{6\sqrt{N}} + O(N^{-1}). \tag{2.9}$$

Formally j^* is given by one of the two valid nearest half-integer values for j, but since which is larger requires knowing N, we will use this expression. This space is increasingly separated from the Dicke space as N increases. Also, the value of j^* does not approach 0 or 1/2, indicating that large N structure, through the lens of degeneracy, is not well–approximated by either a single spin with angular momentum $j = N/2$, nor one with small angular momentum, such as $j = 1/2$.

Given that the maximally degenerate angular momentum subspace is well–approximated by this expression for j^*, it is useful to determine how well dynamics calculated in this subspace represent the entire system dynamics. To formalize this notion, consider the ratio of d_{j^*}, the degeneracy of the j^* subspace, to d_{j^*+1}, the degeneracy of the neighboring j^*+1 subspace:

$$\frac{d_{j^*}}{d_{j^*+1}} = 1 + O(N^{-3/2}). \tag{2.10}$$

The maximally degenerate subspace is not significantly more degenerate than its nearest neighbor. This argument may be extended to show that subspace degeneracy does not vary much locally in general. Thus, even though j^* is the most degenerate subspace, the system dynamics cannot reasonably be approximated by considering dynamics solely in this space.

Within the context of degeneracy–weighted observables, then, there is no single subspace which can accurately mimic the structure and dynamics of the entire Hamiltonian. The minimal collection of angular momentum subspaces that must be considered for a given N may be quantified by the strong support of d_j (Figure 2.2), which is approximately given by the interval $0 \leq j \leq O(\sqrt{N})$, for all allowed values of j. That is, nearly all of the states are contained in the subspaces below some constant multiple of $\sqrt{N}$. The $O(\sqrt{N})$ upper limit can be derived by considering the ratios of the degeneracies of increasingly separated angular momentum subspaces (see appendix for further details).

The insights provided by the computation of j^* and determination of the strong support of d_j have a few important implications. Firstly, that the system must be represented by $O(\sqrt{N})$ subspaces may be of interest to those working in the area of the complexity

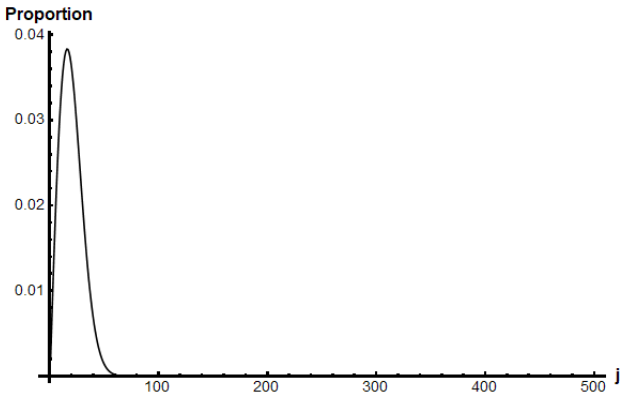

Figure 2.2: Normalized plot of d_j as a function of j, for $N = 1000$ spin-1/2 particles. The maximally degenerate space is the $j = 15$ angular momentum space. This plot clearly indicates that when weighted by degeneracy, the Dicke subspace contributes negligibly as compared to lower j angular momentum subspaces.

of quantum systems. Secondly, this also may be of interest to those simulating quantum systems admitting a similar angular momentum subspace decomposition, in that so long as one has the subspace structure being preserved, any observable that grows sub–exponentially in j, as suggested by (2.53), can be sufficiently modelled using this region of strong support. By restricting computations to this region, we can expect a halving of the dominant order of the computational cost (i.e. an $O(N^4)$ algorithm can be well approximated by an $O(N^2)$ algorithm). In fact, this reduction of order further reduces the effective spin dimensionality of the problem from $O(N^2)$ spin states, to $O(N)$ spin sates, yielding a significant complexity reduction from the original dimension of 2^N.

2.3 Lamb Shift Statistics

In this section, techniques are presented for extracting more information about the Lamb shift coupling matrices without resorting to numerically solving an eigenvalue problem.

2.3.1 Single Angular Momentum Subspace

Given the subspace decomposition of the TC Hamiltonian,

$$\hat{\mathcal{H}} \cong \bigoplus_{j,k} \big(\omega_0 k \mathbb{1}_{j,k} + g_0 L(j,k)\big), \tag{2.11}$$

if one were able to diagonalize $L(j,k)$, then the Hamiltonian would be fully solved. It is instructive to visualize the representation of $L(j,k)$ with respect to $\mathcal{B}_{j,k}$ as in 2.1:

$$\begin{bmatrix} 0 & l_1(j,k) & & & \\ l_1(j,k) & 0 & l_2(j,k) & & \\ & l_2(j,k) & 0 & \ddots & \\ & & \ddots & \ddots & l_n(j,k) \\ & & & l_n(j,k) & 0 \end{bmatrix}. \tag{2.12}$$

Thus, the Lamb shift coupling matrix can be naturally represented as a hollow tridiagonal matrix, a highly structured sparse matrix.

A full closed-form diagonalization of this matrix is unlikely to exist, but there is still a good amount of information that can be extracted. As a first approach we can consider the problem from a numerical linear algebra perspective. It was shown in 2013 that the eigenvalues of this variety of matrix can be computed exactly (to within numerical precision) in $O(n_{j,k} \log n_{j,k})$ floating point operations, a speed-up over the unstructured problem [56]. This algorithm can be used to efficiently extract the Lamb shifts of a given (j,k) space, if desired. The eigenvector problem, given an eigenvalue λ, is then solvable in $O(n_{j,k})$ floating point operations utilizing the Thomas algorithm [57]. This must be done for each of the $n_{j,k}+1$ eigenvalues. Thus, while the cost of producing the set of eigenvalues is $O(n_{j,k} \log n_{j,k})$, the cost of producing the entire eigensystem is $O(n_{j,k}^2)$, dominated by the eigenvector problem. We expect the numerical speedup of finding the eigenvalues to be useful for simulating this system's dynamics and computing state dependent quantities for states defined by classical mixtures across angular momentum subspace, thereby increasing the maximal value for N that can be feasibly simulated on a classical processor.

Given that the eigenvalues of hollow tridiagonal matrices come in oppositely signed pairs, the eigenvalue spectrum of the Lamb shift coupling matrix can be treated as a two parameter family of even sets [58]:

$$\Lambda(j,k) = \{\lambda \,|\, L(j,k)\boldsymbol{v} = \lambda \boldsymbol{v}, \boldsymbol{v} \neq \mathbf{0}\}. \tag{2.13}$$

The fact that the eigenvalues of these coupling matrices is a family of sets and not multi-sets is shown in [59]. Thus, if $|\Lambda(j,k)| = |\mathcal{B}_{j,k}| = n_{j,k}+1$ is odd, there must be exactly one eigenvalue with value $\lambda = 0$. There are a number of useful properties of the collection of Lamb shifts that can be analytically computed, or well-estimated.

Computing the Determinant

A standard parameter of matrices to compute is the determinant, given by the product of the eigenvalues. A two step recursive formula may be used to compute the determinant of the Lamb shift coupling matrix, $L(j,k)$. Let A be a symmetric tridiagonal (Jacobi) matrix with matrix elements,

$$A = \sum_{\alpha=1}^{n+1} a_\alpha \, |\alpha\rangle\langle\alpha| + \sum_{\alpha=1}^{n} b_\alpha \big(\, |\alpha\rangle\langle\alpha+1| + |\alpha+1\rangle\langle\alpha| \, \big), \tag{2.14}$$

and sub-matrices A_α, formed by discarding all basis vectors with index greater than α. Then,

$$\begin{aligned} \det(A) &= \det(A_{n+2}) \\ &= a_{n+1} \det(A_{n+1}) - b_n^2 \det(A_n). \end{aligned} \tag{2.15}$$

Upon computing the determinant of $L(j,k)$, we find that if $n_{j,k}+1$ is odd, then the recurrence terminates with $\det A_0 = 0$, and so $\det L(j,k) = 0$. Otherwise, $n_{j,k}+1$ is even and the determinant is given as

$$\det L(j,k) = (-1)^{\frac{n+1}{2}} l_n^2 l_{n-2}^2 \cdots l_1^2, \tag{2.16}$$

where the dependence of the matrix elements l_α on (j,k) is suppressed for clarity. Through this recursive formula for the determinant, the singular multiplicity of the zero eigenvalue, when $n_{j,k}+1$ is odd, is shown.

Computing the mean

While it is interesting to know that the determinant can be computed efficiently and in a closed form, it does not provide a good, compact description of the structure of the Lamb

shifts. Rather, given the set of Lamb shift eigenvalues, $\Lambda(j,k)$, it is more useful to provide descriptive statistics. The t-th moment is given by

$$\left\langle \Lambda(j,k)^t \right\rangle = \frac{1}{|\mathcal{B}_{j,k}|} \sum_{\lambda \in \Lambda(j,k)} \lambda^t. \tag{2.17}$$

We can avoid computing the eigenvalues explicitly by noticing that the sum over eigenvalues is equivalent to the trace of the Lamb shift coupling matrix. Thus,

$$\left\langle \Lambda(j,k)^t \right\rangle = \frac{1}{|\mathcal{B}_{j,k}|} \operatorname{tr}\left(L(j,k)^t\right). \tag{2.18}$$

Then, given that the Lamb shift coupling matrix is hollow, the mean of the Lamb shifts in each subspace is zero,

$$\langle \Lambda(j,k) \rangle = 0, \tag{2.19}$$

as all the diagonal entries of $L(j,k)$ are zero. This statement can be extended to all odd moments of the Lamb shift eigenvalues. That is, for each coupling matrix, $L(j,k)$,

$$\left\langle \Lambda(j,k)^{2t+1} \right\rangle = 0, \ \forall t \in \mathbb{N}. \tag{2.20}$$

This follows immediately from the fact that, for every $\lambda \in \Lambda(j,k)$, $-\lambda \in \Lambda(j,k)$.

Computing the variance

The variance can be used as an effective measure of the average magnitude of the Lamb shift splittings in each subspace, which in this case is equal to the second moment of $\Lambda(j,k)$:

$$\begin{aligned} \operatorname{Var}(\Lambda(j,k)) &= \left\langle \Lambda(j,k)^2 \right\rangle - \langle \Lambda(j,k) \rangle^2 \\ &= \left\langle \Lambda(j,k)^2 \right\rangle. \end{aligned} \tag{2.21}$$

Computing the variance is then equivalent to determining the trace of the square of the coupling matrix, which is a banded pentadiagonal matrix, explicitly given as

$$\begin{bmatrix} l_1^2 & 0 & l_1 l_2 & & & & \\ 0 & l_1^2 + l_2^2 & 0 & l_2 l_3 & & & \\ l_1 l_2 & 0 & \ddots & \ddots & \ddots & & \\ & l_2 l_3 & \ddots & \ddots & \ddots & l_{n-1} l_n & \\ & & \ddots & \ddots & l_{n-1}^2 + l_n^2 & 0 & \\ & & & l_{n-1} l_n & 0 & l_n^2 & \end{bmatrix} \tag{2.22}$$

Thus, the trace of the square of $L(j,k)$ has a compact closed form expression in terms of the matrix elements $l_\alpha(j,k)$,

$$\operatorname{tr} L(j,k)^2 = 2\sum_{\alpha=1}^{n} l_\alpha(j,k)^2. \tag{2.23}$$

The variance of $\Lambda(j,k)$, for $k \geq k_0(j)$, with $k' = k - k_0(j)$, is then given by the expression

$$\begin{aligned}\operatorname{Var}(\Lambda(j,k)) = &\frac{1}{2}\left|\mathcal{B}_{j,k}\right|^3 - \frac{1}{3}\left|\mathcal{B}_{j,k}\right|^2 (2k' + 4j + 7) \\ &+ \left|\mathcal{B}_{j,k}\right| (2jk' + 2k' + 4j + 7/2) \\ &- \frac{1}{3}(6jk' + 8j + 4k' + 5).\end{aligned} \tag{2.24}$$

Recalling that the dimension of the basis of a (j,k) space is given by $|\mathcal{B}_{j,k}| = \min\{2j+1, k - k_0(j) + 1\}$, when k satisfies $k - k_0(j) > 2j$ the dimension of the space becomes fixed at $2j+1$. And so, for k such that $k - k_0(j) > 2j$, or equivalently $k > N/2 + j$, $\operatorname{Var}(\Lambda(j,k))$ is a linear function in k. This can be seen by substituting $|\mathcal{B}_{j,k}| = 2j+1$ into equation (2.24).

Taking the square root of the variance provides the standard deviation, which has an interpretation as the average distance from the mean. In this sense, for a given subspace of constant angular momentum j, the average Lamb shift is $O(\sqrt{k})$ for $k > N/2 + j$. To describe the full statistics of the Lamb shifts that occur in an ensemble, we must consider all angular momentum subspaces and their respective degeneracies for a given number of excitations, k. Before doing so, it is useful to note an important implication of the statistical structure of the Lamb shifts in arbitrary angular momentum and excitation subspaces.

2.3.2 Rotating–Wave Approximation Revisited

Given that all $L(j,k)$ are non-negative matrices, the maximal absolute value of the eigenvalue, also given by the spectral norm, may be bounded from above and below using the Perron–Frobenius theorem:

$$\min_m \sum_n [L(j,k)]_{mn} \leq \max \Lambda \leq \max_m \sum_n [L(j,k)]_{mn}. \tag{2.25}$$

Applying this theorem shows that $\max \Lambda(j,k)$ is upper bounded by the following cases:

$$\begin{cases} \frac{2}{\sqrt{3}}\sqrt{(2j+k')jk'} & \text{generally} \\ 2[j\sqrt{k'} - \frac{1}{2}\frac{j^2}{\sqrt{k'}} + \frac{1}{8}\frac{j^4}{(k')^{5/2}} + O(\frac{j^5}{(k')^{7/2}})] & 2j \ll k' \\ 2[\frac{1}{\sqrt{2}}k'\sqrt{j} - \frac{1}{8\sqrt{2}}\frac{(k')^2}{\sqrt{j}} + \frac{1}{512}\frac{(k')^4}{j^{5/2}} + O(\frac{(k')^5}{j^{7/2}})] & k' \ll 2j. \end{cases} \tag{2.26}$$

The relations for $\max \Lambda(j,k)$ can narrow the energy range necessary for consideration in experimental design for a given value of N and bounded total energy. Likewise, a lower bound on the maximal splitting can be found via the same argument. This always yields the minimum of the first row and the last row (both of which have a single entry in the coupling matrix).

These bounds on the maximal eigenvalue have an important implication with regard to making a rotating–wave approximation (RWA). As a general rule of thumb, the RWA used for approximating the Dicke Hamiltonian by the Tavis–Cummings Hamiltonian is said to be valid for $g_0\sqrt{N} \ll \omega_0$. Although this rule of thumb is useful for determining whether vacuum Rabi oscillations between the spin ensemble and cavity may be experimentally resolved, it is not a good metric for determining the validity of the RWA. To improve the specificity of this requirement, we first note that, from the lower bound for the maximal eigenvalue,

$$\lim_{j,k\to\infty} \|L(j,k)\|_\infty = \infty, \tag{2.27}$$

meaning that eventually $g_0 \max \Lambda(j,k)$ will approach and exceed $2\omega_0$. Thus, a more accurate condition for justifying a RWA is

$$g_0 \max \Lambda(j,k) \ll \omega_0. \tag{2.28}$$

This constraint puts a limit on the size of j and k that can be considered with this model. A maximally allowed value for k, after which the RWA breaks down, is not a property unique to the TC Hamiltonian, as the JC Hamiltonian's RWA is invalidated when $k \approx \omega_0^2/g_0^2$. Given our upper and lower bounds on $\max \Lambda(j,k)$, we can estimate where the RWA begins to breakdown. As an example, we consider the behavior of the density of states for an $N = 20$ system.

The density of states is a sum of delta functions over all excitation spaces, with location given by the energies of the Lamb-shifted eigenstates, scaled by the weight:

$$n(E) = \sum_{k=0}^{\infty} \sum_{\lambda\in\Lambda(k)} w_k(\lambda)\delta(E - (k\omega_0 + \lambda g_0)). \tag{2.29}$$

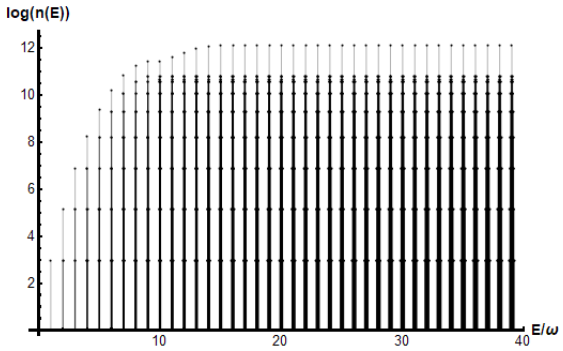

Figure 2.3: Scaled density of states for $N = 20$ spins in the Tavis–Cummings model, with $\omega_0/g_0 = 500$. This is found by diagonalizing the coupling matrices.

When the RWA holds, the distribution of delta functions across neighboring excitation subspaces will be well separated, as show in Figure 2.3. On the other hand, Figure 2.4 illustrates what the energy level structure looks like when the RWA breaks down. In this case, states in a given excitation subspace can overlap with states from neighboring excitation subspaces, breaking the notion of the good quantum number, and invalidating the predictions of the model.

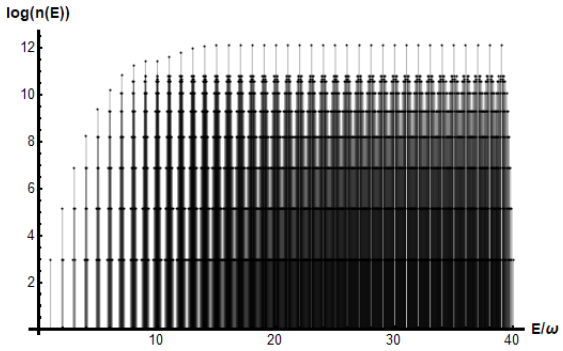

Figure 2.4: Scaled density of states for $N = 20$ spins in the Tavis–Cummings model, with $\omega_0/g_0 = 100$. This is found by diagonalizing the coupling matrices.

2.4 Degeneracy Averaged Lamb Shift Statistics

Given that relaxation and thermal processes in an ensemble tend to suppress collective behavior and spread population over many angular momentum subspaces [24, 30, 31, 60], the utility of descriptive statistics of the Lamb shifts for specific values of j is limited. We may join the above discussions to provide a description of the degeneracy-averaged Lamb shift taken over all subspaces, as a function of ensemble size, N, and total excitation level, k. An expression for the root mean square Lamb shift averaged over the degeneracies across all angular momentum subspaces may then be derived.

To begin, we define a probability distribution on the set of eigenvalues across all values of j at a given value of k. A natural choice is weighting each eigenvalue by its degeneracy:

$$w_k(\lambda) = \sum_j \begin{cases} d_j & \lambda \in \Lambda(j,k) \\ 0 & \text{else} \end{cases} \tag{2.30}$$

The sum over j accounts for the case of repeat eigenvalues across j spaces, although we believe it is generally only the 0 eigenvalue that repeats. For convenience, we also define the set of Lamb shift eigenvalues over k excitations to be given as:

$$\Lambda(k) = \bigcup_j \Lambda(j,k). \tag{2.31}$$

The set of pairs, $(\lambda, \omega_k(\lambda))$ define an unnormalized probability distribution on the Lamb shifts for an N spin TC system with k excitations.

The t-th moment of the Lamb shifts across all angular momentum subspaces is then formally written as

$$\left\langle \Lambda(k)^t \right\rangle = \frac{1}{D_k} \sum_{\lambda \in \Lambda(k)} w_k(\lambda) \lambda^t, \tag{2.32}$$

where D_k is the number of states with k excitations:

$$D_k = \sum_{k'=0}^{k} \binom{N}{k'}. \tag{2.33}$$

Recalling that, if $k < k_0(j) = N/2 - j$, then there are no states of excitation k for the given value of j. In this case, $\Lambda(j,k)$ is empty and does not contribute to the statistics of

this excitation level. Once $k \geq N$, the total number of states present at a given excitation becomes fixed at $D_k = 2^N$.

As with the case of a single angular momentum space, it is better to compute the moments utilizing traces of the Lamb shift coupling matrix, which are computable in $O(n_{j,k})$ floating point operations, as compared to the $O(n_{j,k} \log n_{j,k})$ scaling of the eigenvalue problem. The computational advantage is particularly significant for the second moment, as Equation (2.24) provides a closed-form expression for the trace, dropping the cost to $O(1)$ operations per angular momentum subspace. Using this insight, Equation (2.32) may be rewritten as

$$\left\langle \Lambda(k)^t \right\rangle = \frac{1}{D_k} \sum_j d_j \operatorname{tr}(L(j,k)^t). \tag{2.34}$$

Given that $\Lambda(k)$ is the union of even sets, it is also an even set, such that the odd moments for the Lamb shifts indexed by k excitations are all zero:

$$\left\langle \Lambda(k)^{2t+1} \right\rangle = 0, \ \forall t \in \mathbb{N}. \tag{2.35}$$

Due to the combinatorial nature of the weights on eigenvalues, there is no exact closed form expression for the even moments of the Lamb shift splittings. However, it is computationally feasible to visualize the function for select values of N, as shown in Figure 2.5.

The suppression of the variance for $k < N/2$ can be explained by recalling the partial energy level diagram of Figure 1.3. As each additional angular momentum subspace is considered, the ground state of that j space is introduced into the statistics with energy splitting of zero. Since d_j is an increasing function for $j < j^*$, the dominant element of the distribution of eigenvalues is the ground state of the smallest considered angular momentum subspace. This trend holds true until k approaches $N/2 - j^*$. In the case of $N = 1000$, Equation (2.9) provides $j^* = 15$, hence the suppression of the variance to nearly $k = N/2$.

The linearity of the variance, starting at roughly $k = N/2$, can be explained by noting that the variance of each j–subspace will be linear in k for values of $k > N/2 + j$. Thus, the transition into the linear regime at $k \approx N/2$ is caused by the variance of subspaces in the region of strong support of d_j being most dominant in the linear regime for $k > N/2 + j^*$. Thus, one can expect a linear variance in k for values of $k > N/2 + \sqrt{N}/2 - 1/2 + 1/(6\sqrt{N})$, which is dominated by $N/2$ for large N.

We can efficiently illustrate the trend numerically by performing a regression on the linear regime of the variance for select values of N, and plotting the slope of these lines as a function of N (Figure 2.6).

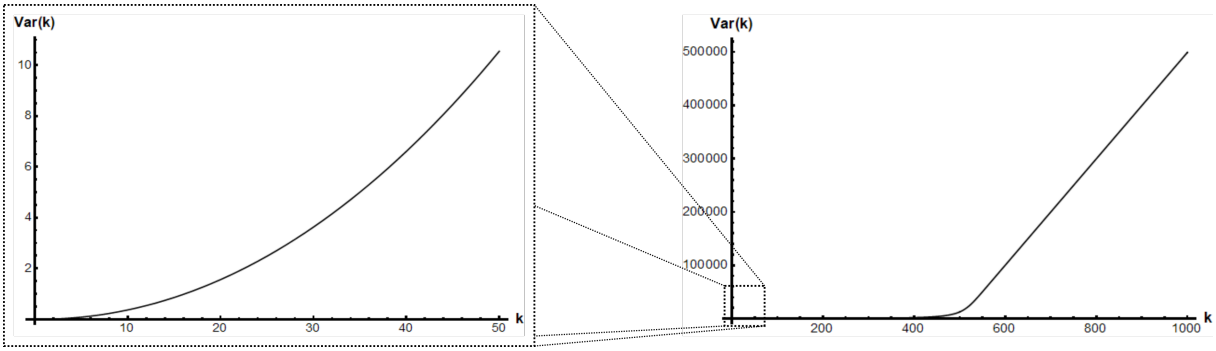

Figure 2.5: Variance of the unit–less ($\hbar = g_0 = 1$) Lamb shift splittings for $N = 1000$ spin–1/2 particles. Notice that the variance becomes linear in k soon after $k = N/2 = 500$. Notice the non-linearity and reduction of scale of the variance in the lower excitation subspaces as compared to the $k > N/2$ subspaces.

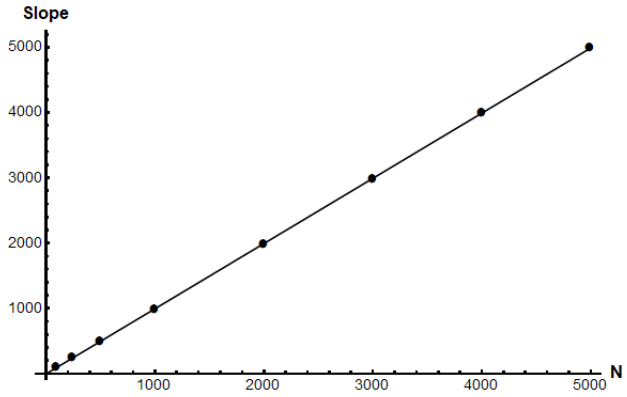

Figure 2.6: Slope of the variance of the collective Lamb shift splittings in the linear regime, for various N. Points mark computed values of the slope for each N. The regression model is $\text{Slope}(N) = 0.9989N - 0.27$, with an R^2 value of nearly 1.

The result of the regression indicates that for the values of k and N considered, the variance is effectively growing at a rate of $0.9989Nk$. In fact, analytically, the variance of the Lamb shift splittings, as a function of k excitations, grows as the product of N and k for $k \geq N$ (see Appendix):

$$\text{Var}(\Lambda(k)) = O(Nk). \tag{2.36}$$

We further conjecture that this result holds for all $k > k^*$, where k^* is some value in the range $N/2 < k^* < N$, and likely depends on N. This can be seen in part by noting that the

dimension of a subspace, $|\mathcal{B}_{j,k}|$, saturates at $2j+1$ when $k = k_0(j)+2j = N/2+j$. Further, since one need only consider the strong support of d_j when averaging (for more details see the appendix), the result could likely be extended to hold if $k^* = N/2 + O(\sqrt{N})$. In the region $k^* < k < N$, the statistics are not exposed to all possible spin states as $D_k < 2^N$. This issue can be avoided by bounding d_j/D_k instead of $d_j/2^N$, for all values of k greater than some k^*. Since D_k is almost constant on this region, the extension should not be too difficult.

2.5 Discussion

This work provides a method to estimate the expected statistics of Lamb shifts for ensembles with a given number of spins, N, spin–cavity interaction strength, g_0, and number of excitations, k. By averaging over subspace degeneracies, we arrive at the well–known result that the effective Lamb shift has a magnitude given approximately by $g_0\sqrt{Nk}$ when averaged over all subspaces. Care must be taken in applying this result, however, as the linearity of the variance in k is invalid for $k < N/2$, as illustrated in Figure 2.5 and mathematically seen in the proof of Equation (2.36) utilizing the region of strong support in the subspaces. This indicates that, while the single excitation splitting prediction of $O(\sqrt{N})$ is indeed valid for states with enough energy under the right conditions, for non–trivial moderate excitation states the variance cannot be approximated as simply. Given that many quantum devices operate exactly in this regime of low to moderate excitation, as dictated by common experimental temperatures of 10 mK to 4K, further examination of the experimental validity of various subspace restriction techniques used to describe experiments on mesoscopic ensembles is required. The tools presented in this work are expected to aid such analysis, permitting more accurate descriptions of mesoscopic ensemble dynamics at a given temperature.

Our results are derived for energy splittings in the static picture. In order to make statements about dynamics of the system, the results will need to be extended to include thermalization effects and an analysis of the evolution of appropriate observables. Considering subspace mixing from thermal effects, local relaxation processes, and field inhomogeneities is also important. Qualitatively large field inhomogeneities will remove all collective behavior, reducing the system to that of a tensor product of spins, while for sufficiently small field inhomogeneity the collective behavior should remain. Quantitatively finding the level of inhomogeneities that can be present likely reduces to the theory eigenvalue perturbations from matrix analysis, a possible starting point would be the tools presented in [61, 62].

As a final note, our results are consistent with various experiments measuring a high–cooperativity state splitting of spin ensembles interacting with high Q cavities, where $g_0\sqrt{N}$ behavior is observed [39, 42, 63, 64]. These experiments are generally run at relatively high power, corresponding to many excitations in the system. It has also been noted that high–cooperativity splitting disappears at sufficiently high drive powers [51, 65]. The coalescence of the splitting into a single peak is indicative of the Tavis–Cummings eigenstructure model becoming invalid, with "classical" behavior emerging due to the smearing of the density of states (Figure 2.4). The tools we've provided in this work should be useful in gaining additional insight into this quantum-classical transition.

2.6 Mathematical Proofs

Proof of Equation (2.9). To derive the value of j^*, we begin by defining the degeneracy function in a convenient form,

$$f(j) = \frac{2j+1}{N/2+j+1}\binom{N}{N/2+j}, \tag{2.37}$$

where j takes integer or half-integer values $0 \leq j \leq N/2$, depending on the parity of N. To prepare for differentiation, the binomial coefficient can be extended to a continuous function

$$\binom{N}{K} = \frac{\Gamma(N+1)}{\Gamma(K+1)\Gamma(N-K+1)}, \tag{2.38}$$

such that Equation (2.37) can be written as a continuous function in j

$$f(j) = \frac{2j+1}{N/2+j+1}\frac{\Gamma(N+1)}{\Gamma(N/2+j+1)\Gamma(N/2-j+1)}. \tag{2.39}$$

We may now differentiate and look for critical values:

$$\frac{d}{dj}f(j) = 4\binom{N}{N/2+j}\frac{\frac{1}{2}(2j+1)(N+2j+2)(H_{N/2-j}-H_{N/2+j})+N+1}{(N+2j+2)^2}. \tag{2.40}$$

In equation (2.40), H_x is the Harmonic series truncated at term x. The degeneracy is then maximal when

$$\frac{1}{2}(2j+1)(N+2j+2)(H_{N/2-j}-H_{N/2+j})+N+1 = 0. \tag{2.41}$$

We can re-cast this result by utilizing the expression for $H_x = \log x + \gamma + O(x^{-1})$, where γ is the Euler-Mascheroni constant ($\gamma \approx 0.577$). This allows us to take the difference of the Harmonic numbers as log's, which cancels the additive term. After simplifying, we are left with

$$\frac{1}{2}(2j+1)(N+2j+2)\log(\frac{N/2-j}{N/2+j}) + N + 1 = 0. \tag{2.42}$$

This is a very tight approximation. If we examine the series expansions of this, we see that taking $j \approx \frac{\sqrt{N}}{2}$ will remove the leading error. We may repeat this procedure, noting that the errors are a Laurent series in $\sqrt{N}$, so we adjust by decreasing powers of $\sqrt{N}$ corrections. Using this, we take as a guess that $j = \frac{\sqrt{N}-1}{2} + \frac{1}{6\sqrt{N}}$, which yields:

$$(3N+1)(3(N^{3/2}+N+\sqrt{N})+1)\frac{\log(\frac{-6N+6\sqrt{N}-2}{3\sqrt{N}(N+\sqrt{N}-1)+1}+1)}{18N} + N + 1. \tag{2.43}$$

When expanded as a series in the limit of large N, we have:

$$\frac{1}{\sqrt{N}} + O(\frac{1}{N}), \tag{2.44}$$

and thus our guess is equal to the true root in the limit of $N \longrightarrow \infty$. Thus,

$$j^* = \frac{\sqrt{N}-1}{2} + \frac{1}{6\sqrt{N}} + O(N^{-1}) \tag{2.45}$$

is the collective spin space with the largest degeneracy, up to error $O(N^{-1})$. ■

Proof of Equation (2.10). We begin by considering the ratio:

$$\frac{d_{j^*}}{d_{j^*+1}} = \frac{N!(2j^*+1)}{(N/2-j^*)!(N/2+j^*+1)!} \cdot \frac{(N/2-j^*-1)!(N/2+j^*+2)!}{N!(2j^*+3)} \tag{2.46}$$

$$= \frac{2j^*+1}{2j^*+3} \cdot \frac{N/2+j^*+2}{N/2-j^*} \tag{2.47}$$

$$= (1-\frac{2}{2j^*+3}) \cdot \frac{1+\frac{2j^*}{N}+\frac{4}{N}}{1-\frac{2j^*}{N}} \tag{2.48}$$

$$= (1-\frac{2}{2j^*+3})(1+\frac{2j^*}{N}+\frac{4}{N})(1+\frac{2j^*}{N}+(\frac{2j^*}{N})^2 + O(((j^*)/N)^3)) \tag{2.49}$$

where the last factor is a geometric series expansion with a ratio of $\frac{2j^*}{N}$. Grouping by powers, using $j^* = O(\sqrt{N})$, we have:

$$1 + [-\frac{2}{2j^*+3} + \frac{2j^*}{N} + \frac{2j^*}{N}] + [\frac{4}{N} - 2\frac{4j^*}{(2j^*+3)N} + 2(\frac{2j^*}{N})^2] + O(N^{-3/2}) \tag{2.50}$$

Now we utilize $j^* = \frac{\sqrt{N}}{2} - \frac{1}{2} + \frac{1}{6\sqrt{N}}$ to evaluate the above:

$$= \quad 1 + 0 + [-\frac{2}{N} + \frac{4}{N} - \frac{4\sqrt{N}}{\sqrt{N}N} + 2(\frac{1}{\sqrt{N}})^2] + O(N^{-3/2}) \tag{2.51}$$

So the ratio of the degeneracies is $1 + O(N^{-3/2})$. ■

Proof of Strong Support for $0 \leq j \leq O(\sqrt{N})$. Recall the computation of the relative population between the maximal angular momentum subspace and its neighbor, and consider the case when the leading term will contribute to the ratio of neighboring values of j. We found that when $\frac{2j}{N} \ll 1$,

$$\frac{d_j}{d_{j+1}} = 1 + [\frac{4j}{N} - \frac{2}{2j+3}] + O(N^{-1}), \tag{2.52}$$

which cancelled when $j = j^*$ since $j^* = \frac{\sqrt{N}}{2} + O(1)$.

Suppose we still have $\frac{2j}{N} \ll 1$, but now we consider a subspace nearby the maximal angular momentum space, such that $j = j^* + \Omega(\sqrt{N})$. The ratio for this value of j is then $1 + \Omega(N^{-1/2})$. This ratio will remain valid for increasing values of j, so long as $\frac{2j}{N} \ll 1$.

To find the ratio of the degeneracies of the next nearest neighbors, we apply this procedure twice, finding

$$\frac{d_j}{d_{j+2}} = (1 + \Omega(1/\sqrt{N}))^2. \tag{2.53}$$

To continue this argument to further subspace degeneracies, listed within the set

$$\{d_j, d_{j+1}, \ldots, d_{j+O(\sqrt{N})}\}, \tag{2.54}$$

we can write a geometric series taken at the infinity limit since the other term will contribute a much smaller portion to the sum. Thus, this series limits to

$$\frac{1}{1 - \frac{1}{1+\Omega(1/\sqrt{N})}} = O(\sqrt{N}). \tag{2.55}$$

We have shown that while the total number of allowed values for j is $O(N)$, the fractional contribution contained in this region is only $O(N^{-1/2})$. Thus we have that of the 2^N possible angular momentum states, *most* of them are contained within the lowest, smallest values of j, $O(\sqrt{N})$ angular momentum subspaces. ■

Proof of Equation (2.24). We will make use of the following summation formulae,

$$\sum_{i=1}^{n} i = \frac{n(n+1)}{2}$$
$$\sum_{i=1}^{n} i^2 = \frac{n(n+1)(2n+1)}{6}$$
$$\sum_{i=1}^{n} i^3 = \frac{n^2(n+1)^2}{4}.$$

Recall that the trace of the square of the coupling matrix can be written exactly as

$$\operatorname{tr} L(j,k)^2 = 2\sum_{\alpha=1}^{n} l_\alpha(j,k)^2 = 2\sum_{\alpha=1}^{n} \big(2\alpha j - \alpha(\alpha-1)\big)\big(k' - \alpha + 1\big). \tag{2.56}$$

Now, grouping the summand by orders of α we have

$$l_\alpha^2(j,k) = \alpha^3 - \alpha^2(2j+1+k'+1) + \alpha(2j+1)(k'+1). \tag{2.57}$$

And so

$$\begin{aligned}\operatorname{tr} L(j,k)^2 = \frac{1}{2}\left|\mathcal{B}_{j,k}\right|^4 - \frac{2}{3}\left|\mathcal{B}_{j,k}\right|^3 (2j+k'+7/2) + \left|\mathcal{B}_{j,k}\right|^2 (4j+2k'+2jk'+7/2) \\ - \frac{2}{3}\left|\mathcal{B}_{j,k}\right| (3jk'+4j+2k+5/2).\end{aligned} \tag{2.58}$$

The variance is then, by definition,

$$\begin{aligned}\operatorname{Var}(\Lambda(j,k)) = \frac{1}{2}\left|\mathcal{B}_{j,k}\right|^3 - \frac{1}{3}\left|\mathcal{B}_{j,k}\right|^2 (2k'+4j+7) \\ + \left|\mathcal{B}_{j,k}\right| (2jk'+2k'+4j+7/2) - \frac{1}{3}(6jk'+8j+4k'+5).\end{aligned} \tag{2.59}$$

■

Proof of Equation (2.26). We begin by transforming the entry values into a continuous function of α so that we may differentiate it. We will use Perron-Frobenius since we have a non-negative matrix and so can bound the maximal eigenvalue by the maximal row sum. To this end we focus on maximizing a single $l_\alpha(j,k)$ entry and double it since the true maximum will occur within one entry of the optimal continuous value choice for α and there are two entries in that row.

Differentiating this we have:

$$\frac{d}{d\alpha}\left[\sqrt{\alpha}\sqrt{2j+1-\alpha}\sqrt{k'-\alpha+1}\right] = \frac{3\alpha^2-4\alpha+2j(-2\alpha+k'+1)-2\alpha k'+k'+1}{2\sqrt{\alpha(\alpha-2j-1)(\alpha-k'-1)}} \tag{2.60}$$

and so this is optimized when:

$$\begin{aligned}\alpha &= \frac{1}{3}\left(2j+k'+2\pm\sqrt{4j^2-2jk'+2j+(k')^2+k'+1}\right) &(2.61)\\ &= \frac{1}{3}\left(2j+k'+2\pm\sqrt{(2j+\frac{1}{2})^2+(k'+\frac{1}{2})^2-2jk'+\frac{1}{2}}\right) &(2.62)\end{aligned}$$

In the above we must exclude the positive sign choice since this results in $\alpha \geq |\mathcal{B}_{j,k}|$, which is beyond the domain for α. With the negative sign choice we note that α is linear in j and k' to first order, so we remove the 1 shifts in our objective function. With this, we have:

$$\begin{aligned}\sqrt{j^2-(\alpha-j)^2}\sqrt{k'-\alpha} &= \sqrt{2j\alpha-\alpha^2}\sqrt{k'-\alpha} &(2.63)\\ &= \sqrt{\alpha}\sqrt{2j-\alpha}\sqrt{k'-\alpha} &(2.64)\end{aligned}$$

Solving for the roots again using this simplified expression provides:

$$\begin{aligned}\alpha &= \frac{1}{3}(2j+k'-\sqrt{4j^2-2jk'+(k')^2})+O(\sqrt{j}+\sqrt{k}) &(2.65)\\ &= \frac{1}{3}(2j+k'-\sqrt{(2j+k')^2-6jk'}) &(2.66)\\ &= \frac{1}{3}(2j+k'-(2j+k')\sqrt{1-\frac{6jk'}{(2j+k')^2}}) &(2.67)\\ &= \frac{1}{3}(2j+k')(1-\sqrt{1-\frac{6jk'}{(2j+k')^2}}) &(2.68)\end{aligned}$$

Observe that $\max_{j,k'}\frac{6jk'}{(2j+k')^2}=\frac{3}{4}$ where $k'=2j$, and $\min_{j,k'}\frac{6jk'}{(2j+k')^2}=0$ when one is constant and the other approaches infinity. This means that:

$$0<\alpha\leq\frac{1}{6}(2j+k') \tag{2.69}$$

Putting this into our expression for the largest eigenvalue, being sure to include the factor of two due to there being a second entry, provides:

$$\begin{aligned}\max \Lambda(j,k) &< 2\sqrt{\frac{1}{6}(2j+k')}\sqrt{2j}\sqrt{k'} && (2.70)\\ &= \frac{2}{\sqrt{3}}\sqrt{(2j+k')jk'}+O(j^{3/4}+(k')^{3/4}) && (2.71)\end{aligned}$$

This expression is mostly relevant when $2j \approx k'$. We now move to the cases of $2j \ll k'$ and $k' \ll 2j$. Returning to our prior expression this is:

$$\begin{aligned}&\sqrt{\frac{1}{3}(2j+k')(1-\sqrt{1-\frac{6jk'}{(2j+k')^2}})}\sqrt{2j-\frac{1}{3}(2j+k')(1-\sqrt{1-\frac{6jk'}{(2j+k')^2}})} && (2.72)\\ &\times\sqrt{k'-\frac{1}{3}(2j+k')(1-\sqrt{1-\frac{6jk'}{(2j+k')^2}})} && (2.73)\\ =\ &\sqrt{\frac{2}{27}(8j^3(\sqrt{1-\frac{6jk}{(2j+k)^2}}-1)+6j^2k+k^3(\sqrt{1-\frac{6jk}{(2j+k)^2}}-1)+3jk^2)} && (2.74)\end{aligned}$$

Taking a series expansion of this and doubling for there being two entries we have:

$$\begin{aligned}\max \Lambda(j,k) &\leq \begin{cases}2\sqrt{j^2k'-j^3+\frac{j^4}{4k'}} & 2j \ll k'\\ 2\sqrt{\frac{j(k')^2}{2}-\frac{1}{8}(k')^3+\frac{1}{128}\frac{(k')^4}{j}} & k' \ll 2j\end{cases} && (2.75)\\ &\approx \begin{cases}2[j\sqrt{k'}-\frac{1}{2}\frac{j^2}{\sqrt{k}}+\frac{1}{8}\frac{j^4}{k^{5/2}}+O(j^5/(k')^{7/2})] & 2j \ll k'\\ 2[\frac{1}{\sqrt{2}}k'\sqrt{j}-\frac{1}{8\sqrt{2}}\frac{(k')^2}{\sqrt{j}}+\frac{1}{512}\frac{(k')^4}{j^{5/2}}+O((k')^5/j^{7/2})] & k' \ll 2j\end{cases} && (2.76)\end{aligned}$$

■

Proof of Equation (2.34). This relation can be seen as the weighted average of averages,

and can thus be derived as follows:

$$\begin{aligned}\left\langle \Lambda(k)^t \right\rangle &= \frac{1}{D_k} \sum_j d_j \left| \mathcal{B}_{j,k} \right| \left\langle \Lambda(j,k)^t \right\rangle \\ &= \frac{1}{D_k} \sum_j d_j \left| \mathcal{B}_{j,k} \right| \frac{\operatorname{tr}(L(j,k)^t}{|\mathcal{B}_{j,k}|} \\ &= \frac{1}{D_k} \sum_j d_j \operatorname{tr}(L(j,k)^t).\end{aligned}$$

■

Lemma 1. *The degeneracies in our system satisfy:*

$$\frac{d_j}{2^N} = O(\frac{1}{N}) \tag{2.77}$$

for all allowed values of j.

Proof. Since $d_j < d_{j^*}$ for each j, we particularize to $j = j^*$. Then, taking only the leading term of $j^* = \sqrt{N}/2$, we have

$$d_{j^*} = \frac{\sqrt{N}/2 + 1}{N/2 + \sqrt{N}/2 + 1} \binom{N}{N/2 + \sqrt{N}/2 + 1}. \tag{2.78}$$

Focusing on the first factor,

$$\frac{2}{\frac{N+1}{\sqrt{N}+1} + 1} = O(1/\sqrt{N}). \tag{2.79}$$

Since $k = N/2 + \sqrt{N}/2 + 1$, we have that $|N/2 - k| = o(n^{2/3})$, we can utilize the following asymptotic equivalence relation [66]:

$$\binom{N}{k} \sim \frac{2^N}{\sqrt{N\pi/2}} e^{-(N-2k)^2/(2N)}. \tag{2.80}$$

Then, using the fact that $N - 2k = \sqrt{N} - 2$, we find that

$$\begin{aligned}e^{-(N-2k)^2/(2N)} &= e^{-(\sqrt{N}-2)^2/(2N)} \\ &= e^{-1/2+2/\sqrt{N}-2/N} \\ &= \frac{1}{\sqrt{e}}\big(1 + O(1/\sqrt{N})\big).\end{aligned} \tag{2.81}$$

Putting together the leading term with the asymptotic equivalence relation, we find

$$\begin{aligned}\binom{N}{N/2+\sqrt{N}/2+1} &\sim \frac{2^N}{\sqrt{N\pi e/2}}\big(1+O(1/\sqrt{N})\big)\\ &= O(2^N/\sqrt{N}).\end{aligned} \tag{2.82}$$

This finally implies

$$d_{j^*} = O(2^N/N), \tag{2.83}$$

and thus it hold that for all allowed j,

$$d_j 2^{-N} = O(1/N). \tag{2.84}$$

■

Proof of Equation (2.36). In order to derive our result, we particularize to $k > N$, since this fixes $D_k = 2^N$ and $k > N/2 + j$ is true for each value of j. Then,

$$\mathrm{Var}(\Lambda(k)) = \frac{1}{2^N}\sum_j d_j \,\mathrm{tr}(L(j,k)^2). \tag{2.85}$$

Recall the trace of the square of a coupling matrix is given by,

$$\begin{aligned}\mathrm{tr}(L(j,k)^2) = \frac{1}{2}\left|\mathcal{B}_{j,k}\right|^4 - \frac{1}{3}\left|\mathcal{B}_{j,k}\right|^3(2k'+4j+7) + \left|\mathcal{B}_{j,k}\right|^2(2jk'+2k'+4j+7/2)\\ - \frac{1}{3}\left|\mathcal{B}_{j,k}\right|(6jk'+8j+4k'+5)\end{aligned} \tag{2.86}$$

Using the fact now that $|\mathcal{B}_{j,k}| = 2j+1$ and $k' = k - N/2 + j$, we find that

$$\mathrm{tr}(L(j,k)^2) = k\big(\frac{8}{3}j^3+4j^2+\frac{4}{3}j\big) - N\big(\frac{4}{3}j^3+2j^2+\frac{2}{3}j\big) + \big(\frac{4}{3}j^3+2j^2+\frac{2}{3}j\big).$$

We focus on only the terms of order k, thus the dominant part of the expression we wish to analyze is given by

$$\frac{4}{3}k(2j^3+3j^2+j). \tag{2.87}$$

It remains to determine the order k contribution to the entire variance, upon averaging over the degeneracies,

$$\mathrm{Var}(\Lambda(k)) = \frac{4}{3}k\sum_j \frac{d_j}{2^N}(2j^3+3j^2+j) + \cdots, \tag{2.88}$$

where the terms of order k^0 will be dropped moving forward.

In order to make the sum over j tractable, we make use of Lemma 1,

$$\frac{d_j}{2^N} = O\big(\frac{1}{N}\big). \tag{2.89}$$

Given that the strong support of the weighting function is from 0 to $O(\sqrt{N})$, we have,

$$\begin{aligned}
\sum_j \frac{4kd_j}{2^N}\frac{2j^3+3j^2-2j}{3} &= \frac{4k}{3}\sum_j O\big(\frac{1}{N}\big)(2j^3+3j^2-2j) \\
&\approx O\big(\frac{k}{N}\big)\sum_{j=0}^{O(\sqrt{N})}(2j^3+3j^2-2j) \\
&= O\big(\frac{k}{N}\big)O(N^2) \\
&= O(Nk).
\end{aligned} \tag{2.90}$$

■

Chapter 3

The Tavis-Cummings Model and Some Dynamics in the Thermal Case

Hybrid quantum systems consisting of a collection of spin-1/2 particles uniformly interacting with an electromagnetic field are important for the development of quantum information processors and other quantum devices. Such systems are often modelled by the Tavis–Cummings model and so having an accurate understanding of the thermal behaviors of this system is needed to understand the behavior of these systems in more realistic environments. In this work we show that the system has a temperature whereby degeneracies in the system become dominant, when in such a temperature regime perturbative expansions for thermal properties in terms of the Lamb shifts are derived as well as numeric methods with optimal scaling, in terms of the size of the spin system. These provide methods for approximating, and bounding, properties of these systems as well as characterizing the dominant population regions, as well as related systems such as coupled-cavity arrays and cavity mediated coupling of collective spin ensembles.

3.1 Introduction

In this chapter, we focus on the collective interaction of a mesoscopic spin ensemble, with N spins, with a single mode quantum electromagnetic field. These systems, in the case of $N = 1$, have been used to verify their quantum nature [33] as well as being a useful tool for designing quantum devices, and so a more full understanding of the thermal properties of these systems could aid further progress in the development of quantum information

processors [9, 11, 12, 67], hybrid quantum devices [13, 14, 15], and radiative cooling of spin ensembles [23, 24, 25, 26, 27], among other possible uses.

In our system we take each particle to be a non-interacting spin-1/2 particle, coupled uniformly to the electromagnetic field. After a rotating wave approximation, this is modeled by the Tavis-Cummings (TC) Hamiltonian,

$$\hat{\mathcal{H}} = \omega_c \hat{a}^\dagger \hat{a} + \omega_s \hat{J}_z + g_0(\hat{a}\hat{J}_+ + \hat{a}^\dagger \hat{J}_-), \tag{3.1}$$

where g_0 is the single particle-mode coupling strength–we work in natural units throughout this work ($\hbar = k_b = 1$) [38].

This work builds off the techniques and results of our prior paper, which formed the first two chapters of this thesis [1]. As shown in our prior work, we have the ability to efficiently compute, as well as provide meaningful statistics on, the energy level structure of the Tavis-Cummings Hamiltonian under a certain set of assumptions. While those results provided some information they failed to provide practical methodology for taking these results and testing them, this work proceeds to carry those results to experimental expectations as well as providing tools of use for other systems with similar structures. Most of the experimental assumptions required here can be realized in a laboratory setting, as we just require that the ensemble be on resonance with the cavity, $\omega_c = \omega_s \equiv \omega_0$, and that $g_0\sqrt{N} \ll \omega_0$ (albeit that this second expression is not quite correct as we argued) and no spin-spin interactions, however, the prior results also did not include thermal effects. Under these assumptions, we have that angular momentum, j, and the number of total excitations, k, that is excitations stored in both the spin ensemble and the cavity, are conserved. This induces a two parameter family of non-interacting subspaces.

This work is organized as follows. It begins with the definitions needed for our analysis. Following this we remark on the temperature regime of particular interest and show that so long as the system is sufficiently above absolute zero there will be nearly no population in the Dicke ($N/2$) subspace, nor in the lowest-excitation levels within the angular momentum subspaces, finding a smooth transition where the degeneracies of this system increasingly dominate. This tends to fall in the 10 mK to 10 K range, although varies with the parameters of the system. If the temperature of the system is low enough that the degeneracy does not dominate, more brute-force methods may be employed. If, however, the temperature is in a more degeneracy dominated regime, the introduced perturbative expansion may be used for computing the partition function and the Boltzmann averaging, which allows us to generate expressions for the shifts in the systems Helmholtz and average energies due to the coupling between the cavity and spin ensemble. Finally, through this perturbative expansion, we are able to generate optimal algorithms for computing many

expectation values, as well as histograms for these properties–bringing the runtime down from $O(N^3)$ to $\Theta(\sqrt{N})$, both with a $O(T)$ dependence on temperature, for temperature T [1].

While we focus on the partition function, average energy of the system, and the Lamb-shift induced fluctuations of the number operator under the self-evolution of the system, the techniques employed and the results shown can be used for other thermodynamic properties. Having access to both quick numerical methods for computing properties of these systems and perturbative expansions for these properties will allow additional insights into this model, as well as systems with similar structures such as coupled-cavity arrays [68, 69, 70], collective spin ensembles with cavity mediated interactions [71, 72], and multi-connected Jaynes-Cummings models and the extension of this work to the Tavis-Cummings version [73, 74]. The utility of this work for a myriad of physically motivated models with applications to a variety of quantum technologies suggests that this work will help with understanding and designing experiments for collective mesoscopic systems.

3.2 Definitions

We include our notations and definitions in this section. The Pauli operators are written in the Zeeman basis. These spin operators can be combined as a sum of tensor products to produce the collective versions of these spin operators. Let N be the number of spin–1/2 particles. Then the collective spin operators are given by

$$\hat{J}_z = \frac{1}{2}\sum_{i=1}^{N} \hat{\sigma}_z^{(i)}, \quad \hat{J}_\pm = \sum_{i=1}^{N} \hat{\sigma}_\pm^{(i)}. \tag{3.2}$$

where the superscript on the Pauli operator indicates action only on the i-th particle.

The action of these operators on a state of total angular momentum j with z component m are given by:

$$\hat{J}_z \left|j,m\right\rangle = m \left|j,m\right\rangle \tag{3.3}$$

$$\hat{J}_\pm \left|j,m\right\rangle = \sqrt{j(j+1) - m(m\pm 1)} \left|j,m\pm 1\right\rangle . \tag{3.4}$$

We note that our Hamiltonian has two good quantum numbers representing conserved quantities, so long as the system is cool enough that the rotating-wave approximation

[1] In this chapter Θ time means that the expression is upper-bounded and lower-bounded by the argument's time complexity.

continues to hold. The first of these is the total angular momentum, j, which determines the eigenvalues of the total angular momentum operator, $\hat{\boldsymbol{J}}^2 = \hat{J}_x^2 + \hat{J}_y^2 + \hat{J}_z^2$, with eigenvalues $j(j+1)$. The second of these conserved quantities is the number of total excitations, k, given as the eigenvalues of the excitation operator,

$$\hat{K} = \hat{a}^\dagger \hat{a} + \hat{J}_z + \frac{N}{2}\mathbb{1}. \tag{3.5}$$

The scaled identity term in the excitation operator ensures excitations are non–negative, as the action of $\hat{J}_z$ on the ground state has eigenvalue $-N/2$.

We recall next the pertinent aspects and definitions from our prior work. Our Hamiltonian may be written in direct sum form as

$$\hat{\mathcal{H}} \cong \bigoplus_{j,k} \left(\omega_0 k \mathbb{1}_{j,k} + g_0 L(j,k)\right)^{\otimes d_j}, \tag{3.6}$$

where $L(j,k)$ are hollow tridiagonal square matrices with known entries and dimension $|\mathcal{B}_{j,k}| = \min\{2j+1, k-k_0(j)+1\}$, with $k_0(j) = N/2 - j$. The set of eigenvalues for $g_0 L(j,k)$ is written as $\Lambda(j,k)$, which are referred to as the *Lamb shifts* for those values of j and k. Some properties of note for these $L(j,k)$ includes that all odd moments of the eigenvalues are zero, while the second moment has an analytic expression, and has expressions for bounds on the largest eigenvalue [1].

The index j runs from $N/2$ to 0 (1/2) when N is even (odd). Each angular momentum space is of dimension $2j+1$. The degeneracy of the subspace with total angular momentum j on N spins is given as

$$d_j = \frac{N!(2j+1)}{(N/2-j)!(N/2+j+1)!}. \tag{3.7}$$

That is, there are d_j disjoint angular momentum subspaces with total angular momentum j present in a direct sum decomposition of $\left(\mathbb{C}^2\right)^{\otimes N}$ [31].

The eigenvalues for one of these coupling matrices may be computed in $O(|\mathcal{B}_{j,k}| \log |\mathcal{B}_{j,k}|)$. Lastly, the degeneracies have a region of strong support of $O(\sqrt{N})$ about j^*, the most degenerate angular momentum subspace, where $j^* \approx \sqrt{N}/2$. This means that the vast majority of the degeneracies lay within this region. These observations aide in our analysis.

3.3 T domain and $g_0 = 0$ case

In this section we begin by providing the solutions to the uncoupled versions of the partition function and average energy, so that they may be used as references with which we compare

the coupled TC model. Notably, the uncoupled case has an analytic solution and so there are no regimes to worry about, whereas the coupled case requires differing approaches depending on the regime. The movement between these regimes is shown, where one is degeneracy dominated and the other is Boltzmann limited, which provides the foundation for our further results as we focus on the rich degeneracy dominated regime.

3.3.1 $g_0 = 0$, or uncoupled, case

Throughout this chapter, we will compare our results with those which would be expected from an uncoupled cavity-spin ensemble system. The uncoupling can be due to $g_0 = 0$, or having a sufficiently large difference between the coefficients ω_s and ω_c. We take the $g_0 = 0$ case so the expressions more closely match those we will obtain later in this work. In this case the reference Hamiltonian is given by $H_0 = \omega_0(a^\dagger a + J_z + \frac{N}{2}\mathbb{1})$ which has a partition function, as shown in Appendix 3.7.1, given by:

$$Z_0 = (1 - e^{-\beta_c \omega_0})^{-1}(1 + e^{-\beta_s \omega_0})^N, \tag{3.8}$$

where $\beta_c = T_c^{-1}$ is the inverse temperature of the cavity, while $\beta_s = T_s^{-1}$ is the inverse temperature of the spin system, which has an average energy of

$$\langle E \rangle_0 = \omega_0(e^{\beta_c \omega_0} - 1)^{-1} + N\omega_0 \frac{e^{-\beta_s \omega_0}}{1 + e^{-\beta_s \omega_0}}. \tag{3.9}$$

This analytical solution holds regardless of the temperature of each of the uncoupled subsystems and could even permit field inhomogeneities for the spins. These equations themselves are of minimal interest on their own, but can help illuminate the differences in the system upon introducing the coupling Hamiltonian and considering the total Tavis–Cummings model. As no analytical solution like Equation (3.8) is known for the Tavis–Cummings model, in the next subsection we consider the various temperature regimes that can be of interest in the Tavis–Cummings model and specify which regime we focus on in the remainder of this work.

3.3.2 Low T, minimal Dicke

Of all the angular momentum subspaces, quite possibly the easiest one to say much about is the Dicke space, which is the completely symmetric subspace. This subspace has particularly nice eigenstates and has been studied extensively [28, 29]. However, this subspace

is only singularly degenerate, $d_{N/2} = 1$, while for larger N all other angular momentum subspaces have significantly greater degeneracies. Even though the Dicke space contains the unique ground state with $k = 0$ excitations there is a temperature at which the exponential suppression due to the Boltzmann factor is no longer significant compared to the vast multiplicity of other angular momentum subspaces and the Dicke space is left with minimal population. This regime shift temperature is, as we shall argue, a small temperature, meaning that if one is not below this value, it is likely not correct to describe the system as being within the Dicke space. This tends to occur for temperatures between 10 mK and 300 mK for small systems of 10^3 spins, above which the Dicke population is minimal.

As a short, simplified argument for the expression for this regime change temperature we consider the following reduced picture. Let $k \leq 1$ and let the system have N spins. In this case only the first two levels in the Dicke space are populated and the $j = \frac{N}{2} - 1$ angular momentum space's lowest energy state is populated. Figure 3.1 shows this subspace of the full spectrum. The partition function of the Dicke subspace is given by $1 + e^{-\beta(\omega_0 - g_0\sqrt{N})} + e^{-\beta(\omega_0 + g_0\sqrt{N})}$, while that due to $j = \frac{N}{2} - 1$ is $(N-1)e^{-\beta\omega_0}$. Then

$$p(\text{Dicke}) = \frac{1 + e^{-\beta(\omega_0 - g_0\sqrt{N})} + e^{-\beta(\omega_0 + g_0\sqrt{N})}}{1 + e^{-\beta(\omega_0 - g_0\sqrt{N})} + e^{-\beta(\omega_0 + g_0\sqrt{N})} + (N-1)e^{-\beta\omega_0}}. \tag{3.10}$$

This is only close to 1 when $1 + e^{-\beta\omega_0} 2\cosh(\beta g_0\sqrt{N}) > (N-1)e^{-\beta\omega_0}$. Since $g_0\sqrt{N} \ll \omega_0$ due to the rotating-wave approximation, we may approximate this requirement with $e^{\beta\omega_0} > (N-1)$, which provides $T < \omega_0/\log(N-1)$, with log being the natural log function throughout this work. Since N is typically large we will take this as

$$T < \omega_0/\log N. \tag{3.11}$$

If further subspaces are included in the denominator this value can only decrease, however, as we show in Appendix 3.7.2, this asymptotic expression is still correct.

The rest of this paper focuses on the regime where $T > \omega_0/\log N$, but the system is still within the rotating-wave approximation. See Figure 3.2 for a pictorial representation of this regime. In this higher temperature regime rich structure and dynamics are exhibited, which will be explored in detail throughout this work. While the consideration of spin ensembles in the "high temperature approximation" is reminiscent of this result, those results sometimes use simplifications not appropriate for our system. In Slichter, it is assumed that the interactions between the spins is effectively *local*, while here we inherently require the system to be *collective* in its behavior [75].

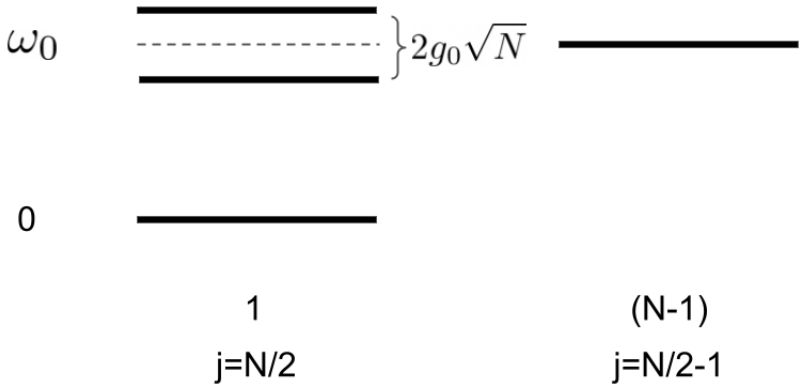

Figure 3.1: This shows the portion of the energy spectrum considered for the regime change argument. The left column is the Dicke subspace, while the second column is the next angular momentum subspace over, while the value above indicates the multiplicity of the degeneracies. The vertical axis indicates the energy of the states.

3.3.3 Higher T, While Still in the Rotating-Wave Approximation

Next, we consider $T > \omega_0/\log N$ and what happens as T is slowly increased. The analytic continuation of the function for the degeneracy of the angular momentum subspaces is a unimodal function with a peak at $j^* = \sqrt{N}/2 - 1/2$ and with the vast majority of the probability mass between 0 and $O(\sqrt{N})$. To gain insights into the behavior of the system as the temperature increases, let us consider the population ratio of adjacent angular momentum subspaces. In particular, for some temperature T we consider the summation over k, resulting in a population ratio of:

$$\frac{p(j)}{p(j+1)} = \frac{d_j(e^{-\beta\omega_0} + 2e^{-2\beta\omega_0} + 3e^{-3\beta\omega_0} + \cdots)}{d_{j+1}(1 + 2e^{-\beta\omega_0} + 3e^{-2\beta\omega_0} + \cdots)} \tag{3.12}$$

$$\approx \frac{d_j e^{-\beta\omega_0}}{d_{j+1}}, \tag{3.13}$$

where for this consideration we use that the Lamb shift splittings are small, $g_0 \max \Lambda(j,k) \ll \omega_0$ so that the rotating-wave approximation holds, and so neglect them here. While one of

	N_c
$T = 10$ mK	$6.96 \cdot 10^{20}$
$T = 100$ mK	121
$T = 300$ mK	4
$T = 1$ K	1

Table 3.1: N_c is the value of N such that $N < e^{\hbar\omega_0/(k_b T)}$, so that mostly the Dicke subspace is populated. The above table uses $\omega_0 = 20\pi$ GHz. It means that for T at and above 1 K the population will not be predominantly in the Dicke space, regardless of the number of spins in the system. When $T = 100$ mK, once the ensemble involves around 120 spins the system is minimally in the Dicke subspace, meaning that for mesoscopic systems population in the Dicke subspace will be minimal.

the above geometric series terminates a term earlier than the other, the size of that term is near zero as xe^{-ax} tends to zero rapidly. More generally the ratio of the populations in angular momentum space j and the Dicke space is given, up to the negligible geometric series terms, by

$$\frac{p(j)}{p(N/2)} = d_j e^{-\beta\omega_0(N/2-j)}, \tag{3.14}$$

which means that this subspace has more population when $d_j e^{-\beta\omega_0(N/2-j)} > 1$, which is when $T > \omega_0(N/2 - j)/\log d_j$. This expression is a monotonic function in j which very slowly increases to a maximal value of $\omega_0/(2\log 2)$, as shown in Appendix 3.7.4. So this regime change temperature in the prior subsection is only a value whereby the population in the Dicke subspace is small, but it is not sufficient to say that further angular momentum subspaces are predominantly populated. Another way to see this is to consider the ratio of the populations in adjacent angular momentum values once again, which provides:

$$\frac{d_j e^{-\beta\omega_0}}{d_{j+1}} > 1 \Rightarrow T > \omega_0/\log(d_{j+1}/d_j). \tag{3.15}$$

The denominator changes sign for $j < j^*$, meaning that there is no temperature where these angular momentum values have a greater probability. However, for $j > j^*$ there will be more population in the smaller angular momentum space once the temperature is sufficiently large, then the width of j^* to $O(\sqrt{N})$ ought to be considered to capture the dominant population. The smallness in the ratio is not sharp though, meaning that a sliding collection of angular momentum values must be considered. This is illustrated in Figure 3.3. Formally the rectangle of what must be considered slides to the left as the

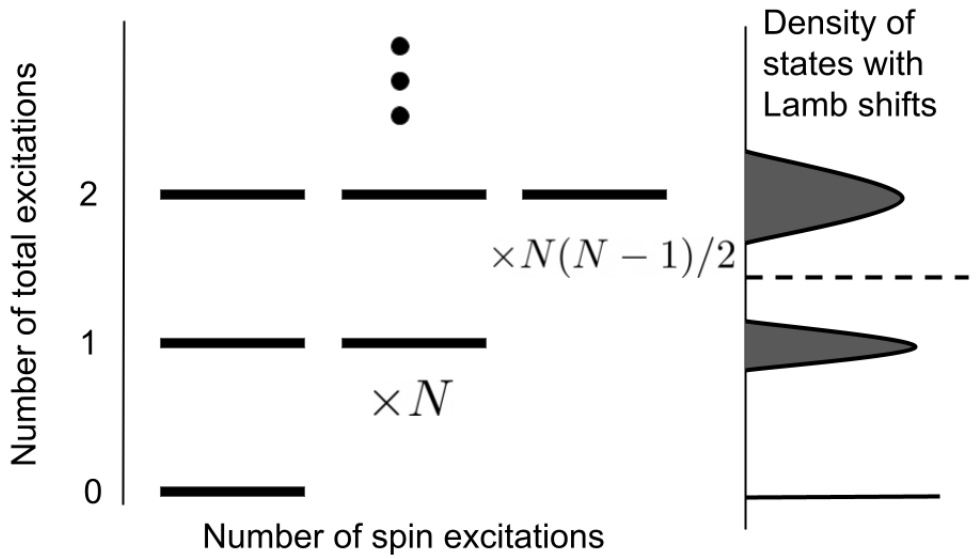

Figure 3.2: This figure shows schematically what the density of states looks like for an ensemble of spins coupled with a cavity. The rotating-wave approximation holds so long as the envelope of states for two different total number of excitations do not overlap.

temperature increases, however, since the region left of j^* is small, the entire thing may be considered without an increase in computational time. Since the ratio is not sufficiently small for most temperatures, we do not know that the subset of angular momentum values which must be considered is asymptotically smaller than N. While on the one hand taking these sums over k would reduce the temperature dependence in the runtime to simulate these systems, the dependency on N is not particularly good, especially once the Lamb shifts are considered. In the next section we consider the impact of including the Lamb shifts on the partition function as well as other expectations.

3.4 Perturbative Expansions and Shifts in Expectations

In the prior section we neglected the effects of the Lamb shifts as they were considered small in comparison to the excitation energy splitting of ω_0. We now include the effects of the Lamb shifts generating a perturbative expansion that can be carried to the desired precision. This provides a more tractable way to describe the system and allows for easier qualitative understanding of it, as well as leading to a faster simulation runtime.

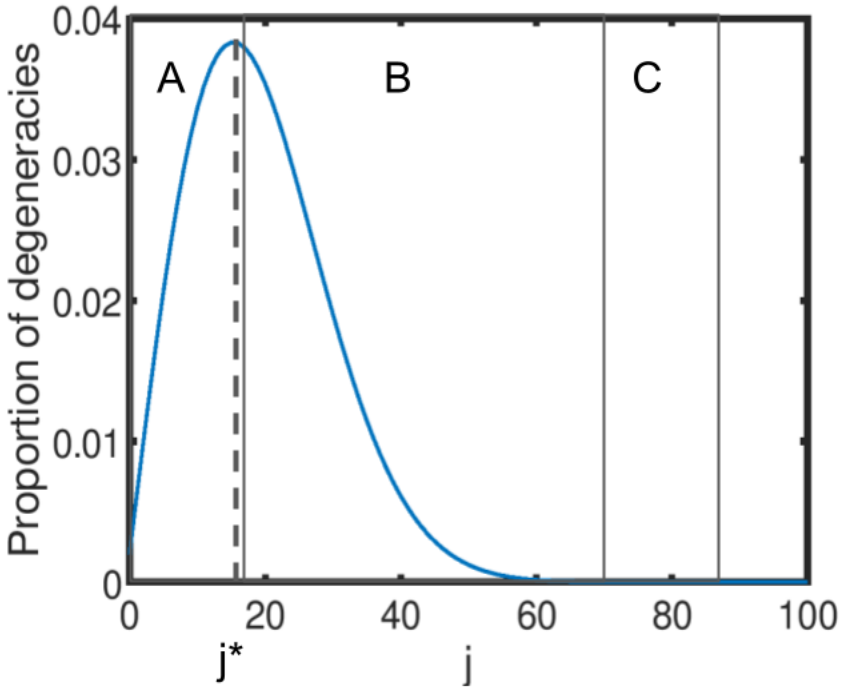

Figure 3.3: For the temperature regime considered, the boxes labelled B and C (right of the j^* line) are the only subspaces with majority population so long as $T < \omega_0/(2\log 2)$. Above this temperature the boxes labelled A and B's angular momentum subspaces must be included. The width is $2\sqrt{N}$ here for both $A+B$ and $B+C$. Plotted for $N = 1000$, zoomed in to the $j \leq 100$ subset.

As the system involves many spins, we take the system as an ensemble, using a density matrix and obeying the canonical Boltzmann distribution for populations. In this statistical mechanics setting, knowing the partition function is of central importance. For the Tavis–Cummings model the partition function is given by:

$$Z_{\text{total}}(\beta) = \sum_{k=0}^{\infty} \sum_{j=j_0(k)}^{N/2} \left(d_j e^{-\beta k \omega_0} \sum_{\lambda \in \Lambda(j,k)} e^{-\beta \lambda g_0} \right), \tag{3.16}$$

where we have defined

$$j_0(k) = \max\left\{N/2 - k,\ N/2 - \lfloor N/2 \rfloor\right\}. \tag{3.17}$$

Upon Taylor expanding and using our results on the parity of eigenvalues we may write $Z_{\text{total}}(\beta) = Z_0(\beta) + Z_{\text{pert}}(\beta)$. In this expression $Z_0(\beta)$ is the partition function of the system with $g_0 = 0$, which is exactly solved in Equation (3.8). $Z_{\text{pert}}(\beta)$ represents the perturbative expansion portion of the total partition function. Throughout the work we will truncate $Z_{\text{pert}}(\beta)$ to only involve the leading term, however, further terms may be included and their structure is discussed in Appendix 3.7.5. In this expansion we have:

$$Z_0(\beta) = \sum_k e^{-\beta k\omega} \sum_j d_j |\mathcal{B}_{j,k}|, \tag{3.18}$$

which is the same as equation (3.8), and

$$Z_{\text{pert}}(\beta) = \frac{(\beta g_0)^2}{2} \sum_k e^{-\beta k\omega} \sum_j d_j |\mathcal{B}_{j,k}| Var(\Lambda(j,k)), \tag{3.19}$$

where we have dropped the higher order terms[2]. While Z_0 corresponds to the case of $g_0 = 0$ it can also be interpreted as the spin ensemble undergoing excitation swaps with the cavity zero times, while Z_{pert} is induced from a double-quantum transition (transferring to the cavity and back, or vice versa) with the next term being a quadruple-quantum transition, and so forth. In effect these perturbative expansion terms provide the correlations induced in the system from the coupling. The strength of these higher order transitions can be neglected compared to the leading perturbative term so long as $\frac{1}{2}(\beta g_0)^2 \text{Var}(\Lambda(j,k)) < 1$ for all j, k with appreciable population, where $\text{Var}(\Lambda(j,k)) = \frac{1}{|\mathcal{B}_{j,k}|} \sum_{\lambda \in \Lambda(j,k)} \lambda^2$ and has an analytic expression [1]. This can be used as a guide for the size of the spin ensemble needed in order to see the effects of the coupling with the cavity, or to know that this perturbative expansion may be truncated as early as it is presented here.

This expansion for the partition function can be used to determine the shifts induced in certain expectations. In principle any expression of the partition function may be computed, but to illustrate the utility, let us consider the shift in the Helmholtz free energy of the system. This is one of the few macroscopic thermodynamic properties that may be computed directly from the quantum model, without specification of other variables. For a closed system at thermal equilibrium we have:

$$\begin{aligned} -\beta\Delta\langle A\rangle &:= -\beta(\langle A\rangle_{Z_{\text{total}}} - \langle A\rangle_{Z_0}) \\ &= \log(Z_0 + Z_{\text{pert}}) - \log Z_0 \\ &= (\log Z_0 + \log(1 + Z_{\text{pert}}/Z_0)) - \log Z_0 \\ &= Z_{\text{pert}}/Z_0 + O((Z_{\text{pert}}/Z_0)^2). \end{aligned} \tag{3.20}$$

[2]By definition, $|\mathcal{B}_{j,k}|\text{Var}(\Lambda(j,k)) = tr(L(j,k)^2)$

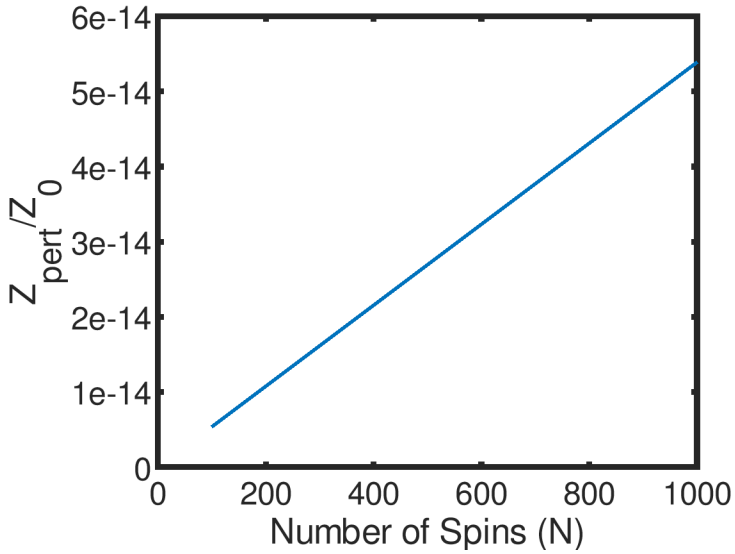

Figure 3.4: Figure of Z_{pert}/Z_0 as a function of N with N in 100 to 1000, $T = 0.3$ K, $g_0 = 200\pi$ Hz, $\omega_0 = 20\pi$ GHz. Equation (3.20) states this is proportional to the first order term in the shift of the Helmholtz free energy due to the coupling: $-\beta\Delta\langle A\rangle$.

As this is a negative value this means that the introduction of the coupling has slightly reduced the amount of free energy in the system, which agrees with intuition as for each excitation a larger portion of the population will reside within the dressed states with the most negative Lamb shift values. A plot of $-\beta\Delta\langle A\rangle$, to first order, is shown in Figure 3.4, numerically computed as a function of N. Over one order of magnitude the ratio is a linear function, so assuming a similar linear trend continues for larger N a system with around 10^{16} spins results in a ratio of $1/100$, leading to an experimentally noticeable shift. For differing temperatures a similar trend occurs, with varying slopes.

Performing a similar analysis, see Appendix 3.7.6, one finds that the average energy shift in the system is given by:

$$\Delta\langle E\rangle := \langle E\rangle_{Z_{\text{total}}} - \langle E\rangle_{Z_0} \tag{3.21}$$

$$\approx (\langle k\rangle_{Z_{\text{pert}}} - \langle k\rangle_{Z_0})\omega_0 - \frac{2}{\beta})\frac{Z_{\text{pert}}}{Z_0}. \tag{3.22}$$

In the above $\langle k\rangle_{Z_{\text{pert}}}$ is the expectation of k over the normalized distribution for $Z_{\text{pert}}(k)$, and $\langle k\rangle_{Z_0}$ is the same but for $Z_0(k)$. This expression for the shift in average energy is also always negative, again matching intuition that having lower-energy dressed states to

populate means that the average energy of the system will be decreased.

While these analytical results are of some interest and use, they are somewhat limited in practical utility. The primary problem is that they still require evaluation of summations to obtain values. In the next section we show that this perturbative expansion may be used to provide a drastic speedup in simulation runtimes of this system.

3.5 Rapid Simulation of Thermal Observables

In the study of mesoscopic systems it is rare to obtain analytical results due to the complexity of such systems. Simulating mesoscopic systems often requires a trade-off between precision and speed, at times using heuristics to bound the accuracy of such methods. Using the tools shown here, we may simulate the Tavis–Cummings model with arbitrarily small error and in optimal runtime dependence on the size of the ensemble. While this work only provides the speedup for the Tavis–Cummings model, a similar methodology might be useful for other systems exhibiting collective behaviors such as a pair of spin ensembles interacting via mean fields.

Before diving into the new results, let us consider the naive approach for computing thermal functions. Assuming one uses the decomposition of the Hamiltonian as a direct sum of spaces labelled by good quantum numbers j and k, this task would require finding the eigenvalues of the terms in the direct sum. These are, up to, $(N+1)\times(N+1)$ matrices, which takes time $O(N^2)$ to solve and there are $O(N)$ of them for each value of k, lastly these eigenvalues must be found for each k of importance, for which there are $O(T)$ of them. Putting these together the total complexity is $O(TN^3)$. A slight improvement can be obtained by using the faster eigenvalue solutions for tridiagonal matrices, but this only reduces the problem to $O(TN^2 \log N)$ generally [56].

To illustrate the result we will consider the computation of the partition function's two components Z_0 and Z_{pert} for some chosen temperature. Z_0 takes $O(1)$ time since it has an analytic expression, so the focus will be on Z_{pert}. To compute Z_{pert} we must perform the sums in:

$$\sum_k e^{-\beta k\omega_0} \sum_j d_j \left[\frac{(\beta g_0)^2}{2} \sum_{\lambda\in\Lambda(j,k)} \lambda^2 + \frac{(\beta g_0)^4}{4!} \sum_{\lambda\in\Lambda(j,k)} \lambda^4 + \dots \right]. \tag{3.23}$$

While one could solve for the eigenvalues λ in the above by finding the roots of the characteristic polynomial for each $L(j,k)$, this can be circumvented by computing traces.

In general the cost of computing the trace is $O(N)$ as the coupling matrices may be as large as $(N/2) \times (N/2)$. If, however, we truncate after the first term, the time to compute $\sum \lambda^2$ is only $O(1)$ since we have an analytic expression for this in terms of j, k, and N. This is a valid approximation so long as $\frac{(\beta g_0)^2}{2} \sum \lambda^2 < 1$. This removes two full powers of N dependence.

Following this, due to the temperature regime that we are in only a small subset of j values contribute much to the summation. From the region of strong support for the degeneracies, we see that $\Theta(\sqrt{N})$ angular momentum values must be considered assuming a selected fractional error δ is permitted, as shown in Appendix 3.7.3. Lastly, the outermost summation is bounded by a geometric series with rate $\beta\omega_0$, so using $O(T)$ terms suffices to capture the majority of the probability density. While $O(T)$ suffices, this bound is of somewhat limited use since T will eventually become large enough that the rotating-wave approximation breaks down for a notable number of populated states. In total, however, this gives a runtime of $O(T\sqrt{N})$. Note that this region of strong support is known to be tightly $\Theta(\sqrt{N})$ meaning that this runtime is *optimal* scaling in the parameter of N. An important caveat to this discussion is that this result only applies for the degeneracy dominated regime, such that $O(\sqrt{N})$ excitations exist in the system, below that it is best to apply brute-force methods due to the comparative smallness of the problem.

If one wished to include any further perturbative terms, the trace must be computed, which at worst will take $\Theta(N)$ time since there are values of j and k with that dimension. The subset of j values that must be considered still remains $\Theta(\sqrt{N})$. This generates a dependency of $\Theta(N^{3/2})$ for including additional terms. If one wished to compute the Lamb shifts themselves, or achieve machine precision, this raises the cost to $O(N^{3/2} \log N)$, which is a modest increase for the additional information gained.

While the above showed the rapidity of computing a scalar, the partition function, our reductions also permit the rapid simulation of some time evolving operators as well. For an observable $\mathcal{O}$ the structure of the summation, with the good quantum numbers j and k, is preserved so long as the operator only depends on j and k, as well as some other parameter that can be summed out. Any function of the cavity and collective spin operators, which includes most observables of interest, satisfy this requirement. While these may be simulated using the same summation, the same rapidity cannot be promised without one more requirement, which is that the operator $\mathcal{O}$ is a subexponential function in j and k–some examples of subexponentially growing functions include J_x, e^{itJ_z}, and $e^{(a^\dagger a^\dagger - aa)it}$. When $\mathcal{O}$ is subexponential the region of strong support in the degeneracies and the geometric series bound on excitations can be applied, otherwise these break down and the full summation must be considered.

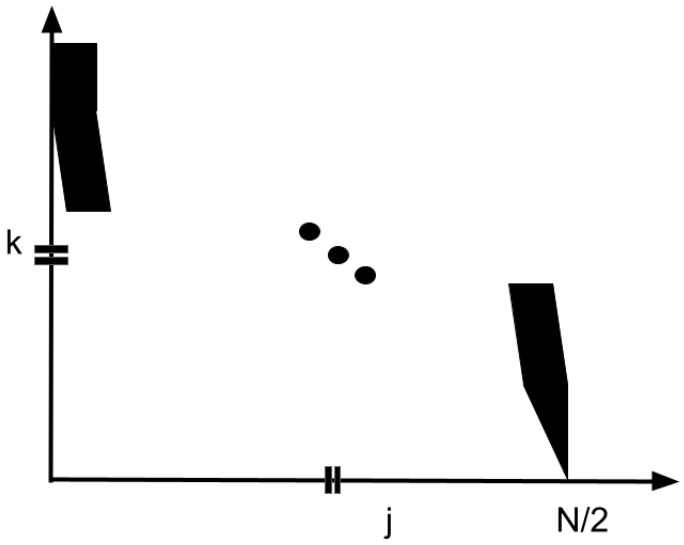

Figure 3.5: Schematic figure showing j values that need summing over for any given k choice. The width of each shape is $\Theta(\sqrt{N})$, aside from the tapered tip of the triangle for which there are insufficiently many angular momentum values available, so all of them are used there.

As a concrete example, we will consider the signal shift for the thermal TC state due to a periodic drive induced by J_x for the observable J_y. Explicitly:

$$\langle J_y e^{it(H_0+H_{\text{int}}+\Omega\cos(\omega_0 t)J_x)}\rho_{\text{thermal}}e^{-it(H_0+H_{\text{int}}+\Omega\cos(\omega_0 t)J_x)}\rangle. \tag{3.24}$$

We find after reductions, as shown in the Appendix 3.7.10, that this reduces to:

$$\sin(\Omega t)\text{tr}(J_z\rho_{\text{thermal}}), \tag{3.25}$$

so the induced shift is, to first order, $\sin(\Omega t)\text{tr}(J_z\rho_{\text{pert}})$. The summations for this are shown in Appendix 3.7.10, whereas Figure 3.6 shows how the shift grows as a function of N and Figure 3.7 shows the periodic behavior.

Naturally, if one wanted to generate a histogram of the populations as a function of k or j the respective summation can be suspended and instead used to generate the points. This is used to show the populations of the terms in the partition function for various temperatures in Figure 3.10. In this figure we see that the population's center drastically shifts as we move into the degeneracy dominated regime ($T = 0.3K$), additionally the width of the distribution increases, as expected.

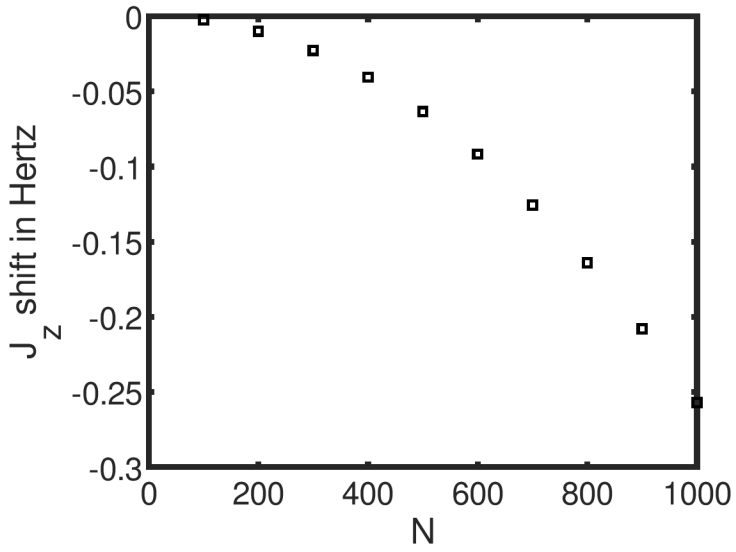

Figure 3.6: The shift in the value of $\mathrm{tr}(\omega_0 J_z \rho_{\mathrm{th}})$ due to the Lamb shifts. The negative sign indicates the availability of lower spin values, weighing the mean down. This is plotted for $T = 0.3$ K, $g_0 = 200\pi$ Hz, $\omega_0 = 20\pi$ GHz, and for N as 100 to 1000. Statistical analysis: $r^2 = 0.9488$, with slope $= 20\pi \cdot 10^9 \cdot -4.502 \cdot 10^{-15}$, intercept $= 20\pi \cdot 10^9 \cdot 9.08 \cdot 10^{-13}$. There seems to be a pretty strong deviation from a straight line, however, so these might not be a good case to extrapolate behavior for high N but provides some experimental signal of sorts.

As one final pair of examples, we can find expressions for the expectations and variances of the uncoupled system and the coupled system in the number operator. Taking the difference of the values for $a^\dagger a$ and $Var(a^\dagger a)$ and dividing by the uncoupled system value, we obtain the following pair of plots, both of which are linear. In effect, these plot the change in the number of photons in the cavity due strictly to the Lamb shifts, and likewise for the variance in the number of photons in the cavity.

A summary of the results are presented in the table below:

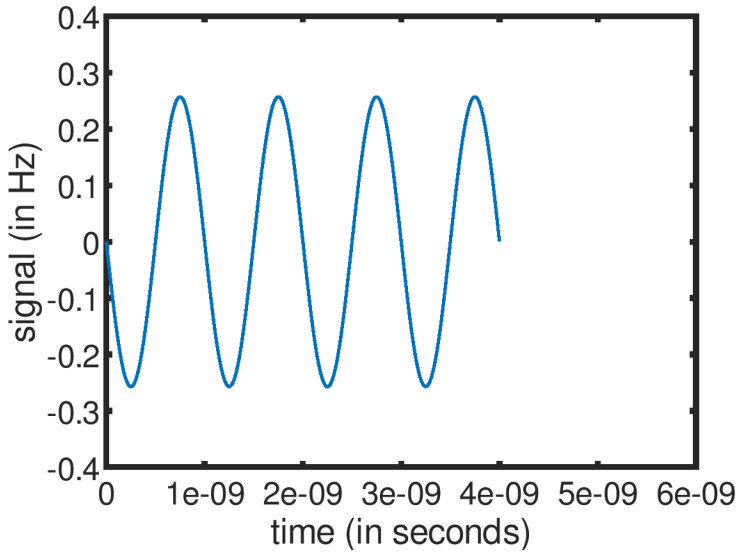

Figure 3.7: The signal of $\omega_0 J_y$ after time t in the rotating-frame of J_z for the driven Hamiltonian $H + \Omega J_x$ with $\Omega = 2\pi$ GHz. This is plotted for $T = 0.3$ K, $g_0 = 200\pi$ Hz, $\omega_0 = 20\pi$ GHz, and $N = 1000$. As stated in Equation (3.119), this is a simple sine times the shift from the prior figure.

3.6 Conclusion

Understanding further details about the interactions between ensembles of spins and cavities enables better control of such systems as well as possibly providing additional observables. These hybrid quantum devices could be used as processors, among other uses. In this work we focused on the Tavis–Cummings model and the thermal properties of this model. In the case of this model we found that the system goes through a smooth transition from having predominantly angular momentum ground states populated to having the population spread out over a collection of $\Theta(\sqrt{N})$ spins, the so-called degeneracy dominated regime. This informs a perturbative expansion for the partition function and general thermal averages in this model. From this expansion, we are able to obtain optimal simulation runtimes at least for many choices of observables.

The body of this work has focused on the case of perfect on-resonance between the cavity and spins, as well as a perfectly homogeneous field. In order to improve the utility of these results the effects of such perfections removal should be analyzed and it should be determined whether current technology inhomogeneities are sufficiently small for the effects

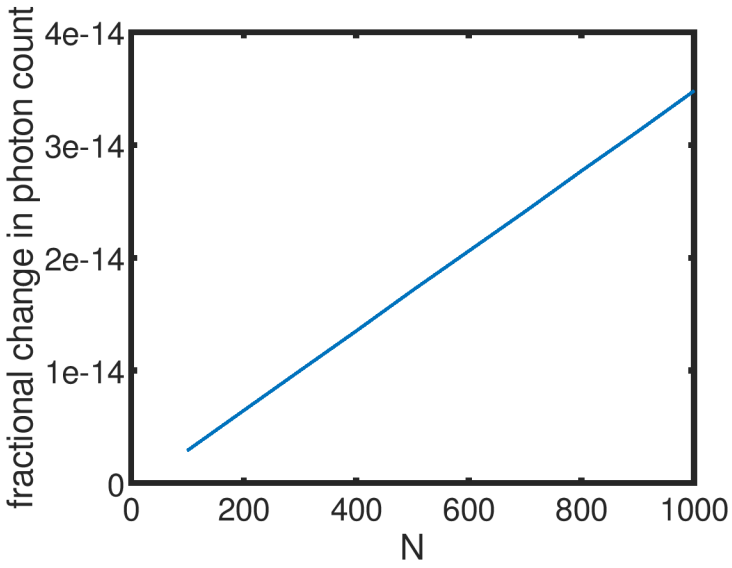

Figure 3.8: The fractional change in the mean number of photons in the cavity as a function of N. This is plotted for $T = 0.3$ K, $g_0 = 200\pi$ Hz, $\omega_0 = 20\pi$ GHz, and $N = 100$ to 1000. This is a linear trend ($r^2 = 1$) with slope $3.54 \cdot 10^{-17}$ and intercept $-6.49 \cdot 10^{-16}$. Once $N \approx 10^{15}$ this fraction would be appreciable.

of these ensemble Lamb shifts to be observed. Considerations of these inhomogeneities are discussed in Appendix 3.7.8, and provide a benchmark with which experimental setups may be compared, as well as when the strength of these perturbations no longer allow our reductions without significant loss of accuracy.

Of note, the complexity of this quantum system has been determined, even in the presence of slight perturbations. This means that within the complexity of quantum systems community and experimental realizations of early-term quantum devices, the Tavis–Cummings model, as considered here, is not sufficiently complex of a system. Either larger perturbations or dipolar couplings should be considered in order to generate a truly "hard" problem for a classical computer to solve.

Lastly these results must be translated fully into an experiment and a prediction for the experimental signal. Figures 3.6, 3.7, 3.11, and 3.12 provide clear expected experimental results which can provide insights into the exact regimes experimentally considered as well as how well this theory matches experiments. This will hopefully inform the parameters in the experiment and permit the resolution of this collective effect and the associated Lamb shifts, as well as better understanding of spin ensemble systems in this regime.

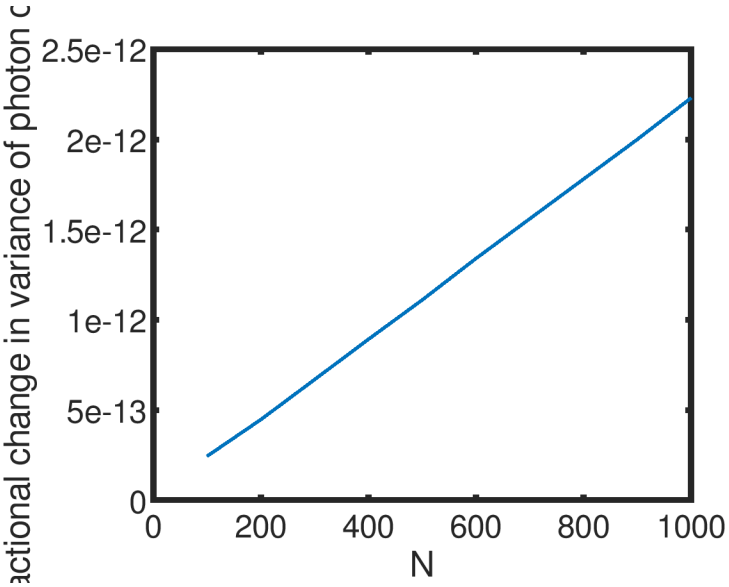

Figure 3.9: The fractional change in the variance of the number of photons in the cavity as a function of N. This is plotted for $T = 0.3$ K, $g_0 = 200\pi$ Hz, $\omega_0 = 20\pi$ GHz, and $N = 100$ to 1000. This is a linear trend ($r^2 = 1$) with slope $2.21 \cdot 10^{-15}$ and intercept $9.4 \cdot 10^{-15}$. Once $N \approx 10^{13}$ this fraction would be appreciable.

3.7 Mathematical Arguments

3.7.1 Computation of $g_0 = 0$ Thermalization Case

Here we show the steps involved in computing the non-interacting partition function and average energy for a spin ensemble and cavity. This involves solving the problem for a cavity and a collection of N collective spins.

For a cavity, the thermal state is given by:

$$\rho_{\text{th}}^{\text{cavity}} = (1 - e^{-\beta\omega_0}) \sum_{k=0}^{\infty} e^{-\beta\omega_0 k} |k\rangle\langle k| \tag{3.26}$$

The partition function for the cavity can then be given by:

$$Z_c = (1 - e^{-\beta\omega_0})^{-1} \tag{3.27}$$

Error	$O(g_0^4)$	$O(g_0^{2c}),\ c>2$	Machine Precision	Naive
Z_{pert}, Z_{tot}, $\Delta\langle A\rangle$, $\Delta\langle E\rangle$	$\Theta(\sqrt{N})$	$\Theta(N^{3/2})$	$O(N^{3/2}\log N)$	$O(N^3)$
$\mathcal{O}(j,k)$ (no ROSS promise)	$O(N)$	$O(N^2)$	$O(N^2\log N)$	$O(N^3)$
$\mathcal{O}(j,k)$ (ROSS promised)	$\Theta(\sqrt{N})$	$\Theta(N^{3/2})$	$O(N^{3/2}\log N)$	$O(N^3)$

Table 3.2: The above table lists the different run times needed for a chosen level of precision, as a function of g_0. The quickest, nontrivial level of precision is markedly faster. For comparison, the time needed in the naive approach is listed. In order to utilize the region of strong support, the observable $\mathcal{O}$ must be a subexponential function in j and k. Note: ROSS stands for region of strong support.

The average energy for a thermalized cavity is then given by:

$$\begin{aligned}
\langle E\rangle_c &= (1-e^{-\beta\omega_0})\sum_{k=0}^{\infty} k\omega_0 e^{-\beta\omega_0 k} && (3.28)\\
&= (1-e^{-\beta\omega_0})\sum_{k=0}^{\infty} -\frac{\partial}{\partial\beta}e^{-\beta\omega_0 k} && (3.29)\\
&= -(1-e^{-\beta\omega_0})\frac{\partial}{\partial\beta}\sum_{k=0}^{\infty} e^{-\beta\omega_0 k} && (3.30)\\
&= \omega_0 e^{\beta\omega_0}(1-e^{-\beta\omega_0})(1-e^{\beta\omega_0})^{-2} && (3.31)\\
&= \omega_0(e^{\beta\omega_0}-1)^{-1} && (3.32)
\end{aligned}$$

For a collection of N uniformly interacting spins the Hamiltonian is given by $\omega_0(J_z+\frac{N}{2}\mathbb{1})$. Note that the eigenstates of this are equivalent to those of $\otimes_{i=1}^N\sigma_z^{(i)}$. As such, we have:

$$\hat{\rho}_{\text{th}}^{\text{spins}} = \otimes_{i=1}^N \frac{e^{-\beta\omega_0}|\uparrow\rangle\langle\uparrow| + |\downarrow\rangle\langle\downarrow|}{1+e^{-\beta\omega_0}} \tag{3.33}$$

The partition function for this portion can be given by:

$$Z_s = (1+e^{-\beta\omega_0})^N \tag{3.34}$$

The average energy is then given by:

$$\langle E\rangle_s = N\omega_0\frac{e^{-\beta\omega_0}}{1+e^{-\beta\omega_0}}. \tag{3.35}$$

The total energy when $g_0 = 0$ is then given by:

$$\langle E\rangle_0 = \langle k\rangle_{Z_0}\omega_0 \tag{3.36}$$

$$= \omega_0(e^{\beta\omega_0} - 1)^{-1} + N\omega_0\frac{e^{-\beta\omega_0}}{1 + e^{-\beta\omega_0}} \tag{3.37}$$

3.7.2 Cutoff Temperature Argument

In this appendix we show that for temperatures above $\omega_0/\log N$, the population within the Dicke subspace is minimal, as well as the population in the low-excitation manifolds being minimal. These will combine into our argument for the number of angular momentum subspaces that must be considered for a given temperature in order to capture the majority of the population in the system.

For our analysis we neglect the Lamb shifts, and at the end argue why they do not change the results, except in high order. To begin with, consider the partial partition function $\tilde{Z}$ composed of only considering the contributions to the partition function of the two angular momentum subspaces with the largest value ($j = N/2$ and $j = N/2-1$). This partial partition function is given by:

$$\tilde{Z} = (1 + 2e^{-\beta\omega_0} + 3e^{-2\beta\omega_0} + \cdots) + N(e^{-\beta\omega_0} + 2e^{-2\beta\omega_0} + 3e^{-3\beta\omega_0} + \cdots) \tag{3.38}$$

$$= \sum_{j=0}^{"\infty"}(j+1)e^{-j\beta\omega_0} + N\sum_{j=0}^{"\infty"} je^{-j\beta\omega_0}, \tag{3.39}$$

where "∞" signifies that these sums are not truly taken to infinity, but rather to $N+1$ and N respectively, then the remaining terms are $N+1$ times the exponential factor and N times the exponential factor, however, since N is large we take it as ∞ for these weighted geometric sums. Note that $\tilde{Z} < Z_0 < Z_{total}$, and so we may bound the probability of being in the $N/2$ subspace by:

$$p(\text{Dicke}) < \frac{\sum_{j=0}^{"\infty"}(j+1)e^{-j\beta\omega_0}}{\tilde{Z}}. \tag{3.40}$$

This will be negligible when $p(\text{Dicke}) \ll 1$, which occurs when the second term in $\tilde{Z}$ dominates. This is promised when:

$$\sum_{j=0}^{"\infty"} e^{-j\beta\omega_0}[(j+1) - Ne^{-\beta\omega_0}j] < 0. \tag{3.41}$$

This can be guaranteed if $Ne^{-\beta\omega_0} > 1 + 1/j$ for all j, which provides $T_c = \omega_0/\log N$. This means that for $T > T_c$ the population in the Dicke subspace must be negligible. As discussed in the main text, while in the rotating-wave approximation regime, the Lamb shifts are small enough to not alter the asymptotic behavior in these expressions, as $g_0 \max \lambda \ll \omega_0$ is required.

Consider the case where the system is cold enough that the maximum number of excitations appreciably excited in the system is given by some $k_{max} \ll N$. With this condition, we can approximate the binomial term in the degeneracy function using the following expression [76]:

$$\binom{N}{k} = (1 + o(1))\frac{N^k}{k!}. \tag{3.42}$$

Motivated by our restriction of the number of excitations to be small and bounded, we consider the degeneracy of the angular momentum ground state with k excitations. Given N spins, the ground state of the subspace with angular momentum j has $k = N/2 - j$ spin excitations.

Then, the degeneracy of the ground state with k excitations is given by

$$d_g(k) = \frac{N - (2k-1)}{N - (k-1)}\binom{N}{N-k}. \tag{3.43}$$

Rearranging this term and utilizing the approximation of the binomial coefficient, we find that

$$d_g(k) = \frac{1}{1 - \frac{k}{N-(2k-1)}}\frac{N^k}{k!}(1 + o(1)). \tag{3.44}$$

Since $k \ll N$, we can safely approximate the degeneracy of the ground state with k excitations as $d_g(k) \approx N^k/k!$.

The dimension of the ground state subspace is 1, and has a zero energy splitting. This implies that the ground state contributions to the partition function are given by,

$$\begin{aligned} Z_g(\beta) &= \sum_{k=0}^{k_{\max}} e^{-\beta k\omega_0}\frac{N^k}{k!} \\ &= \sum_{k=0}^{k_{\max}} \frac{1}{k!}(e^{-\beta\omega_0}e^{\log N})^k \qquad (3.45) \\ &\approx e^{e^{\log N - \beta\omega_0}} \qquad (3.46) \end{aligned}$$

Then the population in these states is given by:

$$\frac{e^{e^{\log N - \beta\omega_0}}}{(1-e^{-\beta\omega_0})^{-1}(e^{-\beta\omega_0/2}+e^{\beta\omega_0/2})^N}, \tag{3.47}$$

which is minimal for $T > T_c$.

Given these properties for temperatures above $\omega_0/\log N$, we then define the *ground state cutoff temperature* to be

$$T_c = \frac{\hbar\omega_0}{k_b \log N}. \tag{3.48}$$

Above this temperature the population in the Dicke subspace and in the lowest energy states will be minimal, so the more full structure of the system must be considered.

3.7.3 Algorithmic scaling

Theorem 2. *For an arbitrary constant error, δ, the runtime to compute a parameter which is a function of j and k, and subexponential in j, is $\Theta(\sqrt{N})$.*

To prove the dependence on N, we begin by noting that d_j has a unique maximum at j^*, about which the ratio of adjacent terms is $1 + O(N^{-3/2})$ [1]. Generally the ratio between two adjacent angular momentum subspaces is given by:

$$\frac{d_j}{d_{j+1}} = \frac{2j+1}{2j+3} \cdot \frac{N/2+j+2}{N/2-j}. \tag{3.49}$$

Differentiating this, we see that there are no valid j values that extremize this expression, and it begins with a ratio of N for $j = N/2 - 1$ and tends to $\frac{1}{3}$ for $j = 0$. Therefore, this ratio is monotonic, and bijective, over the domain of possible j values, having a ratio between $1/3$ and $N - 1$.

Next we will need the following lemma, a well-known result of geometric series:

Lemma 3. *The number of terms that must be summed such that the geometric series with ratio $(1+\epsilon)^{-1}$ has a fractional error of δ is given by $O(\log(\delta^{-1})\epsilon^{-1})$, for $\delta \ll 1$ and $\epsilon \ll 1$.*

Proof. We begin by noting that:

$$\sum_{i=0}^{\infty}(1+\epsilon)^{-i} = \frac{1}{1-\frac{1}{1+\epsilon}} = 1+\epsilon^{-1}. \tag{3.50}$$

So we wish to find t such that:

$$\sum_{i=0}^{t}(1+\epsilon)^{-i} \geq (1-\delta)(1+\epsilon^{-1}) \tag{3.51}$$

Note that this sum is equivalent to:

$$\sum_{i=0}^{t}2^{-i\log(1+\epsilon)} \geq (1-\delta)(1+\epsilon^{-1}) \tag{3.52}$$

Then this is given by:

$$\begin{aligned} t &= O(\log_{(1+\epsilon)^{-1}}(\delta)) && (3.53)\\ &= O(-\log(\delta)/\log(1+\epsilon)) && (3.54)\\ &\approx O(\log(\delta^{-1})/\epsilon) && (3.55) \end{aligned}$$

■

Corollary 4. *For a series of real numbers where the terms monotonically decrease by at least a constant ratio, $1+\epsilon$, the number of terms needed to approximate their sum to relative error δ is $O(\log(\delta^{-1})/\epsilon)$.*

Proof. This is the same as the above, except now we allow the ratio to possibly become more severe than $1+\epsilon$, as our summations will have. ■

Proof of Theorem 2. Fix k. Then the set of possible j values falls in the range $[\max\{j_{min}, \frac{N}{2}-k\}, \frac{N}{2}]$. The ratio of populations between angular momentum subspace j and $j+1$, with j in the range aforementioned, is then given by:

$$r = \frac{d_j}{d_{j+1}}\frac{\mu}{\mu+1}, \tag{3.56}$$

where μ is the number of states available for subspace j (if j is not the smallest value permitted for a given k choice, one could have say the lower 3 levels for j and the lower 4 for $j+1$).

Generally $\frac{d_j}{d_{j+1}} \in (1/3, N-1]$, but suppose we restrict ourselves to j such that $\frac{d_j}{d_{j+1}} \in (1+N^{-1/2}, N-1]$, which occurs for $j = \Theta(j^*) = \Theta(\sqrt{N})$. Now, we wish for $r = 1+\Omega(N^{-1/2})$

to be satisfied. Note that $\mu/(\mu+1)$ begins at $\frac{1}{2}$ and tends to 1, so if we can ensure $\mu/(\mu+1) = 1 - O(N^{-1/2})$ then r will satisfy our desired value. Once $\mu \approx \sqrt{N}$, then:

$$\begin{aligned} \frac{\mu}{\mu+1} &= \frac{\sqrt{N}}{\sqrt{N}+1} && (3.57) \\ &= \frac{1}{1+N^{-1/2}} && (3.58) \\ &\approx 1 - N^{-1/2} && (3.59) \end{aligned}$$

Putting this together, it means that to obtain the sum for some fixed k value, assuming $d_j/d_{j+1} = 1 + N^{-1/2}$, we sum from $\max\{j_{min}, \frac{N}{2} - k\}$ for $O(\sqrt{N})$ terms, then for another $O(\sqrt{N})$ terms whereby these terms converge to within a δ error within $O(\sqrt{N})$ terms from the prior lemma and corollary. Lastly, note that $d_j/d_{j+1} = 1 + N^{-1/2}$ for $j = O(\sqrt{N})$ so when the ratio is below this, there will be at most $O(\sqrt{N})$ more j values to sum. Putting these together, we obtain a δ error, for any constant δ, with only $O(\sqrt{N})$ terms summed.

Lastly, for the matching lower-bound, we can use the result from our prior work, [1], where we showed that $\Omega(\sqrt{N})$ angular momentum values contain the far majority of the degeneracies in the system. This provides a lower-bound for higher excitations whereby most of the degeneracies are available. Together this means that this procedure is effectively optimal in the spin system size, N, with a runtime of $\Theta(\sqrt{N})$. ■

3.7.4 Monotonicity of Population Ratio Temperature

Here we show that the temperature needed to have more population in a low j value than the Dicke value slowly rises to a limiting temperature requirement of $\omega_0/(2\log 2)$. Note that for small j, the following approximation may be made:

$$\begin{aligned} d_j &= \binom{N}{N/2+j} \cdot \frac{2j+1}{N/2+j+1} && (3.60) \\ &\approx \frac{2^N}{\sqrt{N\pi/2}} e^{-(2j)^2/(2N)} \cdot \frac{2j+1}{N/2+j+1} && (3.61) \end{aligned}$$

where the approximation is from [66]. This is to leading order given by 2^N and so:

$$\lim_{N\to\infty} \frac{\omega_0(N/2-j)}{\log d_j} = \frac{\omega_0}{2\log 2}. \quad (3.62)$$

Lastly the expression $\omega_0(N/2-j)/\log d_j$ has a unique root, the above, and is always positive up to j^*. After this temperature the other angular momentum subspaces are populated according to the main text.

3.7.5 Thermal Expectation Expansions

Here we show the error in truncating the expansion for the partition function. The partition function can be used to compute averages directly related to the partition function and also by taking the expectation of the partition function we can compute other averages.

The exact expression for the partition function for our system of interest is given by:

$$Z = \sum_{j,k,\ \lambda\in\Lambda(j,k)} d_j e^{-\beta(k\omega_0 \mathbb{1} + g_0 L(j,k))} \tag{3.63}$$

$$= \sum_k e^{-\beta k\omega_0 \mathbb{1}} \sum_j d_j \sum_{\lambda\in\Lambda(j,k)} e^{-\beta g_0 \lambda}. \tag{3.64}$$

We focus on truncating the inner sum. We set the inner summation as $\tau(j,k,\beta)$. Then Z is:

$$Z = \sum_k e^{-\beta k\omega_0} \tau(j,k,\beta). \tag{3.65}$$

We may then expand τ in a power series. This will allow us to find the bounded error in a truncated expansion. Before beginning, we note that we may assume we have $\|\Lambda(j,k)\|_\infty \ll \omega_0/g_0$, as in this regime the rotating-wave approximation holds, which is needed to have the pair of good quantum numbers utilized in the Tavis–Cummings Hamiltonian.

We begin with an expansion of the innermost sum in τ:

$$\sum_{\lambda\in\Lambda(j,k)} e^{-\beta g_0\lambda} \approx \sum_\lambda 1 - \beta g_0 \sum_\lambda \lambda + \frac{(\beta g_0)^2}{2}\sum_\lambda \lambda^2 - \frac{(\beta g_0)^3}{3!}\sum_\lambda \lambda^3 + \frac{(\beta g_0)^4}{4!}\sum_\lambda \lambda^4 + \dots \tag{3.66}$$

As we showed in our prior work all odd moments of the eigenvalues are zero since eigenvalues come in positive-negative pairs [1]. The number of eigenvalues is $|\mathcal{B}_{j,k}|$, so this expansion is then given by:

$$|\mathcal{B}_{j,k}|(1 + \frac{(\beta g_0)^2}{2}\mathrm{Var}(\Lambda(j,k))) + O((\beta g_0)^4 \sum_\lambda \lambda^4) \tag{3.67}$$

This expansion says that the partition function can be considered as a summation over the states of the uncoupled system plus contributions from second order transitions from the coupling Hamiltonian, and the fourth order, and so forth. We wish for this to truncate, so let's consider what temperatures we can promise the higher order terms to be negligible. Note that $(\frac{1}{2}(\beta g_0)^2 \sum \lambda^2)^2 > \frac{1}{4}(\beta g_0)^4 \sum \lambda^4$, and generally $(\frac{1}{2}(\beta g_0)^2 \sum \lambda^2)^t >$

$\frac{1}{2^t}(\beta g_0)^{2t}\sum\lambda^{2t}$, and so if $\frac{1}{2}(\beta g_0)^2\sum\lambda^2 < 1$ then the higher order terms are all smaller and can be neglected if sufficiently small. This means that the first order correction is dominant so long as $|\mathcal{B}_{j,k}|\frac{(\beta g_0)^2}{2}Var(\Lambda(j,k)) \ll 1$.

Assuming we satisfy this condition we have:

$$\tau(j,k,\beta) \approx \sum_j d_j|\mathcal{B}_{j,k}|(1+\frac{(\beta g_0)^2}{2}\mathrm{Var}(\Lambda(j,k))). \tag{3.68}$$

Including this back in the summation over k, we have:

$$Z_{\text{total}} = Z_0 + Z_{\text{pert}} \tag{3.69}$$

where Z_0 is the partition function when $g_0 = 0$ (just a collection of spins uncoupled with a cavity), and Z_{pert} is the contribution due to the interaction between the cavity and spins.

This also means that the normalization factor, Z^{-1}, can be expanded as:

$$\frac{1}{Z_{\text{total}}} = \frac{1}{Z_0 + Z_{\text{pert}}} \tag{3.70}$$

$$\approx \frac{1}{Z_0}(1-\frac{Z_{\text{pert}}}{Z_0}), \tag{3.71}$$

where the last expression comes from utilizing a truncated geometric series expansion.

3.7.6 Average Internal Energy Shift

We may now compute the average energy of this system, as well as the associated shift induced due to the coupling:

$$\langle E\rangle = -\frac{1}{Z}\frac{\partial}{\partial\beta}Z. \tag{3.72}$$

Applying this to our expression for Z_{total} in (3.65) and applying the chain rule for differentiating, then using the first order correction given by (3.68) we obtain:

$$= \langle k\rangle_Z\omega_0 - \frac{2}{\beta}\frac{Z_{\text{pert}}}{Z}. \tag{3.73}$$

We may now break this into perturbation powers to obtain a more physically meaningful expression. For each line we plug in our expansions and drop higher order terms:

$$= \langle k\rangle_{Z_0} Z_0\omega_0(\frac{1}{Z_0}(1-\frac{Z_{\text{pert}}}{Z_0})) + [Z_{\text{pert}}\langle k\rangle_{Z_{\text{pert}}}\omega_0 - \frac{2}{\beta}Z_{\text{pert}}](\frac{1}{Z_0}(1-\frac{Z_{\text{pert}}}{Z_0})) \quad (3.74)$$

$$= \langle k\rangle_{Z_0}\omega_0(1-\frac{Z_{\text{pert}}}{Z_0}) + \langle k\rangle_{Z_{\text{pert}}}\frac{Z_{\text{pert}}}{Z_0}\omega_0 - \frac{2}{\beta}\frac{Z_{\text{pert}}}{Z_0} \quad (3.75)$$

$$= \langle k\rangle_{Z_0}\omega_0 + ((\langle k\rangle_{Z_{\text{pert}}} - \langle k\rangle_{Z_0})\omega_0 - \frac{2}{\beta})\frac{Z_{\text{pert}}}{Z_0} \quad (3.76)$$

This means that the shift in the average internal energy is given by $\Delta\langle E\rangle = ((\langle k\rangle_{Z_{\text{pert}}} - \langle k\rangle_{Z_0})\omega_0 - \frac{2}{\beta})\frac{Z_{\text{pert}}}{Z_0}$. This expression can be considered as the average excitation difference between the perturbed portion of the system and the uncoupled system, $(\langle k\rangle_{Z_{\text{pert}}} - \langle k\rangle_{Z_0})$, with the addition of a thermally scaling factor of the perturbation expansion variable $-\frac{2}{\beta}\frac{Z_{\text{pert}}}{Z_0}$, and will always be negative, so long as the expansions are valid. This agrees with intuition as having the lower-energy Lamb shifted energy states to place some population into can only decrease the average energy of the system.

3.7.7 Rapid Computation of Expectations with Certain Invariances

Here we outline the analytical results implications for bounding expectations of observables of thermal states of the Tavis–Cummings model as well as the runtime improvements for numerical methods evaluating these expectations. For this we focus on observables with particular invariances, and list them as cases. For each case, $\sum$ means that the variable(s) must be summed over, whereas $\int$ means that that variable is either invariant with respect to that variable or can analytically have its dependence removed. In what follows k is the number of excitations, j is the angular momentum subspace value, and m is the spin value within that angular momentum subspace value.

(a) $\sum j, k, m$: in this case $\mathcal{O}(k, j, m)$ depends on all three parameters. In this case the full summation must be considered which makes the problem nearly intractable and has runtime of $O(TN^2)$. If one can ensure that the region of strong support is satisfied, then this can be reduced to $O(TN)$.

(b) $\sum k, j \int m$: $\mathcal{O}(j, k)$ is the observable. The probabilities are only functions of j and k in this case so $\text{Var}(\Lambda(j, k))$ may be used in the expectation computation. Additionally, so long as $\mathcal{O}(j, k)$ is sub-exponential in j we may use the region of strong

support within the degeneracies to simplify the expression and improve the runtime of computing this expectation. This results in $O(T\sqrt{N})$ time.

(c) $\sum k, \int j, m$: in this case the observable only depends on the number of excitations $\mathcal{O}(k)$. Since the dependency on j is removed and can be tabulated, this loses all dependency on N and requires only $O(T)$ time.

(d) $\sum j, \int k, m$: this follows similar reasoning as the above. The temperature dependence can be removed and summed over independently, meaning just the spin states matter, taking $O(N)$ unless the region of strong support can be provided, in which case this reduces to $O(\sqrt{N})$.

For observables such as J_z the pair of quantum numbers remain valid and so the trace value is basis independent so we just take the summation over $|k, j, m\rangle$. Some examples of these categories include: $a^\dagger a$ and $a + a^\dagger$ in (c) and J_z and J_x in (b). In fact, any function of cavity operators (a and $a^\dagger$) and collective spin operators (J_+, J_-, and J_z) is covered in case (b), with any function that grows subexponentially in j also being able to exploit the region of strong support. Some examples of subexponentially growing functions include J_x, e^{itJ_z}, and $e^{(a^\dagger a^\dagger - aa)it}$.

3.7.8 Perturbations and Inhomogeneities

The following theorem is used, it is a direct consequence from the Bauer-Fike Theorem and Weyl's inequality [77, 78]:

Theorem 5. *Let H and $H + \delta H$ be Hermitian matrices with eigenvalues $\{\lambda_1, \lambda_2, \ldots\}$ and $\{\mu_1, \mu_2, \ldots\}$, respectively, in non-increasing order. Then for all eigenvalues, with index i, we have:*

$$|\lambda_i - \mu_i| \leq \|\delta H\|_2. \tag{3.77}$$

This result naturally extends to the case of block preserving perturbations. The summation structure for our Hamiltonian remains the same so long as $\|\delta H\|_2 \ll \omega_0$. The perturbation expansion needs the variance updated with $tr((H + \delta H)^2) - tr(H + \delta H)^2$, which slightly increases the value, but if small enough perturbations, the net change is effectively nothing.

It is worth noting that formally H, and δH, act on Hilbert spaces with countably infinite bases, so without the thermal effects the norm may not converge. If one requires block

preserving perturbations, then the level of perturbation needs only be bounded by ω_0 within each block, and so the infiniteness of the Hilbert space is circumvented. Some examples of block preserving perturbations include those which preserve the angular momentum and total excitation quantum numbers, which would include most forms of field and coupling inhomogeneities, but would not include dipolar interactions or individual spin orientation perturbations.

Formally these operators are semi-bounded Hermitian operator on a countably infinite space and the results are rigorous so long as $\|\delta H\|_2$ is bounded [79]. Fortunately, the Hilbert spaces of H and $H + \delta H$ are effectively truncated at large k since the rotating-wave approximation breaks down, which results in the loss of the good quantum numbers and the lack of validity for the direct sum decomposition.

As an explicit example, let us consider dipolar flip-flop coupling between pairs of spins:

$$\delta H_{ff} = d_{ij}(\sigma_+^{(i)}\sigma_-^{(j)} + \sigma_-^{(i)}\sigma_+^{(j)}), \quad i \neq j. \tag{3.78}$$

Note that this is independent of the number of excitations in the cavity so the Hilbert space can be taken as a direct sum over the number of excitations in the cavity, meanning that we only require $\|\delta H_{ff}\|_2 \ll \omega_0$ within each block. We then have:

$$\begin{aligned} \|\delta H_{ff}\|_2 &= \sqrt{tr(\delta H_{ff}\delta H_{ff})} && (3.79)\\ &= \sqrt{\sum_{ij} 2d_{ij}^2}. && (3.80) \end{aligned}$$

Then this says that interaction due to dipolar flip-flops does not change the summation structure so long as $\sum_{ij} 2d_{ij}^2 \ll \omega_0^2$. If one wished to bound this in some lattice-like scenario where each spin couples predominantly with $O(1)$ spins, then the total summation will have $\sum_{ij} 2d_{ij}^2$ going as $O(N)$. If no such restriction is made, then there will be $O(N^2)$ terms in the summation.

3.7.9 Number Operator Expectation Fractional Shift and Variance Fractional Shift

To compute the expectation of the number operator under self-evolution, we will need to compute $\hat{n}_{\text{pert}}(j,k) := \text{tr}(\omega_0 a^\dagger a L^2(j,k))$. Written using $k' = k - k_0(j)$ and following the

notations used in [1], we may compute:

$$
\begin{aligned}
& tr(a^\dagger a L^2(j,k)) && (3.81)\\
= \;& \langle 1_{j,k}|a^\dagger a|1_{j,k}\rangle l_1^2(j,k) + \langle |\mathcal{B}_{j,k}||a^\dagger a||\mathcal{B}|_{j,k}\rangle l^2_{|\mathcal{B}_{j,k}|}(j,k) && (3.82)\\
& + \sum_{\alpha=2}^{|\mathcal{B}_{j,k}|-1} \langle \alpha_{j,k}|a^\dagger a|\alpha_{j,k}\rangle (l_\alpha^2(j,k) + l_{\alpha+1}^2(j,k)) && (3.83)\\
= \;& (k'-1)(2j)(k') + (k'-|\mathcal{B}|)(|\mathcal{B}|(2j-(|\mathcal{B}|-1))(k'+1-|\mathcal{B}|) && (3.84)\\
& + \sum_{\alpha=2}^{|\mathcal{B}|-1} (k'-\alpha)(\alpha(2j-\alpha+1)(k'-\alpha+1) + (\alpha+1)(2j-\alpha)(k'-\alpha)) && (3.85)\\
= \;& (k'-1)(2j)(k') + (k'-|\mathcal{B}|)(|\mathcal{B}|(2j-(|\mathcal{B}|-1))(k'+1-|\mathcal{B}|) && (3.86)\\
& + \sum_{\alpha=2}^{|\mathcal{B}|-1} [(-2)\alpha^4 + (1+4j+4k')\alpha^3 + (-1-8jk'-2k'^2-k')\alpha^2 && (3.87)\\
& + (4jk'^2 - 2jk' + k')\alpha + (2jk'^2)] && (3.88)\\
= \;& 2jk'(k'-1) + [-|\mathcal{B}|^4 + (2j+2k')|\mathcal{B}|^3 + (-4jk'-2j-k'^2-3k'-1)|\mathcal{B}|^2 && (3.89)\\
& + (2jk'^2 + 2jk' + k'^2 + k')|\mathcal{B}| && (3.90)\\
& + A\frac{1}{30}(6|\mathcal{B}|^5 - 15|\mathcal{B}|^4 + 10|\mathcal{B}|^3 - |\mathcal{B}| - 30) + B\frac{1}{4}(|\mathcal{B}|^4 - 2|\mathcal{B}|^3 + |\mathcal{B}|^2 - 4) && (3.91)\\
& + C\frac{1}{6}(2|\mathcal{B}|^3 - 3|\mathcal{B}|^2 + |\mathcal{B}| - 6) + D\frac{1}{2}(|\mathcal{B}|^2 - |\mathcal{B}| - 2) + E(|\mathcal{B}| - 2) && (3.92)\\
= \;& \frac{A}{5}|\mathcal{B}|^5 + (-1 - \frac{A}{2} + \frac{B}{4})|\mathcal{B}|^4 + (2j + 2k' + \frac{A}{3} - \frac{B}{2} + \frac{C}{3})|\mathcal{B}|^3 && (3.93)\\
& + (-4jk' - 2j - k'^2 - 3k' - 1 + \frac{B}{4} - \frac{C}{2} + \frac{D}{2})|\mathcal{B}|^2 && (3.94)\\
& + (2jk'^2 + 2jk' + k'^2 + k' - \frac{A}{30} + \frac{C}{6} - \frac{D}{2} + E)|\mathcal{B}| && (3.95)\\
& + (2jk'(k'-1) - A - B - C - D - 2E) && (3.96)\\
= \;& -\frac{2}{5}|\mathcal{B}|^5 + \frac{1}{4}(1+4j+4k')|\mathcal{B}|^4 + \frac{1}{6}(-16jk' - 4k'^2 - 2k' - 9)|\mathcal{B}|^3 && (3.97)\\
& + \frac{1}{4}(8jk'^2 - 4jk' - 4j - 4k' - 1)|\mathcal{B}|^2 && (3.98)\\
& + \frac{1}{30}(60jk'^2 + 50jk' + 20k'^2 + 10k' - 3)|\mathcal{B}| && (3.99)\\
& + 2(-3jk'^2 + 4jk' - 2j + k'^2 - 2k' + 1) && (3.100)
\end{aligned}
$$

Evaluating this at the two regimes $|\mathcal{B}| = \min\{2j+1, k'+1\}$, we obtain:

$$\frac{16}{5}j^5 - \frac{16}{3}j^4k' + 4j^4 + \frac{8}{3}j^3k'^2 - \frac{20}{3}j^3k' - 16j^3 + 4j^2k'^2 - \frac{2}{3}j^2k' - 25j^2 \\ - \frac{14}{3}jk'^2 + \frac{26}{3}jk' - \frac{81}{5}j + 2k'^2 - 4k' \quad (3.101)$$

and

$$\frac{1}{3}jk'^4 + jk'^3 - \frac{16}{3}jk'^2 + 8jk' - 4j - \frac{1}{15}k'^5 - \frac{1}{12}k'^4 - \frac{11}{6}k'^3 - \frac{47}{12}k'^2 - \frac{101}{10}k', \quad (3.102)$$

respectively. These are analytical expressions still.

We wish to find, where ρ_{th} is the coupled thermal state, the perturbative term of which is computed using $\hat{n}_{\text{pert}}(j,k)$:

$$\text{fractional mean shift} := \frac{\text{tr}(\omega_0 a^\dagger a \rho_{\text{th}}) - \text{tr}(\omega_0 a^\dagger a \rho_0)}{\text{tr}(\omega_0 a^\dagger a \rho_0)} \quad (3.103)$$

Second moment

We begin by defining $\hat{n}^{(2)}_{\text{pert}}(j,k) := \text{tr}(\omega_0^2 (a^\dagger a)^2 L^2(j,k))$. Using a similar method as just before, we may compute:

$$
\begin{aligned}
& \text{tr}((a^\dagger a)^2 L^2(j,k)) && (3.104)\\
= \; & \langle 1_{j,k}|(a^\dagger a)^2|1_{j,k}\rangle l_1^2(j,k) + \langle |\mathcal{B}_{j,k}||(a^\dagger a)^2||\mathcal{B}|_{j,k}\rangle l^2_{|\mathcal{B}_{j,k}|}(j,k) && (3.105)\\
& + \sum_{\alpha=2}^{|\mathcal{B}_{j,k}|-1} \langle \alpha_{j,k}|(a^\dagger a)^2|\alpha_{j,k}\rangle (l_\alpha^2(j,k) + l_{\alpha+1}^2(j,k))\\
= \; & (k'-1)^2(2j)(k') + (k'-|\mathcal{B}|)^2(|\mathcal{B}|(2j-(|\mathcal{B}|-1))(k'+1-|\mathcal{B}|) && (3.106)\\
& + \sum_{\alpha=2}^{|\mathcal{B}|-1} (k'-\alpha)^2(\alpha(2j-\alpha+1)(k'-\alpha+1) + (\alpha+1)(2j-\alpha)(k'-\alpha))\\
= \; & (k'-1)^2(2j)(k') + (k'-|\mathcal{B}|)^2(|\mathcal{B}|(2j-(|\mathcal{B}|-1))(k'+1-|\mathcal{B}|) && (3.107)\\
& + \sum_{\alpha=2}^{|\mathcal{B}|-1} [2\alpha^5 + (-1-4j-6k')\alpha^4 + (1+12jk'+6k'^2+2k')\alpha^3\\
& + (-12jk'+2jk'-2k'^3-k'^2-2k')\alpha^2 + (4jk'^3-4jk'^2+k'^2)\alpha + (2jk'^3)]\\
= \; & |\mathcal{B}|^5 + (-2j-3k'-2)|\mathcal{B}|^4 + (6jk'+2j+3k'^2+5k'+1)|\mathcal{B}|^3 && (3.108)\\
& + (-6jk'^2-4jk'-k'^3-4k'^2-2k')|\mathcal{B}|^2\\
& + (2jk'^3+2jk'^2+k'^3+k'^2)|\mathcal{B}| + (2jk'^3-4jk'^2+2jk')\\
& + A\frac{1}{12}(2|\mathcal{B}|^6 - 6|\mathcal{B}|^5 + 5|\mathcal{B}|^4 - |\mathcal{B}|^2 - 12)\\
& + B\frac{1}{30}(6|\mathcal{B}|^5 - 15|\mathcal{B}|^4 + 10|\mathcal{B}|^3 - |\mathcal{B}| - 30) + C\frac{1}{4}(|\mathcal{B}|^4 - 2|\mathcal{B}|^3 + |\mathcal{B}|^2 - 4)\\
& + D\frac{1}{6}(2|\mathcal{B}|^3 - 3|\mathcal{B}|^2 + |\mathcal{B}| - 6) + E\frac{1}{2}(|\mathcal{B}|^2 - |\mathcal{B}| - 2) + F(|\mathcal{B}| - 2)
\end{aligned}
$$

Grouping by powers of $|\mathcal{B}|$, we obtain:

$$
\begin{aligned}
&= \frac{A}{6}|\mathcal{B}|^6 + (1 - \frac{A}{2} + \frac{B}{5})|\mathcal{B}|^5 + (-2j - 3k' - 2 + \frac{5}{12}A - \frac{B}{2} + \frac{C}{4})|\mathcal{B}|^4 && (3.109)\\
&\quad +(6jk' + 2j + 3k'^2 + 5k' + 1 + \frac{B}{3} - \frac{C}{2} + \frac{D}{3})|\mathcal{B}|^3 && (3.110)\\
&\quad +(-6jk'^2 - 4jk' - k'^3 - 4k'^2 - 2k' - \frac{A}{12} + \frac{C}{4} - \frac{D}{2} + \frac{E}{2})|\mathcal{B}|^2\\
&\quad +(2jk'^3 + 2jk'^2 + k'^3 + k'^2 - \frac{B}{30} + \frac{D}{6} - \frac{E}{2} + F)|\mathcal{B}|\\
&\quad +(2jk'^3 - 4jk'^2 + 2jk' - A - B - C - D - E - 2F)\\
&= \frac{1}{3}|\mathcal{B}|^6 + \frac{1}{5}(-1 - 4j - 6k')|\mathcal{B}|^5 + (3jk' + \frac{3}{2}k'^2 + \frac{1}{2}k' - \frac{5}{12})|\mathcal{B}|^4 && (3.111)\\
&\quad +(-\frac{10}{3}jk' + \frac{2}{3}j - \frac{2}{3}k'^3 - \frac{1}{3}k'^2 + \frac{4}{3}k' + \frac{1}{6})|\mathcal{B}|^3\\
&\quad +(2jk'^3 - 8jk'^2 + 4jk' - \frac{3}{2}k'^2 - \frac{1}{2}k' + \frac{1}{12})|\mathcal{B}|^2\\
&\quad +(2jk'^3 + 4jk'^2 - \frac{5}{3}jk' + \frac{2}{3}k'^3 + \frac{1}{3}k'^2 - \frac{1}{3}k' - \frac{1}{15})|\mathcal{B}|\\
&\quad +(-jk'^3 + 4j + 2k'^3 - 6k'^2 + 6k' - 2)
\end{aligned}
$$

Evaluating this at the two regimes $|\mathcal{B}| = \min\{2j + 1, k' + 1\}$, we obtain:

$$
\begin{aligned}
&-\frac{64}{15}j^6 + \frac{48}{5}j^5k' - \frac{32}{5}j^5 + 24j^4k'^2 - \frac{56}{3}j^4k' - \frac{4}{3}j^4 + \frac{8}{3}j^3k'^3 + \frac{40}{3}j^3k'^2 - \frac{64}{3}j^3k' + \frac{4}{3}j^3\\
&+4j^2k'^2 + 2j^2k'^2 - \frac{16}{3}j^2k' + \frac{1}{3}j^2 + \frac{1}{3}jk'^3 + \frac{2}{3}jk'^2 - \frac{2}{3}jk' + \frac{56}{15}j + 2k'^3 - 6k'^2 + \frac{29}{5}k' - \frac{21}{10}
\end{aligned} \tag{3.112}
$$

and

$$
-\frac{13}{10}k'^6 + \frac{21}{5}jk'^5 - \frac{1}{30}k'^5 + \frac{8}{3}jk'^4 + \frac{1}{12}k'^4 - \frac{13}{3}jk'^3 + 2k'^3 - \frac{5}{3}jk'^2 - \frac{25}{4}k'^2 + \frac{86}{15}k' + \frac{58}{15}j - \frac{21}{10} \tag{3.113}
$$

respectively. These are analytical expressions still. From here the fractional variance shift can be found using linearity of the trace and thermal density state.

3.7.10 Driven Solution

We will consider the result of:

$$
\mathrm{tr}(J_y e^{it(H + 2\Omega\cos(\omega_0 t)J_x)}\rho_{th}e^{-it(H+2\Omega\cos(\omega_0 t)J_x)}) \tag{3.114}
$$

Note that since $\rho_{\text{th}} \propto e^{-\beta H}$ we may commute the evolution of H_{int} around it as H_{int} (without the rotating-wave approximation) commutes with J_x. Further the term $a^\dagger a$ in H_0 commutes with J_y, so we may cancel that term as well. Then this reduces to:

$$\text{tr}(J_y e^{it(\omega_0 J_z + 2\Omega\cos(\omega_0 t)J_x)}\rho_{\text{th}} e^{-it(\omega_0 J_z + 2\Omega\cos(\omega_0 t)J_x)}). \tag{3.115}$$

We will now move into the rotating frame defined by $\omega_0 J_z$ for the Hamiltonian $\omega_0 J_z + 2\Omega\cos(\omega_0 t)J_x$. This becomes ΩJ_x [23]. Our expression is now:

$$\text{tr}(e^{-it\Omega J_x} J_y e^{it\Omega J_x}\rho_{\text{th}}). \tag{3.116}$$

If we only keep the terms with constant number of excitations, we obtain from [23] that:

$$\begin{aligned}
\text{tr}(e^{-it\Omega J_x} J_y e^{it\Omega J_x}\rho_{\text{th}}) &= \text{tr}(\frac{1}{2}(e^{-i\Omega t}(J_y + iJ_z) + e^{i\Omega t}(J_y - iJ_z))\rho_{\text{th}}) && (3.117)\\
&= \text{tr}(\cos(\Omega t)J_y\rho_{\text{th}}) + \text{tr}(\sin(\Omega t)J_z\rho_{\text{th}}) && (3.118)\\
&= \sin(\Omega t)\text{tr}(J_z\rho_{\text{th}}), && (3.119)
\end{aligned}$$

where the first trace is zero due to not preserving the number of excitations.

Computing $\mathrm{tr}(\omega_0 J_z \rho_{\mathrm{th}})$ first non-zero change:

$$\begin{aligned}
& \mathrm{tr}(J_z L^2(j,k)) && (3.120)\\
= \;& (1-j)l_1^2(j,k) + (|\mathcal{B}|-j)l_{|\mathcal{B}|}^2(j,k) + \sum_{\alpha=2}^{|\mathcal{B}|-1}(\alpha-j)(l_\alpha^2(j,k)+l_{\alpha+1}^2(j,k)) && (3.121)\\
= \;& (1-j)(2j)(k') + (|\mathcal{B}|-j)(|\mathcal{B}|(2j-(|\mathcal{B}|-1))(k'+1-|\mathcal{B}|) && (3.122)\\
& + \sum_{\alpha=2}^{|\mathcal{B}|-1}(\alpha-j)(\alpha(2j-\alpha+1)(k'-\alpha+1)+(\alpha+1)(2j-\alpha)(k'-\alpha))\\
= \;& |\mathcal{B}|^4 + (-3j-k'-2)|\mathcal{B}|^3 + (2j^2+3jk'+4j+k'+1)|\mathcal{B}|^2 && (3.123)\\
& +(-2j^2k'-2j^2-jk'-j)|\mathcal{B}| + (-2j^2k'+2jk')\\
& + \sum_{\alpha=2}^{|\mathcal{B}|-1} 2\alpha^4 + (-1-6j-2k')\alpha^3 + (1+4j^2+j+6jk')\alpha^2\\
& +(-4j^2k'-j+2jk')\alpha + 2j^2k'\\
= \;& |\mathcal{B}|^4 + (-3j-k'-2)|\mathcal{B}|^3 + (2j^2+3jk'+4j+k'+1)|\mathcal{B}|^2 && (3.124)\\
& +(-2j^2k'-2j^2-jk'-j)|\mathcal{B}| + (-2j^2k'+2jk')\\
& +A\frac{1}{30}(6|\mathcal{B}|^5-15|\mathcal{B}|^4+10|\mathcal{B}|^3-|\mathcal{B}|-30) + B\frac{1}{4}(|\mathcal{B}|^4-2|\mathcal{B}|^3+|\mathcal{B}|^2-4)\\
& +C\frac{1}{6}(2|\mathcal{B}|^3-3|\mathcal{B}|^2+|\mathcal{B}|-6) + D\frac{1}{2}(|\mathcal{B}|^2-|\mathcal{B}|-2) + E(|\mathcal{B}|-2)\\
= \;& \frac{A}{5}|\mathcal{B}|^5 + (1-\frac{A}{2}+\frac{B}{4})|\mathcal{B}|^4 + (-3j-k'-2+\frac{A}{3}-\frac{B}{2}+\frac{C}{3})|\mathcal{B}|^3 && (3.125)\\
& +(2j^2+3jk'+4j+k'+1+\frac{B}{4}-\frac{C}{2}+\frac{D}{2})|\mathcal{B}|^2\\
& +(-2j^2k'-2j^2-2jk'-j-\frac{A}{30}+\frac{C}{6}-\frac{D}{2}+E)|\mathcal{B}|\\
& +(-2j^2k'+2jk'-A-B-C-D-2E)\\
= \;& \frac{2}{5}|\mathcal{B}|^5 + \frac{1}{4}(-1-6j-2k')|\mathcal{B}|^4 + \frac{1}{6}(8j^2+12jk'+2j-3)|\mathcal{B}|^3 && (3.126)\\
& +\frac{1}{4}(-8j^2k'+4jk'+6j+2k'+1)|\mathcal{B}|^2\\
& +\frac{1}{30}(60j^2k'-40j^2-60jk'-10j+3)|\mathcal{B}|\\
& +(-2j^2k'-4j^2-6jk'+6j+2k'-2)
\end{aligned}$$

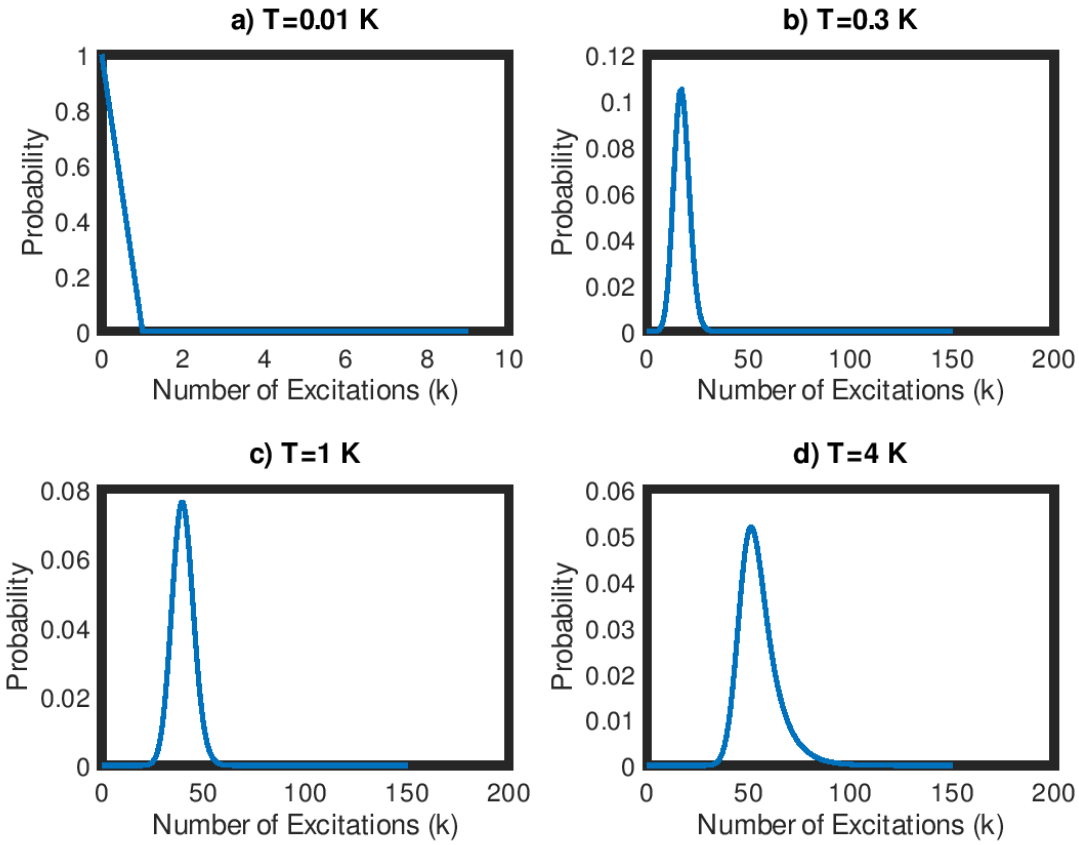

Figure 3.10: Figure of the distribution of the population for Z_0 as a function of the number of excitations in the system (k). These are plotted for $N = 100$, $\omega_0 = 20\pi$ GHz.

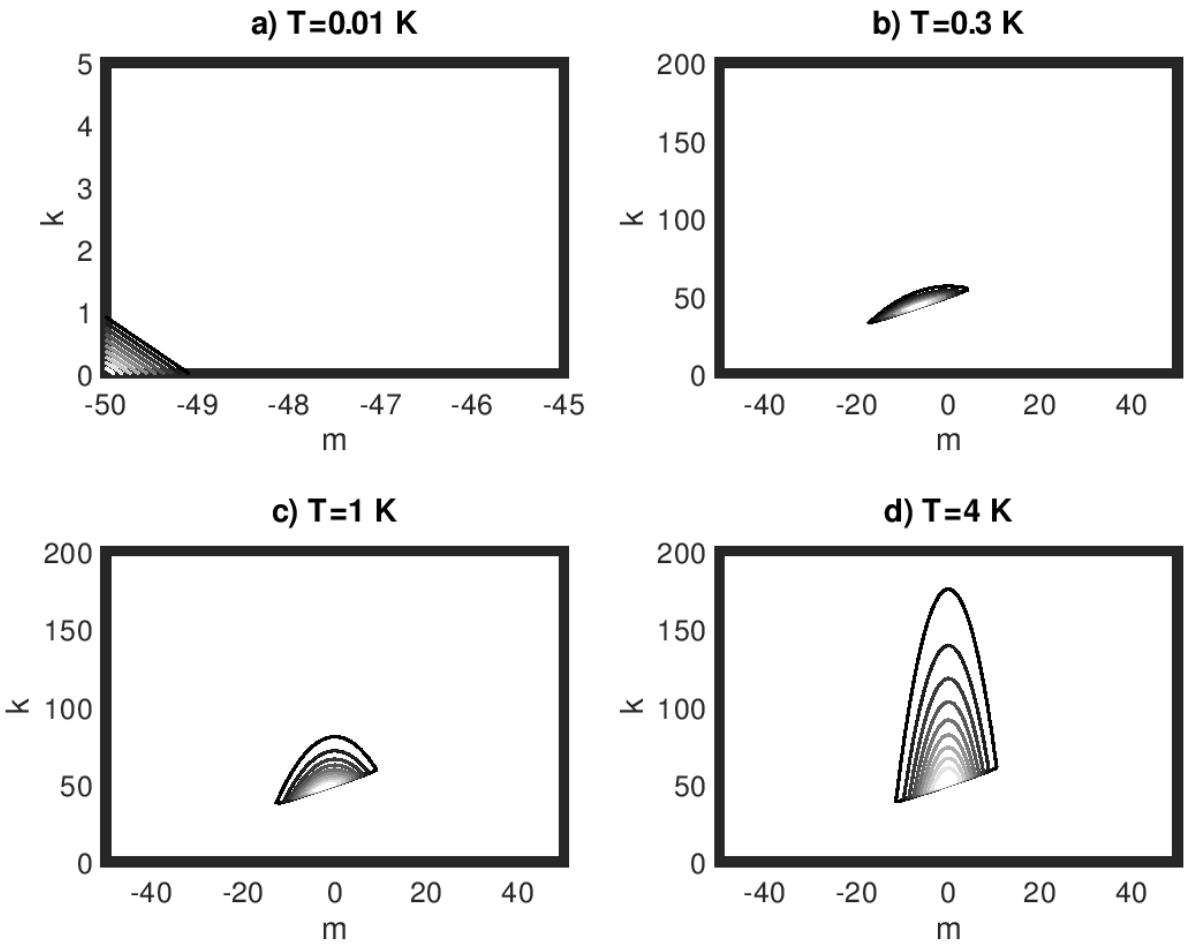

Figure 3.11: Figure of the distribution of the population for Z_{total} as a function of the number of excitations in the system (k) against the secondary spin quantum number (m). These are plotted for $N = 100$, $g_0 = 200\pi$ Hz, and $\omega_0 = 20\pi$ GHz. Note that for $T = 0.01$ Kelvin the population is essentially in the Dicke subspace and global groundstate.

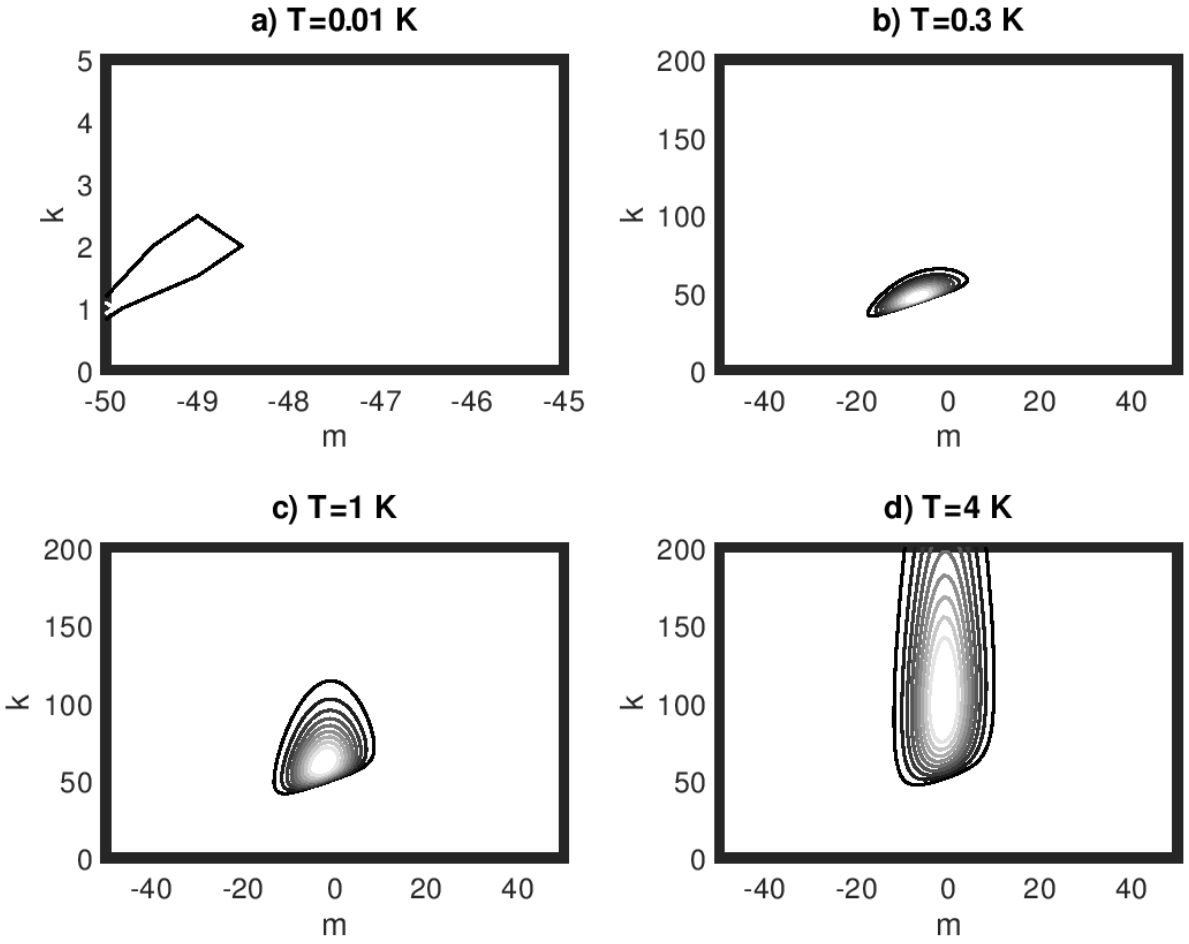

Figure 3.12: Figure of the distribution of the population for Z_{pert}, the Lamb shifts alone, as a function of the number of excitations in the system (k) against the secondary spin quantum number m. These are plotted for $N = 100$, $g_0 = 200\pi$ Hz, and $\omega_0 = 20\pi$ GHz. Note that for $T = 0.01$ Kelvin the population is essentially in the Dicke subspace and global groundstate. The volumes, normalized by Z_{total}, are given by $2.81 \cdot 10^{-16}$, $1.25 \cdot 10^{-15}$, $3.82 \cdot 10^{-16}$, and $7.91 \cdot 10^{-17}$, respectively.

Part II

Higher-dimensional Quantum Error-Correcting Codes

The Protection of Higher-dimensional Quantum Information Overview

Quantum computers are often envisioned as operating on 2-level quantum systems, known as qubits. However, if one permits the use of more levels, also known as larger local-dimensions, a larger computational space becomes available per particle. In this part we explore a slight extension of the traditional stabilizer method generating additive quantum error-correcting code.

In chapter 4 we provide a brief introduction to classical error-correcting codes only so that the analogous terms can be defined in the case of quantum error-correcting codes. When discussing quantum error-correcting codes we briefly discuss how syndrome measurements can be performed in non-destructive ways, making the connection, and important differences, between the classical and quantum cases clear–defining the stabilizer formalism.

In chapter 5 we discuss how we may transform stabilizer codes designed for one local-dimension into codes that exist for any local-dimension choice. This means that particularly if the local-dimension of a quantum device were easily able to be tuned then these same codes can be used regardless of which local-dimension is selected. From there we prove that so long as the local-dimension is sufficiently large the distance of these codes can be promised to remain at least as high, while for smaller local-dimensions the distance can be manually verified. Through these methodology we construct a number of error-correcting codes which have their parameters preserved regardless of the choice of local-dimension. While these methods do not provide codes which are strictly better than those already known, it provides a broader perspective on stabilizer codes and may aid in better understanding of Pauli operator centered algorithms.

Chapter 4

Introduction to Quantum Error-Correcting Codes

Our goal in this chapter is to begin from classical additive error-correcting codes and show the mapping to their quantum analog of stabilizer codes.

4.1 Classical Error-Correcting Codes

To begin, let us consider possibly the simplest encoding procedure. Let us encode the single bits as:

$$0 \mapsto 000, \quad 1 \mapsto 111. \tag{4.1}$$

Now, if any single bit flip occurs, we can still take the majority vote to decode the bit. If, however, two bit flips occurs, then we will incorrectly decode the bit. As a general principle we will assume that errors that involve more bit flips will occur less often.

This simple repetition code protects our bit against any single bit flip. If we wish to protect against two bit flips, then we would need to encode our single bit into five bits, such as by encoding:

$$0 \mapsto 00000, \quad 1 \mapsto 11111. \tag{4.2}$$

We could continue in this way, creating more and more protected encodings of our bit. Unfortunately, the *rate* of the code, number of logical bits per physical bits, is only $\frac{1}{3}$ at most. If we instead batch encodings into blocks, we can improve this rate significantly.

If we consider parities of bits instead of simply taking majority vote we can generate better encodings. For this we have the following definitions:

Definition 6. *For a classical block code C the parity check matrix $\boldsymbol{H}$ states which parities to consider when attempting to determine the error.*

Definition 7. *For a classical block code C the generator matrix $\boldsymbol{G}$ has rows which form the basis for the physical bits used in the encoding of the bits.*

By construction we will require $\mathbf{H}\mathbf{G}^T = 0$ so that any member, v, in the vector space formed from the rows of $\mathbf{G}$ still satisfies $\mathbf{H}v = 0$. Let us revisit the repetition code, which we can restate in terms of these block matrices:

$$\begin{bmatrix} 1 & 1 & 0 \\ 0 & 1 & 1 \end{bmatrix} \begin{bmatrix} 1 & 1 & 1 \end{bmatrix}^T = 0. \tag{4.3}$$

Note that both the 000 and 111 codewords are represented by the generator matrix since the vector space is over $\mathbb{Z}_2$.

As an important example, we can consider the Hamming code, which has parity check matrix:

$$\mathbf{H} = \begin{bmatrix} 1 & 1 & 1 & 1 & 0 & 0 & 0 \\ 1 & 1 & 0 & 0 & 1 & 1 & 0 \\ 1 & 0 & 1 & 0 & 1 & 0 & 1 \end{bmatrix}. \tag{4.4}$$

This columns of this matrix are all three digit binary strings aside from the all zero string. We will not bother writing out the codewords since they provide no additional insights. The rate of this code is $4/7$ since the column null space has dimension four. Notice though that for any single physical bit flip it will pull out one column from $\mathbf{H}$, which is guaranteed to be unique. This means that we can correct any single bit flip. If, however, two bit flips occur then we will not be able to differentiate that two bit flip from the single bit flip that generates the same parity check value. This brings us to defining the parameters of classical block code:

- n: the number of physical bits used to generate protected logical bits. The number of columns in the parity check matrix $\mathbf{H}$.
- k: the number of logical bits. This is given by the dimension of the column null space of $\mathbf{H}$.
- d: the distance of the code. This is given by the minimal number of columns of $\mathbf{H}$ which are linearly dependent over $\mathbb{Z}_2$.

The construction of good parity check matrices, and hence good classical codes, has been well-studied and is not the focus of this work, so we leave this topic here. We have introduced the essential parameters of classical additive error-correction and will next discuss how this idea, with some modifications, can be imported to the quantum realm.

4.2 Quantum Error-Correcting Codes

In an ideal world we would just use classical error-correction in the quantum realm as well. Unfortunately there are some properties of quantum systems that prevent this. If one measures the parity of the quantum bits this causes the collapse of the quantum state making your quantum computer just about the same as a classical computer, so clearly we should avoid measuring our encoded states. We also cannot simply copy the encoded states and perform measurements to determine the error on that copy and apply the correction on the original. The no-cloning theorem prevents this [80]. A different solution must be used: indirect measurement of the parities.

Definition 8. *A qubit is a normalized vector in* $\mathbb{C}^2$

For qubits we must protect against changes in the ratio of the entries, both real value (bit-flip) and imaginary value (phase-flip). In order to discuss the indirect measurement method, we must introduce a few essential qubit gates.

We begin with the most fundamental building blocks, the Pauli gates (also known as the Pauli matrices):

$$X = \begin{bmatrix} 0 & 1 \\ 1 & 0 \end{bmatrix}, \quad Z = \begin{bmatrix} 1 & 0 \\ 0 & -1 \end{bmatrix}, \quad Y = \begin{bmatrix} 0 & -i \\ i & 0 \end{bmatrix} \tag{4.5}$$

where we have written these matrices in the computational basis, $|0\rangle$ and $|1\rangle$. Alongside these, we also have the following pair of gates:

$$H = \frac{1}{\sqrt{2}} \begin{bmatrix} 1 & 1 \\ 1 & -1 \end{bmatrix}, \quad CNOT = \begin{bmatrix} 1 & 0 & 0 & 0 \\ 0 & 1 & 0 & 0 \\ 0 & 0 & 0 & 1 \\ 0 & 0 & 1 & 0 \end{bmatrix} \tag{4.6}$$

where the former is called the Hadamard gate and the latter the CNOT gate. The Hadamard gate transforms between bit ($|0\rangle$, $|1\rangle$) basis and phase ($|+\rangle$, $|-\rangle$) basis. The CNOT gate conditionally performs a NOT (X) gate on a target register based on if the controlling register is a $|0\rangle$ or $|1\rangle$.

With these gates we can generate the quantum analog of the classical repetition code. We begin encoding $|0\rangle$ into $|000\rangle$ and $|1\rangle$ into $|111\rangle$, meaning that if we wish to encode $\alpha|0\rangle + \beta|1\rangle$ we would encode it as $\alpha|000\rangle + \beta|111\rangle$. We will use a pair of auxiliary qubits, preset as $|0\rangle$, to determine the parity of our bits. We will use the registers in our encoded

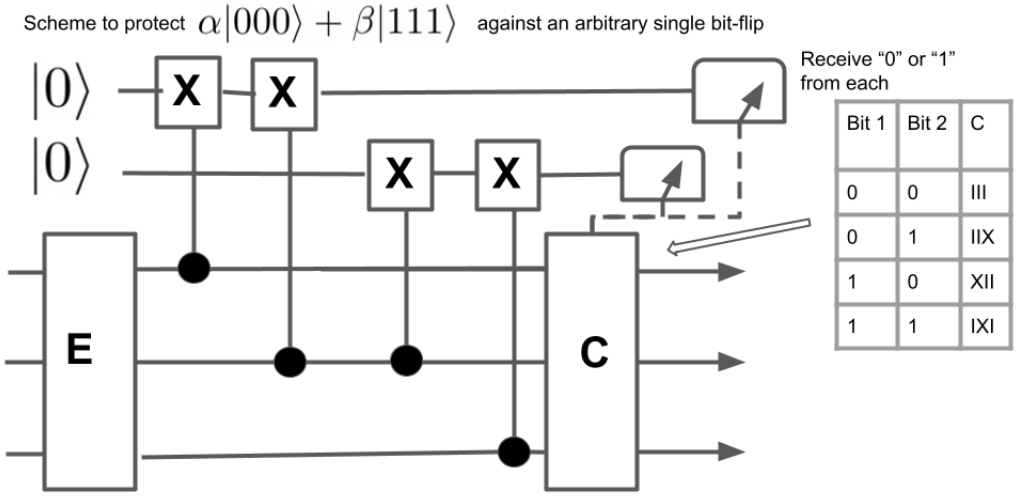

Figure 4.1: Our first circuit for protecting a qubit against a single bit-flip error through non-destructive measurements. In this diagram the E block is where an error may have occurred, whereas the C block is the correction applied, based on what measurement values are obtained from the auxiliary qubits.

state as the controls for CNOT gates with the auxiliary qubits as the targets. The CNOT gates will be placed following the pattern of parity checks used for the repetition code. This is illustrated in Figure 4.1.

First, let us make sure that if no error occurs we get a trivial change on the auxiliary qubits. In this case each auxiliary qubit receives a pair of flips, returning them to their original value. If we then measure these auxiliary qubits, we will get "0" for both. Now suppose a single bit flip occurs. The parities of the auxiliary qubits will be altered by whichever physical register receives the error. This results in a unique pair of final values allowing us to determine which single bit flip occurred, then correct the discovered error (up to a higher order). This means that we have successfully imported this code from the classical setting to the quantum setting.

This is only sufficient for protecting a single qubit against a bit flip. We need to also protect against phase flips in order to fully protect our qubit. To aid in our construction of a phase-flip protected qubit and parity checking circuit, let us reconsider the prior example, although altering some gates. These changes are shown in Figure 4.2. In this circuit now the auxiliary qubits are flipped if and only if the bit flip (X gates) that occur during the

error phase do not commute with the parity checking control-phase (CZ) gates.

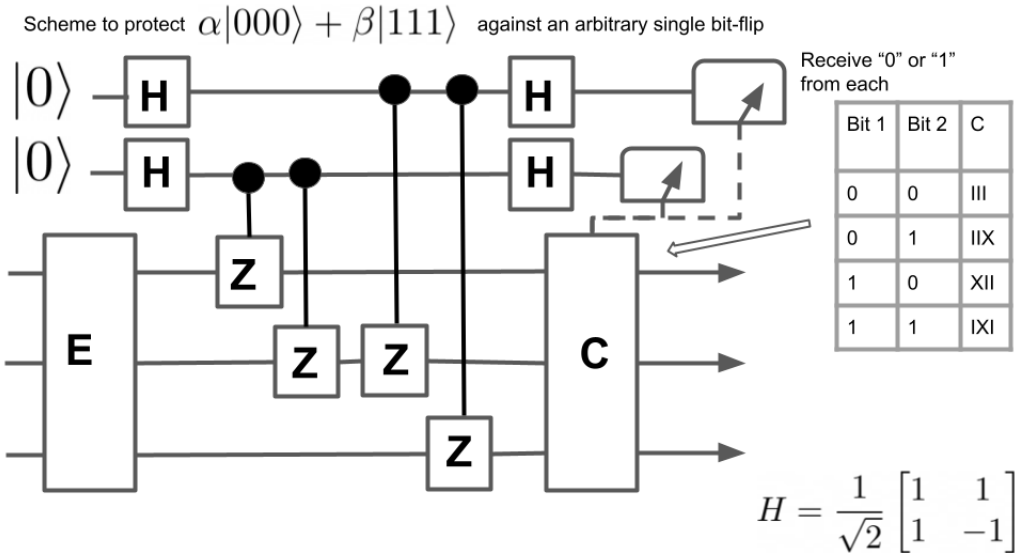

Figure 4.2: Our new circuit for protecting a qubit against a single bit-flip error through non-destructive measurements. In this diagram the E block is where an error may have occurred, whereas the C block is the correction applied, based on what measurement values are obtained from the auxiliary qubits.

We can use this alternate form now to create a circuit which protects against an arbitrary single register phase flip. This time we encode the state as $\alpha|{+}{+}{+}\rangle + \beta|{-}{-}{-}\rangle$, and simply replace the CZ in the circuit with CNOT gates. Again the read out values from the auxiliary qubits will be given by the parity of the commutator of the error with these parity check control gates. The phase-flip protection scheme is shown in Figure 4.3. This idea can be combined together to generate the Shor 9-qubit code as a simple concatenation of these two codes [81]. Generally, we do not need to consider these circuits, but instead just focus on the commutators of the errors with the parity check control X and control Z gates, allowing us to step away from these circuits and instead focus on Pauli operators.

As of this point the relationship to classical error-correction has been loose, however, the connection can be solidified significantly. We would need a parity check-like matrix to still differentiate between the non-commuting term occurring from an X operator or a Z operator, so we must allow for the power of each of these operators to be taken into account. This leads to the symplectic representation for stabilizers:

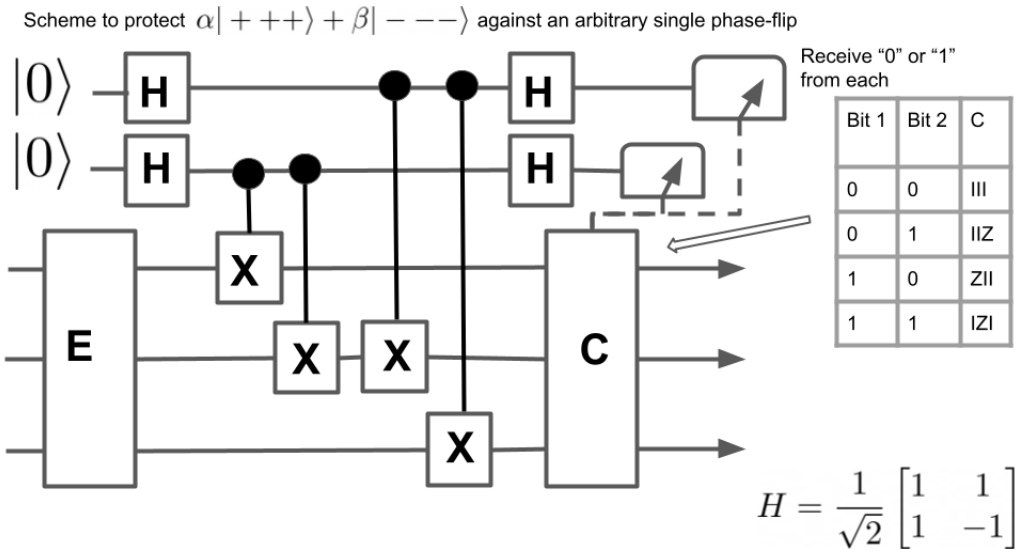

Figure 4.3: Our circuit for protecting a qubit against a single phase-flip error through non-destructive measurements. In this diagram the E block is where an error may have occurred, whereas the C block is the correction applied, based on what measurement values are obtained from the auxiliary qubits.

Definition 9. *The symplectic representation of an n register Pauli operator, $X^{\vec{a}}Z^{\vec{b}}$, transforms the Pauli to a $2n$ length binary vector $\vec{a} \bigoplus \vec{b}$.*

This definition will be extended in the following chapter, but suffices for the discussion here. The inner product needed to match the commutation requirements of Paulis is given by:

Definition 10. *Let $p_1 = X^{\vec{a}_1}Z^{\vec{b}_1}$ and $p_2 = X^{\vec{a}_2}Z^{\vec{b}_2}$. Then p_1 and p_2 commute if and only if $\vec{a}_1 \cdot \vec{b}_2 + \vec{a}_2 \cdot \vec{b}_1 = 0 \mod 2$.*

Since we are truly working with matrices in the quantum case, quantum states which are unaltered by each of these parity checks would require that all of these parity checks commute with each other. This means that a stabilizer code requires that all generators commute with each other. With this, we finally are able to write quantum codes in forms strongly reminiscent of classical error-correcting codes.

As an important example, let us consider the Steane code [82]. As Pauli operators this

can be given by the following parity checking Pauli operations:

$$\langle XXXXIII, XXIIXXI, XIXIXIX, ZZZZIII, ZZIIZZI, ZIZIZIZ\rangle. \tag{4.7}$$

If we instead write this in the symplectic representation we may write:

$$\left[\begin{array}{ccccccc|ccccccc} 1&1&1&1&0&0&0&0&0&0&0&0&0&0\\ 1&1&0&0&1&1&0&0&0&0&0&0&0&0\\ 1&0&1&0&1&0&1&0&0&0&0&0&0&0\\ 0&0&0&0&0&0&0&1&1&1&1&0&0&0\\ 0&0&0&0&0&0&0&1&1&0&0&1&1&0\\ 0&0&0&0&0&0&0&1&0&1&0&1&0&1 \end{array}\right]. \tag{4.8}$$

In particular, this code is given by using the seven physical bit Hamming code to perform the parity check in each of the bit and phase bases. This code then protects against any single bit-flip or phase-flip error, which form a complete error-basis [83].

The Pauli operators for a code form a commuting group, while in the symplectic representation they form a vector space over a finite field. This means that different group members, formed from compositions of generators, correspond to different linear combinations of the basis vectors in the symplectic representation. Given this, we will interchangeably refer to the stabilizer group or the vector space for a given collection of Pauli operators forming a group.

Then in analogy with classical codes, we have the following parameters for a qubit stabilizer code:

- n: the number of physical qubits used to encode the logical qubits. In the symplectic representation this is given by the number of columns in one of the two parts.
- k: the number of logical qubits which are protected by the stabilizer code. While not apparent from this construction, this is given by n minus the rank of the matrix, which is effectively the column null space of one portion of the matrix [84].
- d: the distance of the stabilizer code. This is given by the lowest *Pauli weight* operator that commutes with the parity checking generators for the stabilizer code, but is itself not represented by those parity checking generators (in the stabilizer group).

With these definitions we see then that the Steane code has $n = 7$, $k = 1$, and $d = 3$. Generally there are full methodologies for constructing stabilizer codes with all sorts of

parameters. In the next chapter we discuss a new method for constructing stabilizer codes, focusing on higher local-dimensional quantum systems. As of this time it is primarily of pedagogical use, but could provide essential insights for other problems due to its non-standard approach.

Chapter 5

Local-dimension-invariant Stabilizer Codes

5.1 Motivation

The ability to perform classical computation within an arbitrarily small error rate was shown by Shannon in the 40's [85]. He provided a theoretical framework showing that modern classical computation would be possible. From that point, there arose a new challenge of finding actual codes that could best implement Shannon's result. This in turn pushed coding theory into a new realm, inspiring codes such as the Hamming code family and BCH codes [86], and later leading to incredible ideas such as Polar codes [87] and Turbo codes [88].

As computational power progressed, there began to be investigations into the potential power of using quantum phenomena as a computational tool. This brought those same questions explored for classical computers back into question. This led to various ideas to try to bring over classical codes in some form or another. Among some of the earlier ideas was the stabilizer formalism [89], CSS codes [90, 91], and teleportation [92]. Many classical coding theory methods have been generalized into this new quantum setting, such as Polynomial codes (a generalization of BCH and cyclic codes) [93, 94], Polar codes [95], and Turbo codes [96, 97]–including results such as a complete list of all perfect codes [98].

Having protected quantum information is an essential piece of being able to perform quantum computations. There are a variety of methods to help protect quantum information such as those discussed in [99], but here we focus on the common tool used for

correcting quantum errors known as stabilizer codes, the quantum analog of classical additive codes [84, 100].. In this work we focus on stabilizer codes as they are the quantum analog of classical linear codes. Even with error-correcting codes, having sufficient amounts of protected quantum information to perform useful tasks is still an unresolved challenge. A way to retain a similarly sized computational space while reducing the number of particles that need precise controls is to replace the standard choice of qubits with *qudits*, quantum particles with q levels, also known as local-dimension q [101]. Throughout this work we require q to be a prime so that each nonzero element has a unique multiplicative inverse over $\mathbb{Z}_q$. This restriction can likely be removed, but for simplicity and clarity we only consider this case. This relationship for the growth of computational states can also be captured in the formula for the number of logical codewords for a qudit stabilizer code, q^k, which states that the number of codewords grows exponentially with the local-dimension q as the base, so increasing q increases the amount of information protected per particle [6]. Experimental realizations of qudit systems are currently underway [102, 103, 104, 105, 106], so having more error-correcting codes will aid in protecting such systems.

This means that we also need error-correction methods for these qudit systems. Prior work on qudit codes often depends on having a classical code which satisfies the conditions needed for CSS code construction, or a similar orthogonality requirement (such as [107, 108, 109]). This allows for the generation of many qudit quantum codes, however, at times these codes can require very strict relations between the number of bases for the particles (sometimes called the local dimension of the system) as defined in Definition 11, the number of particles, and the number of logical qudits. This can result in these codes being less useful for constructed qudit systems. This work aims to tackle this problem by working to reduce this level of restriction by allowing codes to be used for qudits of a different number of bases than they were initially designed for. While most codes have been designed for a given local-dimension value, Chau showed that both the 5-qubit [110] and 9-qubit [111] codes could be transformed into qudit codes with the same parameters and minimal modifications to the code. In some regards one may consider this work as a tool somewhat similar in nature to CSS code construction: CSS allows classical to quantum code construction whereas this allows for quantum to quantum code construction.

This chapter is organized as follows. We begin by extending our definitions from the prior chapter to permit qudit operations, as well as a few more definitions needed for this chapter. Following this we provide a few simple examples of stabilizer codes which can be applied regardless of the local-dimension of the underlying device in Section 5.3. Following this we show that any stabilizer code can be put into a form which could be used regardless of the local-dimension–so called local-dimension-invariant (LDI) codes. In the section after that we prove that so long as the system has a sufficiently large local-dimension we can

promise that the distance of the code is at least the same, if not higher. In section 5.6 we consider the possibility of applying a code designed for some initial local-dimension system on a device with a smaller local-dimension and whether the distance could still be preserved. We then proceed to consider the class of stabilizer codes known as Calderbank-Shor-Steane (CSS) codes and show that at least one non-trivial family of codes can be used regardless of the local-dimension and still have at least as high a distance. We then move to discussing a few more examples of LDI codes, including a topological example, using this to highlight the importance in the selection of the LDI representation. Finally we conclude with the implications of this work as well as many possible future directions to carry this line of work.

5.2 Definitions

In this section we define the majority of the tools used in this chapter. We begin by recalling some common definitions and results for qudit Pauli operators. For a more complete guide on qudit stabilizer codes, we recommend [6].

A qubit is defined as a two level system with states $|0\rangle$ and $|1\rangle$. We define a qudit as being a quantum system over q levels, where q is prime. We denote by $\mathbb{Z}_q$ the set $\{0, 1, \ldots q-1\}$. When $q = 2$ we refer to each register as a qubit, while for any value of q we call each register a qudit. In order to speak more generally and not specify q, we will often times refer to each register as a particle instead.

Definition 11. *Generalized Paulis for a particle over q orthogonal levels (local-dimension q) are given by:*

$$X_q|j\rangle = |(j+1) \mod q\rangle, \quad Z_q|j\rangle = \omega^j|j\rangle \tag{5.1}$$

with $\omega = e^{2\pi i/q}$, where $j \in \mathbb{Z}_q$.

When $q = 2$, these are the standard qubit operators. For notational clarity, we will drop the subscript on these operators. These matrices, and their compositions, like their qubit counterparts, form a nice error basis [83, 6]. These operators also form a group, which over a single particle is indicated by $\mathbb{P}_q$. This group structure is preserved over tensor products of these operators, so a generalized Pauli acting on n particles will be in the group $\mathbb{P}_q^n$.

Definition 12. *A stabilizer group, also called here stabilizer code, $\mathbf{S}$ with commuting generators $\{s_i\}$ is defined as the subgroup of all n-qudit generalized Paulis formed from all multiplicative compositions ($\circ$) of these generators. This subgroup must not contain a non-trivial multiple of the identity.*

Since each operator has order q, a collection of $n-k$ compositionally independent generators for this stabilizer group will have q^{n-k} elements. We recall for the reader, the well-known result [6]:

Theorem 13. *For any stabilizer code with $n-k$ qudit stabilizers and n physical qudits, there will be q^k mutually orthogonal basis stabilizer states, or codewords.*

We will work under the assumption that errors on distinct particles are independent and we will assume the error model on each qudit is the depolarizing channel. This is a standard choice. Given this error model we will predominantly be interested in the number of non-identity terms in any error as the exponent of the error term increases with this. This gives us the following definition:

Definition 14. *The weight of an n-qudit Pauli operator is given by the number of non-identity operators in its tensor product statement.*

We note that, so long as no ambiguity exists, we suppress $\otimes$. We only include $\otimes$ to make register changes explicit.

Working with tensors of operators can be challenging, and so we make use of the following well-known mapping from these to vectors. This mapping is sometimes referred to as the symplectic representation, but we use alternative notation in this work to provide some notational flexibility utilized in this work. By representing these operators as vectors at times the solution to a problem can become far more tractable.

Definition 15 (ϕ representation of a qudit operator)**.** *We define the linear surjective map:*

$$\phi_q : \mathbb{P}_q^n \mapsto \mathbb{Z}_q^{2n} \tag{5.2}$$

which carries an n-qudit Pauli in $\mathbb{P}_q^n$ to a $2n$ vector mod q, where we define this mapping by:

$$I^{\otimes i-1} X_q^a Z_q^b I^{\otimes n-i} \mapsto \left(0^{i-1}\ a\ 0^{n-i} \middle| 0^{i-1}\ b\ 0^{n-i}\right), \tag{5.3}$$

which puts the power of the i-th X operator in the i-th position and the power of the i-th Z operator in the $(n+i)$-th position of the output vector. This mapping is defined as a homomorphism with: $\phi_q(s_1 \circ s_2) = \phi_q(s_1) \oplus \phi_q(s_2)$, where $\oplus$ is component-wise addition mod q. We denote the first half of the vector as $\phi_{q,x}$ and the second half as $\phi_{q,z}$.

Equivalently we can state this mapping as:

$$\phi_q\left(\bigotimes_{t=1}^{n} X^{a_t} Z^{b_t}\right) = \left(\bigoplus_{t=1}^{n} a_t\right) \bigoplus \left(\bigoplus_{t=1}^{n} b_t\right), \tag{5.4}$$

where in the above $\bigoplus$ is a direct sum symbol. We will write a vertical bar between the vector for the X powers and the vector for the Z powers mostly for ease of reading.

When $q = 2$ this is the standard mapping used in the qubit stabilizer formalism. We may invert the map ϕ_q to return to the original n-qudit Pauli operator with the global phase being undetermined. We make note of a special case of the ϕ representation:

Definition 16. *Let q be the dimension of the initial system. Then we denote by ϕ_∞ the mapping:*

$$\phi_\infty : \mathbb{P}_q^n \mapsto \mathbb{Z}^{2n} \tag{5.5}$$

where no longer are any operations taken $\mod$ *some base, but instead carried over the full set of integers.*

The ability to define ϕ_∞ as a homomorphism still (and with the same rule) is a portion of the results of this work–shown in Theorem 20. Our definition of ϕ_q is the standard choice for working with stabilizers over q bases, however, our ϕ_∞ allows us to avoid being dependent on the number of bases our system has when working with our stabilizers. Formally we will write a code in ϕ_q, perform some operations, then write it in ϕ_∞, then select a new local-dimension q' and use $\phi_{q'}$. We shorten this to write it as ϕ_∞, and can later select to write it as $\phi_{q'}$ for some prime q' by taking element-wise $\mod q'$. While the operators in ϕ_∞ all commute, normalization of the codewords for infinitely many levels becomes a potential problem.

As an example of the difference in the ϕ representations, consider the following:

$$\phi_2(X \otimes Z^{-1} \otimes I \otimes XZ) = (1\ 0\ 0\ 1 \mid 0\ 1\ 0\ 1), \quad \phi_\infty(X \otimes Z^{-1} \otimes I \otimes XZ) = (1\ 0\ 0\ 1 \mid 0\ -1\ 0\ 1). \tag{5.6}$$

The commutator of two operators in this picture is given by the following definition:

Definition 17. *Let s_i, s_j be two qudit Pauli operators over q bases, then these commute if and only if:*

$$\phi_q(s_i) \odot \phi_q(s_j) = 0 \mod q \tag{5.7}$$

where $\odot$ is the symplectic product, defined by:

$$\phi_q(s_i) \odot \phi_q(s_j) = \oplus_k [\phi_{q,z}(s_j)_k \cdot \phi_{q,x}(s_i)_k - \phi_{q,x}(s_j)_k \cdot \phi_{q,z}(s_i)_k] \tag{5.8}$$

where $\cdot$ is standard integer multiplication $\mod q$ *and $\oplus$ is addition* $\mod q$.

Equivalently the commutator of two generalized Paulis, p_1 and p_2, is written and computed as $\phi(p_1) \odot \phi(p_2) = \vec{a}^{(1)} \cdot \vec{b}^{(2)} - \vec{b}^{(1)} \cdot \vec{a}^{(2)}$, with $\cdot$ as the standard dot product. This is not formally a commutator, but when this is zero, or zero modulo the local-dimension, the two operators commute, while otherwise it is a measure of number of times an X operator passed a Z operator without a corresponding Z operator passing an X operator. When $q = 2$, this becomes the standard commutation relations between qubit Pauli's and is particularly simplified since addition and subtraction mod 2 are identical.

Definition 18. *A stabilizer code, specified by its $n - k$ generators, is characterized by the following set of parameters:*

- *n: the number of (physical) particles that are used to protect the information.*
- *k: the number of encoded (logical) particles.*
- *d: the distance of the code, given by the lowest weight of an undetectable generalized Pauli error. An undetectable generalized Pauli error is an n-qudit Pauli operator which commutes with all elements of the stabilizer group, but is not in the group itself.*

These values are specified for a particular code as $[[n, k, d]]_q$, where q is the local-dimension of the qudits.

Stabilizer codes come in two varieties: degenerate and non-degenerate codes. We pause for a moment here to discuss how degenerate codes, a uniquely quantum coding feature, differ from non-degenerate codes. Degenerate codes are different in the following equivalent ways. Firstly, they may have multiple errors with the same syndrome value and that map to different physical states, but upon recovery still map back to the same logical state. Secondly, degenerate codes may have generators, aside from the identity operator, which have lower weight than the distance of the code. These two differences make degenerate codes markedly different from their non-degenerate counterpart. Degenerate codes, while having these extra nuances, are a crucial class of stabilizer codes as any quantum analog of a low-density parity-check (LDPC) code with high distance will need to be a degenerate code.

To aid in determining which error might have occurred the *syndrome* values are computed by finding the commutator of the error with each of the generators for the stabilizer code.

A stabilizer code is written in the ϕ representation as a matrix whose rows are a set of $n - k$ generators for the subgroup. There are some operations that we may perform which must preserve the parameters of the code, these include, in the ϕ representation:

– Row swaps, corresponding to relabelling the generators.

– Swapping columns i and $i+n$ with j and $j+n$, corresponding to relabelling particles.

– Multiplying a row by any number in $\{1, \ldots, q-1\}$, corresponding to composing that generator with itself.

– Adding row i to row j, corresponding to composing the operators.

– Swapping column i with -1 times column $i+n$, corresponding to a discrete-fourier transform (DFT) on particle i; the qudit analog of the Hadamard gate.

We neglect the phase gate, $\sqrt{Z}$, since we do not use it here, but it would also preserve the parameters of the code. Note though that the SUM gate (qudit CNOT gate) will not usually preserve the distance of the code so we do not allow ourselves to perform that operation on our codes [112]. Now that the tools have been presented we proceed to our results.

5.3 Simple Examples

Consider the following example of generators for a stabilizer group: $\langle XX, ZZ \rangle$. As a qubit code this forms a valid stabilizer code with codeword:

$$\frac{|00\rangle + |11\rangle}{\sqrt{2}} \tag{5.9}$$

and the commutator of these generators can be seen to be: $(1) + (1) = 2 \equiv 0 \mod 2$. Now suppose we wish to use this code for a qutrit system. In order to do that we must transform these generators into ones which have commutator 0, this can be achieved with $\langle XX^{-1}, ZZ \rangle$, whose powers are congruent mod 2 to the original code. In this case $\phi_\infty(X \otimes X^{-1}) \odot \phi_\infty(Z \otimes Z) = 0$. This means that not only can this be used for qutrits, but for all prime number of bases. The codeword in the qutrit case is:

$$\frac{|00\rangle + |12\rangle + |21\rangle}{\sqrt{3}} \tag{5.10}$$

and the generalization of this for the codewords of a q level system is a simple extension. We simply make each term in the codeword have the entries sum to a multiple of the qudit

dimension so that the ZZ operator has a $+1$ eigenvalue:

$$\frac{1}{\sqrt{q}}(\sum_{j=1}^{q}|j \mod q, q-j \mod q\rangle). \tag{5.11}$$

If we look at the generators of this code, there is no single qudit operator that commutes with the generators, thus the distance of this invariant form of the code is still $d = 2$.

This is not the only example of a code that can be turned into a form that is able to be used regardless of the local-dimension. Another great example is the 5-qubit code [110]. In fact, no changes are needed:

$$\langle XZZXI, \quad IXZZX, \quad XIXZZ, \quad ZXIXZ\rangle. \tag{5.12}$$

From inspection this can be seen to have commutators 0, and so this is a valid stabilizer code for qudits, and it can also be checked that this code will always have distance 3. There is also the 9-register code [111].

It is helpful to have a couple of examples, however, it has been unknown whether it is always possible to put stabilizer codes into an invariant form. We move forward from here to show that this can always be done, and a method of how to do this. The remainder of this chapter delves into various aspects related to this question.

5.4 Methods for Constructing Local-dimension-invariant Stabilizer Codes

In the prior section we saw a few examples of codes which can be used regardless of what local-dimension our qudits have. In this section we show that it is always possible, and with a constructive method, to put a stabilizer code into a local-dimension-invariant form. The prescriptive method shown is not unique, so we briefly discuss a couple of slight modifications which can be of use, as well as a particular property of some codes which can be preserved.

We begin with the following definition, motivated by the prior section's observations and the definition for ϕ_∞:

Definition 19. *A stabilizer code S is local-dimension-invariant (LDI) if and only if:*

$$\phi_\infty(s_i) \odot \phi_\infty(s_j) = 0, \quad \forall s_i, s_j \in S \tag{5.13}$$

We now show that all qudit stabilizer codes can be written in an LDI form. This shows that we can form valid stabilizer groups over any number of bases, but says nothing about the distance of these codes. This aspect is treated in the section immediately following.

Theorem 20. *All stabilizer codes can be transformed into a local-dimension-invariant form.*

Proof. Let $\{s_1, \ldots, s_{n-k}\}$ be a set of stabilizer generators for a qudit code over q levels, with q prime. We must construct a set of stabilizers, $\{s'_1, \ldots, s'_{n-k}\}$, such that:

(a) $\phi_\infty(s'_i) \equiv \phi_q(s_i) \mod q$, for all i

(b) $\phi_\infty(s'_i) \odot \phi_\infty(s'_j) = 0$, for all $i \neq j$.

Without loss of generality, we assume that our stabilizers are given in canonical form:

$$\begin{pmatrix} \phi(s_1) \\ \vdots \\ \phi(s_{n-k}) \end{pmatrix} = \left(\begin{array}{cc|cc} I_{n-k} & X_2 & Z_1 & Z_2 \end{array} \right). \tag{5.14}$$

We define the strictly lower diagonal matrix, L, with entries:

$$L_{ij} = \begin{cases} 0 & i \leq j \\ \phi_\infty(s_i) \odot \phi_\infty(s_j) & i > j \end{cases} \tag{5.15}$$

and define $s'_1, \ldots, s'_{n-k}$ such that:

$$\begin{pmatrix} \phi(s'_1) \\ \vdots \\ \phi(s'_{n-k}) \end{pmatrix} = \left(\begin{array}{cc|cc} I_{n-k} & X_2 & Z_1 + L & Z_2 \end{array} \right). \tag{5.16}$$

We show that $s'_1, \ldots, s'_{n-k}$ satisfy the conditions.

(a) Since $\phi_\infty(s_i) \odot \phi_\infty(s_j) \equiv 0 \mod q$ for all $i \neq j$, we observe that $L_{ij} \equiv 0 \mod q$ for all entries. By adding rows of L to our stabilizers, we have not changed the code modulo q.

(b) For $i > j$, we observe that:

$$\begin{aligned}
&\phi(s_i') \odot \phi(s_j') \\
&= (\phi(s_i) + (0 \mid L_i\ 0)) \odot (\phi(s_j) + (0 \mid L_j\ 0)) \\
&= \phi(s_i) \odot \phi(s_j) + \phi(s_i) \odot (0 \mid L_j\ 0) \\
&\quad + (0 \mid L_i\ 0) \odot \phi(s_j) + (0 \mid L_i\ 0) \odot (0 \mid L_j\ 0) \\
&= \phi(s_i) \odot \phi(s_j) + 0 - L_{ij} + 0 \\
&= 0.
\end{aligned}$$

■

Example 21. *Consider the 7-qubit Steane code with parameters* $[[7, 1, 3]]_2$*, denote it by* Ξ *[82]. The* ϕ *representation is given by:*

$$\phi_2(\Xi) = \left[\begin{array}{c|c} H & 0 \\ 0 & H \end{array}\right] \tag{5.17}$$

where H *is the parity-check matrix for the classical Hamming code given by:*

$$H = \begin{bmatrix} 1 & 0 & 0 & 1 & 0 & 1 & 1 \\ 0 & 1 & 0 & 1 & 1 & 0 & 1 \\ 0 & 0 & 1 & 0 & 1 & 1 & 1 \end{bmatrix}. \tag{5.18}$$

We will put this into a local-dimension-invariant form using the method shown in Theorem 20. We begin by putting this in standard form, performing operations $\mod 2$*:*

$$\phi_2(\Xi) = \left[\begin{array}{ccccccc|ccccccc} 1 & 0 & 0 & 0 & 0 & 0 & 1 & 0 & 0 & 0 & 0 & 1 & 1 & 0 \\ 0 & 1 & 0 & 0 & 0 & 0 & 0 & 0 & 0 & 0 & 1 & 1 & 1 & 0 \\ 0 & 0 & 1 & 0 & 0 & 0 & 1 & 0 & 0 & 0 & 1 & 0 & 1 & 0 \\ 0 & 0 & 0 & 1 & 0 & 0 & 0 & 1 & 1 & 0 & 0 & 0 & 0 & 1 \\ 0 & 0 & 0 & 0 & 1 & 0 & 0 & 0 & 1 & 1 & 0 & 0 & 0 & 1 \\ 0 & 0 & 0 & 0 & 0 & 1 & 0 & 1 & 1 & 1 & 0 & 0 & 0 & 0 \end{array}\right]. \tag{5.19}$$

Now that we have the code expressed in standard form we construct the matrix containing the symplectic inner products, no longer taking operation over mod 2*. The anti-symmetric matrix* $[\odot]$ *representing the symplectic inner products between the stabilizers and the re-*

sulting L matrix for this code are given below:

$$[\odot] = \begin{bmatrix} 0 & 0 & 0 & 2 & 0 & 0 \\ 0 & 0 & 0 & 0 & 0 & 0 \\ 0 & 0 & 0 & 0 & 2 & 0 \\ -2 & 0 & 0 & 0 & 0 & 0 \\ 0 & 0 & -2 & 0 & 0 & 0 \\ 0 & 0 & 0 & 0 & 0 & 0 \end{bmatrix} \Rightarrow L = \begin{bmatrix} 0 & 0 & 0 & 0 & 0 & 0 \\ 0 & 0 & 0 & 0 & 0 & 0 \\ 0 & 0 & 0 & 0 & 0 & 0 \\ -2 & 0 & 0 & 0 & 0 & 0 \\ 0 & 0 & -2 & 0 & 0 & 0 \\ 0 & 0 & 0 & 0 & 0 & 0 \end{bmatrix}. \tag{5.20}$$

Adding this to our standard form, we have an invariant form for the Steane code given by:

$$\phi_\infty(\Xi) = \left[\begin{array}{ccccccc|ccccccc} 1 & 0 & 0 & 0 & 0 & 0 & 1 & 0 & 0 & 0 & 0 & 1 & 1 & 0 \\ 0 & 1 & 0 & 0 & 0 & 0 & 0 & 0 & 0 & 0 & 1 & 1 & 1 & 0 \\ 0 & 0 & 1 & 0 & 0 & 0 & 1 & 0 & 0 & 0 & 1 & 0 & 1 & 0 \\ 0 & 0 & 0 & 1 & 0 & 0 & 0 & -1 & 1 & 0 & 0 & 0 & 0 & 1 \\ 0 & 0 & 0 & 0 & 1 & 0 & 0 & 0 & 1 & -1 & 0 & 0 & 0 & 1 \\ 0 & 0 & 0 & 0 & 0 & 1 & 0 & 1 & 1 & 1 & 0 & 0 & 0 & 0 \end{array}\right]. \tag{5.21}$$

Since now all stabilizer generators from $\phi_\infty(\Xi)$ commute, this form of the code is a valid stabilizer code over any number of bases. We do not know, however, what the distance of this code is from this. We address this in Example 31.

We will want to know the size of the maximal entry in this invariant form for our bound on ensuring the distance of the code is at least preserved. The bound on the maximal entry is provided from the above proof:

Corollary 22. *The maximal element in $\phi_\infty(S)$, B, is upper bounded by:*

$$(2 + k(q-1))(q-1). \tag{5.22}$$

Proof. As before, we begin with S in standard form. For any $i \neq j$, there are at most k entries, those entries which are not part of the Identity portion of the standard form, in which both $\phi_{q,x}(s_i)$ and $\phi_{q,z}(s_j)$ are non-zero and bounded above by $q-1$, and a single entry, corresponding to the sole nonzero entry in the Identity portion of the standard form, in which one is 1 whereas the other is bounded above by $q-1$. This gives us a bound on the inner product of: $k(q-1)^2 + (q-1)$. This is a bound on the size of an entry in our invariant stabilizer of $q - 1 + k(q-1)^2 + (q-1) = (2 + k(q-1))(q-1)$. ■

Example 23. *In this example we show that CSS codes remain CSS codes under this transformation. Consider a general CSS code given by:*

$$\phi(\Xi) = \left[\begin{array}{ccc|ccc} I_{k_1} & X_{k_2} & X_{n-(k_1+k_2)} & 0 & 0 & 0 \\ 0 & 0 & 0 & Z_{k_1} & I_{k_2} & Z_{n-(k_1+k_2)} \end{array}\right] \tag{5.23}$$

where we have put the two block matrices into approximately standard form. Now, we perform Hadamards (or discrete Fourier transforms) on the k_2 sized middle blocks. We then have:

$$\phi(\Xi) = \left[\begin{array}{ccc|ccc} I_{k_1} & 0 & X_{n-(k_1+k_2)} & 0 & X_{k_2} & 0 \\ 0 & I_{k_2} & 0 & Z_{k_1} & 0 & Z_{n-(k_1+k_2)} \end{array}\right]. \tag{5.24}$$

Now, we note that the first k_1 stabilizers exactly commute with each other, i.e., inner product 0 in the ϕ_∞ sense, and likewise for the k_2 other stabilizer generators. Now we simply need to consider the case where we pick generators from each of the halves. We consider the matrix $[\odot]$, as above. This has nonzero entries for rows in k_2 when the columns are in k_1. Likewise for when the rows are in k_1, the entries are nonzero for columns in k_2. Thus we only add entries to Z_{k_1} and X_{k_2} with $[\odot]$ and, hence, certainly also for our L matrix. In fact, the L matrix adds entries only to Z_{k_1} since it is lower triangular. Given the new invariant form matrix, we may now invert our initial step of applying discrete Fourier transforms and we will still have a CSS code.

While the proof of Theorem 20 used $L_{ij} = \phi_\infty(s_i) \odot \phi_\infty(s_j)$ in order to generate a single LDI form, we may generate other LDI forms by altering the added L matrix. We note two of these now: $L^{(+)}$ and $L^{(-)}$.

Definition 24. *$L^{(+)}$ ($L^{(-)}$) has $L^{(+)}_{ij}$ ($L^{(-)}_{ij}$) is $\phi_\infty(s_i) \odot \phi_\infty(s_j)$ if the symplectic product is greater than zero (less than zero).*

These alternative L matrices each provide a different property. Firstly, using $L^{(+)}$ allows $\phi_\infty(S)$ to have only non-negative entries. There are certain properties that are only generally true for matrices with non-negative entries, so this can perhaps be of use. Additionally, this could be of use for systems formally with countably infinite local-dimension, such as Bosonic systems, where operators with negative powers are not feasible. Secondly, $L^{(-)}$ permits a slight reduction in the bound for the maximal entry in $\phi_\infty(S)$, as the following Lemma shows:

Lemma 25. *The maximal entry in $\phi_\infty(S)$, B, can be at most $(1 + k(q-1))(q-1)$, and generally $B \leq \max_{i,j} |\phi_\infty(s_i) \odot \phi_\infty(s_j)|$.*

Upon putting the code into canonical form this follows immediately from the definition of $L^{(-)}$ as each entry will be whatever value was already in that location (values in $\mathbb{Z}_q$) minus the absolute value of the inner product, which will be at most the absolute value of the inner product. While this is a small improvement on the value of B, since it will be the base of an exponential expression this amounts to a larger improvement in the overall cutoff value.

While these are a few ways of generating LDI forms, there are a very large number of options. Finding a collection of entries, which are congruent to zero modulo the initial local-dimension, that generates all trivial commutations is equivalent to finding solutions to a system of linear, homogeneous, Diophantine equations with a large surplus of variables [113]. Given this, there is good reason to believe that far tighter bounds on B may be possible.

5.5 LDI Proofs of Distance Promise Bounds

Now that we know that all qudit codes can be put into an LDI form, we now prove that at least for sufficiently large local-dimension values we can ensure that the distance of the code is at least preserved. We find a cutoff on the number of bases in the underlying space needed to at least preserve the distance.

Theorem 26. *For all primes $p > p^*$, with p^* a cutoff value greater than q, the distance of an LDI form for a non-degenerate stabilizer code $[[n, k, d]]_q$ used for a system with p bases, $[[n, k, d']]_p$, has $d' \geq d$.*

To make claims about the distance of the code we begin by breaking down the set of undetectable errors into two sets. These definitions highlight the subtle possibility of the distance reducing upon changing the local-dimension.

Definition 27. *An unavoidable error is an error that commutes with all stabilizers and produces the $\vec{0}$ syndrome over the integers.*

These correspond to undetectable errors that would remain undetectable regardless of the number of bases for the code since they always exactly commute under the symplectic inner product with all stabilizer generators–and so all members of the stabilizer group. Since these errors are always undetectable we call them unavoidable errors since changing the number of bases would not allow this code to detect this error. This then provides the following insight:

Remark 28. *The distance of a code over the integers is given by the minimal weight member in the set of unavoidable errors. The distance over the integers is represented by d^*, and so $d^* \geq d$. This value is also the minimum number of columns of the stabilizer generator matrix that are linearly dependent over the integers (or equivalently over the rationals), in the symplectic sense.*

We also define the other possible kind of undetectable error for a given number of bases, which corresponds to the case where some syndromes are multiples of the number of bases:

Definition 29. *An artifact error is an error that commutes with all stabilizers but produces at least one syndrome that is only zero modulo the base.*

These are named artifact errors as their undetectability is an artifact of the number of bases selected and could become detectable if a different number of bases were used with this code. Each undetectable error is either an unavoidable error or an artifact error. We utilize this fact to show our theorem.

Proof. The ordering of the stabilizers and the ordering of the registers does not alter the distance of the code. With this, ϕ_∞ for the stabilizer generators over the integers can have the rows and columns arbitrarily swapped.

Let us begin with a code over q bases and extend it to p bases. The errors for the original code are the vectors in the kernel of ϕ_q for the code. These errors are either unavoidable errors or are artifact errors. We may rearrange the rows and columns so that the stabilizers and registers that generate these entries that are nonzero multiples of q are the upper left $2d \times 2d$ minor, padding with identities if needed. The factor of 2 occurs due to the number of nonzero entries in ϕ_∞ being up to double the weight of the Pauli. The stabilizer(s) that generate these multiples of q entries in the syndrome are members of the null space of the minor formed using the corresponding stabilizer(s).

Now, consider the extension of the code to p bases. Building up the qudit Pauli operators by weight j, we consider the minors of the matrix composed through all row and column swaps. These minors of size $2j \times 2j$ can have a nontrivial null space in two possible ways:

- If the determinant is 0 over the integers then this is either an unavoidable error or an error whose existence did not occur due to the choice of the number of bases.
- If the determinant is not 0 over the integers, but takes the value of some multiple of p, then it's $0 \mod p$ and so a null space exists.

Thus we can only introduce artifact errors to decrease the distance. By bounding the determinant by p^*, any choice of $p > p^*$ will ensure that the determinant is a unit in $\mathbb{Z}_p$, and hence have a trivial null space since the matrix is invertible.

Now, in order to guarantee that the value of p is at least as large as the determinant, we can use Hadamard's inequality to obtain:

$$p > p^* = B^{2(d-1)}(2(d-1))^{(d-1)} \tag{5.25}$$

where B is the maximal entry in ϕ_∞. Since we only need to ensure that the artifact induced null space is trivial for Paulis with weight less than d, we used this identity with $2(d-1) \times 2(d-1)$ matrices.

When $j = d$, we can either encounter an unavoidable error, in which case the distance of the code is d or we could obtain an artifact error, also causing the distance to be d. It is possible that neither of these occur at $j = d$, in which case the distance becomes some d' with $d < d' \leq d^*$. ■

We alluded prior to this proof that the code over the integers has distance at least as large. To determine how many bases are needed to ensure we have distance d^*, we simply extend our above result to obtain the cutoff expression, whereby no further distance improvements can be obtained from embedding the code–suggesting that another code ought to be used.

Corollary 30. *For a non-degenerate stabilizer code we obtain the integer distance d^* when:*

$$p > B^{2(d^*-1)}(2(d^*-1))^{d^*-1}. \tag{5.26}$$

After this value the distance cannot be improved through embedding. If d^* is unknown, this can be upper bounded by using $n-k$ in place of d^*.

Proof. This follows from the above proof. The looser bound comes from $d^* \leq n-k$, so we can evaluate this at $d^* = n-k$ to obtain the loosest condition. ■

As a brief example of using this theorem, let us consider the Steane code again:

Example 31. *In our example of the Steane code, Corollary 22 tells us that the maximal entry is at most 3, but from our application of the method given in Theorem 20, we have $B = 1$ so we defer to this value since it's the true maximal entry value. The original distance was $d = 3$. This means that for all primes larger than $1^{2\cdot 2}(2 \cdot 2)^2 = 16$ we are guaranteed that the distance is preserved. For primes below that value, we can manually*

check and apply alternate manipulations if needed. Given that all entries are ± 1*, we know that the determinant of all the minors of interest are bounded by* 4*, all primes at least as large as* 5 *preserve the distance. Through manual checking 3 is also not a possible minor determinant, so all primes preserve the distance for our LDI form of the Steane code.*

We also have the following theorem which provides an alternative bound utilizing the structure of the symplectic product more directly as well as block matrix formulas:

Theorem 32. *For all primes* $p > p^*$ *the distance of an LDI representation of a non-degenerate stabilizer code* $[[n, k, d]]_q$ *over* p *bases,* $[[n, k, d']]_p$*, has* $d' \geq d$*, where we may use as* p^* *the value:*

$$(B(q-1)(d-1)(1+(d-1)^2(q-1)^{d-1}(d-2)^{(d-2)/2}))^{d-1}, \tag{5.27}$$

with q *the initial local-dimension,* d *the distance of the initial code, and* B *the maximal entry in the* ϕ_∞ *representation of the code.*

Proof. Let us begin with a code with local-dimension q and apply it to a system with local-dimension p. The errors for the original code are the vectors in the kernel of ϕ_q for the code. These errors are either unavoidable errors or are artifact errors. The stabilizers that generate these multiples of q entries in the syndrome are members of the null space of the minor formed using the corresponding stabilizers.

Now, consider the extension of the code to p bases. Building up the qudit Pauli operators by weight j, we consider the minors of the matrix. These minors of size $2j \times 2j$ can have a nontrivial null space in two possible ways:

- If the determinant is 0 over the integers then this is either an unavoidable error or an error whose existence did not occur due to the choice of the number of bases.
- If the determinant is not 0 over the integers, but takes the value of some multiple of p, then it's $0 \mod p$ and so a null space exists.

Thus we can only introduce artifact errors to decrease the distance. By bounding the determinant by p^*, any choice of $p > p^*$ will ensure that the determinant is a unit in $\mathbb{Z}_p$, and hence have a trivial null space since the matrix is invertible.

We next utilize the structure of the symplectic product more heavily in order to reduce the cutoff local-dimension. Note that for a pair of Paulis in the ϕ representation, we may

write:

$$\begin{aligned}\phi(s_1) \odot \phi(s_2) &= \phi(s_1) \begin{bmatrix} 0 & -I_n \\ I_n & 0 \end{bmatrix} \phi(s_2)^T \quad (5.28)\\ &:= \phi(s_1) g \phi(s_2)^T \quad (5.29)\end{aligned}$$

and so we may consider the commutation for the generators with some Pauli u as being given by $\bigoplus_{i=1}^{n-k}(\phi(s_i)g)\phi(u)^T$, where $\bigoplus$ is a direct sum symbol here, indicating that a vector of syndrome values is returned. This removes the distinction between the two components and allows the symplectic product to act like the normal matrix-vector product. Now, notice that for any Pauli weight j operator, we will have up to j nonzero entries in the X component of the ϕ representation and up to j nonzero entries in the Z component. This means that up to j columns in each component will be involved in any commutator.

Next, note that to ensure that an artifact error is not induced it suffices to ensure that there is a nontrivial kernel, induced by the local-dimension choice, which is ensured so long as any $2(d-1) \times 2(d-1)$ minor does not have a determinant which is congruent to the local-dimension. This can be promised by requiring the local-dimension to be larger than the largest possible determinant for such a matrix. Since there will be at most j nonzero entries in each component it suffices to consider j columns from each component and subsets of $2j$ rows of this.

From this reduction, we need only ensure that the local-dimension is larger than the largest possible determinant for this $2j \times 2j$ minor. Let us denote this minor by:

$$\begin{bmatrix} X_1 & Z_1 \\ X_2 & Z_2 \end{bmatrix}, \quad (5.30)$$

where each block has dimensions $j \times j$. The maximal entries are $q-1$ for X_1 and X_2, whereas for Z_1 and Z_2 it is bounded by B. We now use the block matrix identity:

$$det \begin{bmatrix} X_1 & Z_1 \\ X_2 & Z_2 \end{bmatrix} = det(X_1) det(Z_2 - X_2 X_1^{-1} Z_1). \quad (5.31)$$

Since all entries in X_1 are integers and the determinant is, by construction, nonzero, the maximal entry in X_1^{-1} will be at most that of the largest cofactor of X_1. The largest cofactor, $\tilde{C}$, will be at most $(q-1)^{d-2}(d-2)^{(d-2)/2}$, as provided by Hadamard's inequality. The largest entry in $Z_2 - X_2 X_1^{-1} Z_1$ is then upper bounded by $B(1 + (q-1)\tilde{C}(d-1)^2)$. From here, we may apply Hadamard's inequality for determinants again using the given entry bounds, using that each block has dimensions up to $(d-1) \times (d-1)$, which provides

$p^* = (q-1)^{d-1}(d-1)^{d-1}(B(1+(q-1)\tilde{C}(d-1)^2))^{d-1}$, or alternatively expressed in terms of our fundamental variables as

$$(B(q-1)(d-1)(1+(d-1)^2(q-1)^{d-1}(d-2)^{(d-2)/2}))^{d-1}. \tag{5.32}$$

In the case of $q = 2$ this reduces to $(B(d-1)(1+(d-1)^2(d-2)^{(d-2)/2}))^{d-1}$.

Lastly, when $j = d$, we can either encounter an unavoidable error, in which case the distance of the code is d or we could obtain an artifact error, also causing the distance to be d. It is possible that neither of these occur at $j = d$, in which case the distance becomes some d' with $d < d' \leq d^*$, with d^* being the distance of the code over the integers. ■

Before concluding this section, we provide a brief comparison of this bound to the original one of $B^{2(d-1)}(2(d-1))^{(d-1)}$. The new bound only depends on B^{d-1} opposed to the original $B^{2(d-1)}$, which as the bound on B depends on k means that for codes, or code families, with larger k values the new bound can provide a tighter expression. Unfortunately, however, this new bound is doubly-exponential in the distance of the code d, having a dependency of roughly d^{d^2} opposed to the prior dependency of d^d, so if one is attempting to promise the distance of a code with a larger distance, this new bound is likely to be far less tight. In summary, this alternative bound is not per se better, however, since one may simply use whichever of the bounds is tighter this alternative bound may provide a lower requirement for the local-dimension needed in order to ensure that the distance of the code is at least preserved.

5.5.1 Degenerate Codes

Degenerate codes are a uniquely quantum phenomenon, which suggests that they are a crucial class of quantum error-correcting codes in order to obtain certain properties. For a degenerate quantum error-correcting code we must avoid undetectable errors, but also detectable errors which produce the same syndrome but do not map to the same physical codeword. Any LDPC-like quantum error-correcting code will be degenerate, as, equivalently, a quantum error-correcting code is degenerate if there is some stabilizer group member with lower weight than the distance of the code and by construction one would aim to have a high distance for a quantum LDPC code but still $O(1)$ weight for each generator. We show now that a similar distance promise may be made in the degenerate case as was possible in the non-degenerate case, and remark on what differences exist between the two classes in the local-dimension-invariant framework in the next section.

Theorem 33. *For all primes $p > p^*$ the distance of an LDI representation of a degenerate stabilizer code $[[n, k, d]]_q$ over p bases, $[[n, k, d']]_p$, has $d' \geq d$, where p^* is the same function of n, k, d, and q as before.*

Proof. In the case of non-degenerate codes all undetectable errors, up to distance d, were in the normalizer of the generators, $\mathcal{N}(S)$, as the weight of all members of the stabilizer group have weight at least d. For degenerate codes we only need to be concerned about elements in $\mathcal{N}(S)/S$, as now there are some members of the stabilizer group which might have weight below d. The latter set is a subset of the former ($\mathcal{N}(S)/S \subset \mathcal{N}(S)$), and so the same distance promise is obtained as before. ■

Notice that all Paulis with weight less than d that are in S produce a syndrome that is all zeros, over the integers, and so may appear to be within the category of unavoidable errors when syndromes are computed. This means that when checking the distance this must carefully be taken into account, otherwise the members in S may be mistaken for these errors leading to an erroneous distance value.

This means that just like non-degenerate quantum codes, we may also promise the distance of the code in the degenerate case, and with the same cutoff bound. This provides both classes of stabilizer codes and so provides a distance promise for all stabilizer codes.

5.5.2 Brief Aside: MDS Codes

The quantum Singleton bound is given by $n - k \geq 2(d - 1)$ [114]. All stabilizer codes must satisfy this bound. One could aim to design codes which saturate this universal bound. Such codes are called Maximally Distance Separated (MDS) codes.

Corollary 34. *Given an MDS code with parameters $[[n, k, d]]_q$, we may generate an MDS code with parameters $[[n, k, d]]_p$ for all $p > p^*$.*

This suggests that perhaps MDS codes, while optimal in some sense (saturating the quantum Singleton bound), and their MDS property may not be the best metric for optimality when considering local-dimension choices as well [115]. The generalized quantum Hamming bound is local-dimension aware, however, codes which saturate this bound–known as perfect codes–are fully enumerated and cannot have distance 5 or above [98]. Additionally the generalized quantum Hamming bound does not always hold for degenerate stabilizer codes. This means that perhaps focusing on the MDS property of codes is not a great metric for quality always.

5.6 Opposite Direction Distance Promises

The above provides a condition on the number of bases needed to ensure the distance of the code is at least preserved, but one could also ask, given an LDI code, whether that code can be used over fewer bases. We provide a bound on this with the following:

Lemma 35. *For a non-degenerate code, for all $p < p^{**}$, with p^{**} a cutoff value less than q (possibly ≤ 2), the distance of $[[n, k, d]]_q$ over p bases, $[[n, k, d']]_p$, must have $d' < d$.*

Proof. Let $t = \lfloor \frac{d-1}{2} \rfloor$. The qudit quantum Hamming bound requires the initial code to satisfy:

$$\sum_{j=0}^{t} \binom{n}{j} (q^2 - 1)^j \leq q^{n-k}. \tag{5.33}$$

Now we consider applying the code over p levels. Then we may bound:

$$\binom{n}{t} (p^2 - 1)^t \leq \sum_{j=0}^{t} \binom{n}{j} (p^2 - 1)^j. \tag{5.34}$$

Likewise, when $p \geq 2$ we may bound:

$$p^{n-k} \leq (p^2 - 1)^{n-k}. \tag{5.35}$$

Combining these we have:

$$\binom{n}{t} (p^2 - 1)^t \leq (p^2 - 1)^{n-k}. \tag{5.36}$$

Then we violate the initial inequality if:

$$p < \sqrt{1 + \binom{n}{t}^{1/((n-k)-t)}} = p^{**} \tag{5.37}$$

This means that p^{**} is only a valid bound when it is larger than 2, otherwise this result is trivially true since we no longer have a quantum code. ■

Combining these results mean that distance *may* be preserved for $p^{**} \leq p < p^*$, while for $p > p^*$ it is guaranteed to have the distance preserved. For the region of values of p where the distance might be preserved, one can manually check and attempt another LDI form to try to make the distance preserved for the desired number of bases.

The expression for p^{**} was derived by using the generalized quantum Hamming bound, which holds for all non-degenerate codes, however, for degenerate codes this bound does not always hold as there is no longer a bijective relationship between correctable errors and syndromes. This means that for a general degenerate code we have the following Lemma:

Lemma 36. *There is no corresponding p^{**} that holds for arbitrary degenerate codes.*

While not all degenerate quantum codes obey the generalized quantum Hamming bound, there are certain code families which do [107, 116]. For those code families the exact same expression for p^{**} holds as did for non-degenerate codes.

The non-existence of a p^{**} expression for arbitrary degenerate codes provides an opportunity. Consider a code whose initial local-dimension q is far larger than 2. In the non-degenerate case this p^{**} provides a local-dimension value below which the distance of the code must decrease, but for degenerate codes the lack of this means that it may be possible to apply the code over a far smaller local-dimension, even local-dimension 2, and still preserve all of the parameters, and particularly the distance. This suggests that it may be possible to import codes into lower local-dimension values than previously expected.

We conclude this section by briefly summarizing the distance promises. We will be referring to figure 5.1, where the x-axis is the local-dimension and the y-axis is promise on the distance of the code. Below p^{**} we know that the distance of the code must be lower than the initial distance d. For $p^{**} < p < q$, we have no information about the distance of the code from any of our results. Codes in this region would be those which can be applied over a smaller local-dimension than their initial design. Following this, we know that at local-dimension q the distance is unchanged as the LDI form does not alter the code over q. Between q and p^* we again have no promises on the distance of the code, however, we do have multiple expressions for p^*, so any further reductions in this value would lower the cutoff value for the local-dimension needed to preserve the distance of the code. In section 5.8 we show a particular case whereby this cutoff can be slightly super quadratically improved. Proceeding, between p^* and $p^*(d^*)$ we know that the distance of the code must be at least d but could be as high as d^* (the distance over the integers). Finally, for local-dimensions larger than $p^*(d^*)$ we know that the distance of the code must be d^*. It is possible that $d^* = d$, however, it is not certain, hence we make the distinction in the schematic diagram.

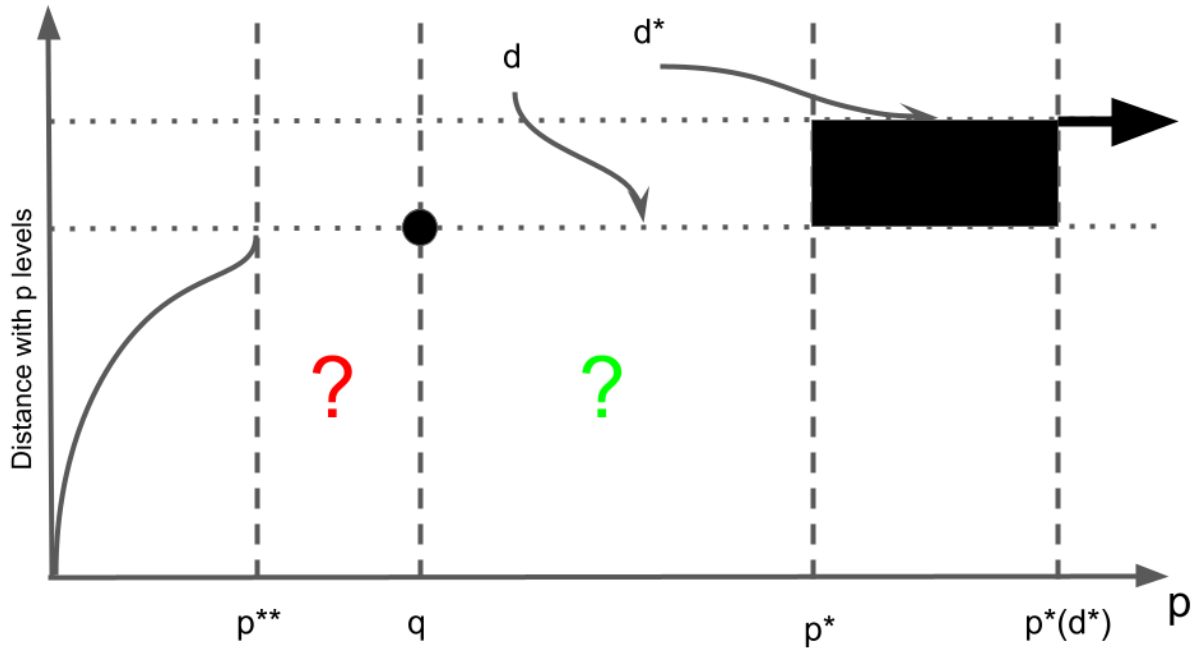

Figure 5.1: Distance promises in the non-degenerate code case for LDI codes. Along the x-axis is the newly selected local-dimension for the LDI code transformed from initial local-dimension q.

5.7 Logical Operators for LDI Codes

Besides from the stabilizers we also need logical operators to perform computations over the encoded qudits. Now we show how to construct such invariant logical operators.

Lemma 37. *We may define invariant logical operators, $\mathcal{L}_\infty$, for the stabilizer code* $\mathbf{S}$ *as well.*

Proof. Each logical operator is in $N(\mathbf{S})/\mathbf{S}$, the normalizer of $\mathbf{S}$ excluding $\mathbf{S}$, and there are k X logical operators and k Z logical operators. This means that we could, if we desired, generate a code $\mathbf{S}'$ whose generators are $\mathbf{S} \cup L_X$. This will have rank n and can be written in standard form as:

$$\left[I_n | * \right] \tag{5.38}$$

meaning that L_X may be diagonalized within the last k qudits. This can also be done with L_Z.

Then, since these logical operators are compositionally independent, they must be linearly independent in the ϕ representation, meaning $rank(L_X \cup L_Z) = 2k$. Now, if we take the standard form for $\mathbf{S}$ and append L_X, L_Z as additional rows we have:

$$\begin{bmatrix} \mathbf{S} \\ L_X \\ L_Z \end{bmatrix} = \left[\begin{array}{ccc|cc} I_{n-k} & A & | & B & C \\ 0 & D & | & E & F \\ 0 & G & | & H & J \end{array}\right] \tag{5.39}$$

From the above observation it is possible to compose the generators for L_X, L_Z to generate the matrix:

$$\left[\begin{array}{ccc|cc} I_{n-k} & A & | & B & C \\ 0 & I_k & | & E' & F' \\ 0 & G' & | & H' & I_k \end{array}\right] \tag{5.40}$$

At this point we focus on fixing the commutators between elements of L_X and L_Z. Since the first k qudits will always contribute 0 to the commutator we drop those columns:

$$\left[\begin{array}{c|c} I_k & F' \\ G' & I_k \end{array}\right] \tag{5.41}$$

We can further reduce this to:

$$\left[\begin{array}{c|c} I_k & 0 \\ 0 & I_k \end{array}\right] \tag{5.42}$$

This trivially satisfies the required relations:

$$\phi_q(\bar{X}_i) \odot \phi_q(\bar{Z}_j) = \delta_{ij} \tag{5.43}$$

$$\phi_q(\bar{X}_i) \odot \phi_q(\bar{X}_j) = \phi_q(\bar{Z}_i) \odot \phi_q(\bar{Z}_j) = 0, \quad \forall i, j \tag{5.44}$$

Throughout these computations we have updated E' and H'. We now simply apply Theorem 20 to each logical operator in turn appended to $\phi(\mathbf{S})$. ■

Remark 38. *This process does not alter our invariant stabilizer form, so our bound from earlier still holds.*

5.8 Calderbank-Shor-Steane (CSS) Case

We now proceed to a new result related to local-dimension-invariant (LDI) codes in the case of Calderbank-Shor-Steane (CSS) codes. In Example 23, we showed that CSS structure

can be preserved when transformed into an LDI form. CSS codes have a set of independent generators only using X operators or Z operators for each generator.

Figure 5.2 illustrates the initial distance promises proven for arbitrary stabilizer codes, as well as the improvements to be shown in the case of CSS codes. For local-dimensions p with $q < p < p^*$, the distance of the code is uncertain. For this uncertainty region the distance could be lower, it could be the same, or it could even be higher, however, it must be determined manually. It is conjectured that for $q \leq p$ the distance can be at least preserved, however, this is only known to be possible for a few codes, such as the 5, 7, and 9 particle codes [110, 2, 111]. This section adds to this collection an infinite family. While the distance is promised to be at least the same for $p^* < p$, the caveat is that the current bound for p^* for an arbitrary stabilizer code is very large: $p^* = B^{2(d-1)}(2(d-1))^{d-1}$ with B being the largest entry in the LDI form. This value is typically large, so reductions to it is crucial to make the technique of more practical use. In the class of CSS codes we may reduce this cutoff value roughly quadratically: $p^*_{CSS} \approx \sqrt{p^*}$.

Theorem 39. *For all primes p, $p > p^*_{CSS}$, with $p^*_{CSS} = B^{d-1}(d-1)^{(d-1)/2}$, the distance of a local-dimension-invariant CSS code with parameters $[[n,k,d]]_q$ used over p levels with parameters $[[n,k,d']]_p$, has $d' \geq d$.*

The proof of Theorem 39 follows using largely the same argument as before.

Proof. We begin by recalling that Example 23 showed that LDI codes, using the given method, preserve CSS structure. CSS codes take the structure:

$$\left[\begin{array}{c|c} \mathcal{X} & 0 \\ 0 & \mathcal{Z} \end{array}\right]. \tag{5.45}$$

The distance preservation property may then be considered separately within the two blocks $\mathcal{X}$ and $\mathcal{Z}$. This effectively reduces the Pauli weight of an error to the Hamming weight of the error within a single error-axis. Each block only has nonzero valued syndrome values for Z and X terms in a Pauli respectively. Given this, the Pauli weight for any error activating syndromes in just the $\mathcal{X}$ portion is the same as the Hamming weight for those operators. This is likewise the case for the $\mathcal{Z}$ portion. This then means that in order to have an undetectable error it must be undetectable within the $\mathcal{X}$ portion and within the $\mathcal{Z}$ portion.

Next, undetectable errors correspond to nontrivial kernels of matrix minors. Consider building up the errors composed solely of Z operators by their Hamming weight w. The kernel is nontrivial if the $w \times w$ matrix minor corresponding to this Hamming string has

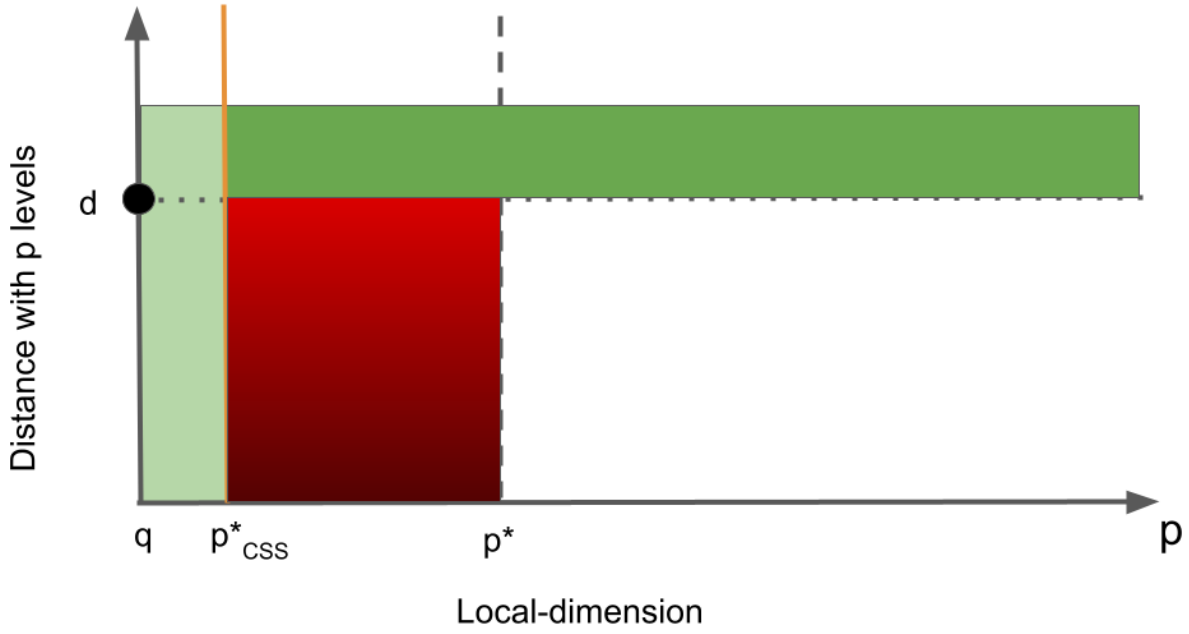

Figure 5.2: This schematic image illustrates the effect of finding a reduced expression for the cutoff value for the distance promise. The light green area on the left is the set of local-dimension values which must have their distance manually checked, the red region is the set of local-dimension values which must have their distance manually checked for a CSS code if the general p^* expression is used, whereas when p^*_{CSS} is used that region automatically has the distance promised.

a determinant that is congruent to zero modulo the local-dimension. To avoid tracking the locations of the Hamming weights we allow ourselves to arbitrarily permute the entries within each portion of the CSS code. The determinant for a minor can be zero in two different ways:

- If the determinant is 0 over the integers then this error is either an unavoidable error or an error whose existence did not occur due to the choice of the local-dimension.
- If the determinant is not 0 over the integers, but is merely some multiple of the local-dimension, then this corresponds to an artifact error.

This means that we only have to worry about this second case lowering the distance upon changing the local-dimension. If the determinant of this minor can be guaranteed to be

smaller than the local-dimension then we are promised that the distance will at least remain the same. We may bound the determinant of a $w \times w$ matrix minor using Hadamard's inequality, which we evaluate at $d-1$ since we only need to ensure no artifact errors are induced prior to weight d. This then provides:

$$p^*_{CSS} = B^{d-1}(d-1)^{(d-1)/2}. \tag{5.46}$$

Then so as long as the local-dimension is larger than this no Z error will result in a distance lower than d. This same argument can be made for X errors, which completes the proof. ■

In essence this is based on needing only to perform the prior distance promise proof over each of the two blocks in these codes and only needing to worry about the Pauli weight of the error in each block being the same as the Hamming weight. This is slightly better than a quadratic improvement over the general p^* bound. This is a step toward decreasing the value of p^* significantly enough to make this method of practical use. Let us consider the utility of this improvement for the qubit Hamming family, with parameters $[[2^N-1, 2^N-1-2N, 3]]_2$. The first member of this family, H_3, is known as the Steane code with parameters $[[7,1,3]]_2$ [82]. An LDI form, with parameters $[[7,1,\geq 3]]_q$, for this code was found earlier in this chapter as:

$$\phi_\infty(H_3) = \left[\begin{array}{ccccccc|ccccccc} 1&0&0&0&0&0&1&0&0&0&0&1&1&0\\ 0&1&0&0&0&0&0&0&0&0&1&1&1&0\\ 0&0&1&0&0&0&1&0&0&0&1&0&1&0\\ 0&0&0&1&0&0&0&-1&1&0&0&0&0&1\\ 0&0&0&0&1&0&0&0&1&-1&0&0&0&1\\ 0&0&0&0&0&1&0&1&1&1&0&0&0&0 \end{array}\right]. \tag{5.47}$$

We return this code to CSS form by applying DFTs on particles 4, 5, and 6:

$$\phi_\infty(H_3) = \left[\begin{array}{ccccccc|ccccccc} 1&0&0&0&1&1&1&0&0&0&0&0&0&0\\ 0&1&0&1&1&1&0&0&0&0&0&0&0&0\\ 0&0&1&1&0&1&1&0&0&0&0&0&0&0\\ 0&0&0&0&0&0&0&-1&1&0&-1&0&0&1\\ 0&0&0&0&0&0&0&0&1&-1&0&-1&0&1\\ 0&0&0&0&0&0&0&1&1&1&0&0&-1&0 \end{array}\right]. \tag{5.48}$$

Using the bound for p^* without knowing the code is CSS but knowing that the maximal entry is 1, we find $p^* = 16$. This leaves a handful of primes still to verify the distance over.

If instead we use Theorem 39 with the known maximal entry of 1 we obtain $p^* = 1^2 2^{2/2}$, which is 2. This means that the distance of this code is always at least preserved. While this was discussed before, this provides a quicker way to obtain this fact and illustrates the improvements obtained here.

The prior description of an LDI representation for the Steane code used the prescriptive method for generating an LDI form for the code, however, we could have equivalently performed the following alteration:

$$\phi_2(H_3) = \left[\begin{array}{ccccccc|ccccccc} 1 & 1 & 1 & 1 & 0 & 0 & 0 & 0 & 0 & 0 & 0 & 0 & 0 & 0 \\ 0 & 1 & 1 & 0 & 1 & 1 & 0 & 0 & 0 & 0 & 0 & 0 & 0 & 0 \\ 0 & 1 & 0 & 1 & 1 & 0 & 1 & 0 & 0 & 0 & 0 & 0 & 0 & 0 \\ 0 & 0 & 0 & 0 & 0 & 0 & 0 & 1 & 1 & 1 & 1 & 0 & 0 & 0 \\ 0 & 0 & 0 & 0 & 0 & 0 & 0 & 0 & 1 & 1 & 0 & 1 & 1 & 0 \\ 0 & 0 & 0 & 0 & 0 & 0 & 0 & 0 & 1 & 0 & 1 & 1 & 0 & 1 \end{array}\right]. \tag{5.49}$$

We then put the code into an LDI form by flipping the signs of some of the entries, producing:

$$\phi_\infty(H_3) = \left[\begin{array}{ccccccc|ccccccc} 1 & 1 & 1 & 1 & 0 & 0 & 0 & 0 & 0 & 0 & 0 & 0 & 0 & 0 \\ 0 & 1 & 1 & 0 & 1 & 1 & 0 & 0 & 0 & 0 & 0 & 0 & 0 & 0 \\ 0 & 0 & 1 & 1 & 0 & 1 & 1 & 0 & 0 & 0 & 0 & 0 & 0 & 0 \\ 0 & 0 & 0 & 0 & 0 & 0 & 0 & 1 & -1 & 1 & -1 & 0 & 0 & 0 \\ 0 & 0 & 0 & 0 & 0 & 0 & 0 & 0 & 1 & -1 & 0 & 1 & -1 & 0 \\ 0 & 0 & 0 & 0 & 0 & 0 & 0 & 0 & 0 & 1 & -1 & 0 & -1 & 1 \end{array}\right]. \tag{5.50}$$

Intuitively, we select signs so that the Z rows add to zero, and also add to zero within the blocks corresponding to those in the X rows. This also satisfies the same distance promise–always having distance at least 3, regardless of the local-dimension. In fact, we can extend this method of flipping the signs of some entries in this code to that of the whole family of codes within the $[[2^N - 1, 2^N - 1 - 2N, 3]]_2$ family. We show that this sign flipping can always generate an LDI representation for the code. In particular, we find that for this family we can prove a tight bound on the value of the maximal entry:

Lemma 40. *For the qubit quantum Hamming code family with parameters* $[[2^N - 1, 2^N - 1 - 2N, 3]]_2$*, there is an LDI representation such that* $B = 1$ *for all members of the family.*

Recall that this family is generated by each column being one of the nonzero binary strings of length N in each the X component and the Z component. We will take the register placement of each string to be the same in the X component and the Z component.

Proof. We begin by noting that for the $N = 3$ case we already have the Steane code discussed just above (equation (5.50)). We will now prove inductively that we may always generate an LDI form such that $B = 1$. Let H_N^∞ be the N-th family member such that all generators in H_N^∞ commute with those of H_N. Next, consider for $N \geq 4$, one can write the next member of the family in terms of the prior member as:

$$\phi_2(H_{N+1}) = \left[\begin{array}{ccc|ccc} 1 & 1^{\otimes 2^N-1} & 0^{\otimes 2^N-1} & 0 & 0 & 0 \\ 0 & H_N & H_N & 0 & 0 & 0 \\ 0 & 0 & 0 & 1 & 1^{\otimes 2^N-1} & 0^{\otimes 2^N-1} \\ 0 & 0 & 0 & 0 & H_N^\infty & H_N^\infty \end{array}\right], \tag{5.51}$$

with the superscript $\otimes$ indicating repetition of that value. However, this version of the code is not in an LDI representation. We make the following sign changes and then verify that this version is an LDI representation:

$$\phi_\infty(H_{N+1}^\infty) = \left[\begin{array}{ccc|ccc} 1 & 1^{\otimes 2^N-1} & 0^{\otimes 2^N-1} & 0 & 0 & 0 \\ 0 & H_N & H_N & 0 & 0 & 0 \\ 0 & 0 & 0 & 1 & v & 0^{\otimes 2^N-1} \\ 0 & 0 & 0 & 0 & H_N^\infty & H_N^\infty \end{array}\right], \tag{5.52}$$

where $v = (-1 \bigoplus 1)^{\otimes 2^{N-1}-2} \bigoplus (-1)$. By the inductive hypothesis all operators in H_N commute with those of H_N^∞. Next, the first row commutes with the first nontrivial row in the Z component as there are an equal number of -1 and $+1$ in v. The sum of each row in H_N^∞ is 0, again due to alternating signs, and so the first row commutes with all rows in H_N^∞. We must lastly ensure that v commutes with each row in H_N. Consider the most recently added row in H_N. This will be given by $1^{\otimes 2^{N-1}} \bigoplus 0^{\otimes 2^{N-1}-1}$, which will commute with v. The following rows will be those of $(0 \bigoplus H_{N-2} \bigoplus H_{N-2})^{\otimes 2}$, which delves one level further down the classical Hamming family. The second repetition of $(0 \bigoplus H_{N-2} \bigoplus H_{N-2})$ trivially commutes as the entries in the Z component are all zero. We then just need $v \odot (0 \bigoplus H_{N-2} \bigoplus H_{N-2}) = 0$. Note that H_{N-2} has an odd number of columns $(2^{N-2} - 1)$, and so the symplectic product terms from the first H_{N-2} will begin with the $+1$ term in v and then alternate, while for the second H_{N-2} the terms will begin with the -1 term in v and then alternate. This means that for every $+1$ there is a -1 and so they commute. ■

While the ability to write this family in an LDI representation only using $\{0, \pm 1\}$ as the entries is of limited interest, applying this result with Theorem 39 we obtain:

Corollary 41. *All qubit Hamming codes have an LDI representation that has distance at least* 3*, meaning that this generates a* $[[2^N - 1, 2^N - 2N - 1, \geq 3]]_q$ *code family for all* $N \geq 3$ *and* q *a prime.*

Proof. This family is a CSS code family. This result then follows from the CSS distance promise for LDI codes and the above Lemma showing that $B = 1$ may be achieved for this family. ■

This shows that the local-dimension-invariant form is at least in some cases able to provide tight expressions that allow for the full importing of code families for larger local-dimension systems. Additionally, this provides another qudit code family, a particularly non-trivial one, with two parameters N and q.

5.9 Additional Examples

To help ground some of the discussions, we provide some more examples next. These illustrate the utility of this framework as well as providing clear examples whereby the choice of LDI form can significantly change the distance promise that can be made.

Example 42. *Consider the qubit code with generators $\langle s_1, s_2\rangle = \langle X^{\otimes n}, Z^{\otimes n}\rangle$, with $n \geq 4$ being an even number. This code has parameters $[[n, n-2, 2]]_2$. $|\phi_\infty(s_1) \odot \phi_\infty(s_2)| = n$, so directly applying Lemma 25, $B = n-1$ is obtained. This provides a bound of $2(n-1)^2$ via the prior bound, while with the new bound shown here this is $(n-1)$. The results then say that the distance is preserved for $p > n-1$.*

Let us take the LDI form for the code as $\langle X^{1-n}X^{\otimes(n-1)}, Z^{\otimes n}\rangle$. Observe that all weight one Paulis do not commute with at least one generator for the code, whereas $IZZ^{-1}I^{\otimes(n-3)}$ is an unavoidable error, so the distance is always $d = 2$.

While this suggests that the determinant bound we showed is incredibly loose, we can write the qubit code in a different LDI form as $\langle (XX^{-1})^{\otimes(n/2)}, Z^{\otimes n}\rangle$. For this form $B = 1$, which provides $p^* = 2$, using either bound, which means that the distance is always at least preserved. This illustrates the impact of careful selection of the LDI form used, and suggests that perhaps with a careful choice of LDI form the bounds provided can be tight for a given code.

Example 43. *As another example let us consider the Shor code, with parameters $[[9, 1, 3]]_2$, and consider a local-dimension-invariant form for it. The Shor code is a degenerate code as the inner blocks of the code have some repeated syndromes. The code has a maximal symplectic product of 2, meaning that there is an LDI form which has $B = 1$. One such*

option is the following set of generators:

$$\langle XX^{-1}II^{\otimes 6},\ IXX^{-1}I^{\otimes 6},\ I^{\otimes 3}XX^{-1}II^{\otimes 3},$$
$$I^{\otimes 3}IXX^{-1}I^{\otimes 3}, I^{\otimes 6}XX^{-1}I,\ I^{\otimes 6}IXX^{-1},$$
$$Z^{\otimes 6}I^{\otimes 3},\ I^{\otimes 3}Z^{\otimes 6}\rangle. \quad (5.53)$$

Using $B = 1$, the bound from [2] is tighter, which provides $p^* = 16$, meaning that so long as the local-dimension is 17 or larger the distance will be at least 3. From here, manual checking, for local-dimensions 3, 5, 7, 11, and 13, verifies that the distance is always preserved. There already was a 9-register code [111], however, this contextualizes the result within the local-dimension-invariant framework. For completeness, a set of logical operators for this code is given by $\bar{X} = XX^{-1}XX^{-1}XX^{-1}XX^{-1}X$ and $\bar{Z} = Z^{\otimes 9}$, which was initially neglected in the definition of the code [111]. For the logical operators we only require that they do not commute with each other, but do commute with the generators for the code–here $\bar{X} \odot \bar{Z} \neq 0$.

5.9.1 The Toric Code

All of the examples considered so far have been traditional stabilizer codes. In more near-term applications of quantum error-correction topological codes have become of greater interest. Amongst topological codes is the toric code, proposed by Kitaev, which has a distance that is the square root of the number of qubits. We examine the toric code here and show how we can put it into an LDI form that always preserves the distance.

The toric code is constructed on a square grid of qubits and its dual square grid also as qubits. The code is CSS with the stabilizer generators given as X operators on the edges of each grid square, and Z operators on the cross from the intersection of squares, see Figure 5.3. We make the proposed modifications in the figure, flipping the power of opposing pairs of Pauli operators within each generator. This allows for compositions to still perfectly commute with all other generators. This simple change provides an LDI form for the code, but does not, yet, guarantee that the distance is preserved.

For the toric code, the logical operators are completely topologically winding strings of a single Pauli operator. This is what gives the code the high distance as the weight of the logical operators is a lower bound on the distance for non-degenerate codes such as this. As an ansantz, we take these same logical operators and consider the coset equivalent forms for them upon interacting with the stabilizer generators. In Figure 5.4 we show two characteristic examples. The top example imagines applying the X stabilizer from below

the middle X operator, which deforms the string. This is exactly the same action as the qubit case, except the left edge is a -1 power instead of $+1$. Consider, however, if we apply the same generator from above. Then the string is deformed like the in qubit case but there is also an added *bridge* in the operator that is impossible in the qubit case (it disappears upon taking $\mod 2$). Now, this behavior could be extended and we could generate more bridges, however, no bridge can fully wind around the torus and generate a non-trivial action on the logical space. This means that the distance is still preserved, although these peculiar bridges appear for the non-qubit case. As of this time, it is not clear whether these bridges provide some possible other changes to the toric code, aside from singular strings not always being the logical operator, but rather strings with possible multiplicities in them.

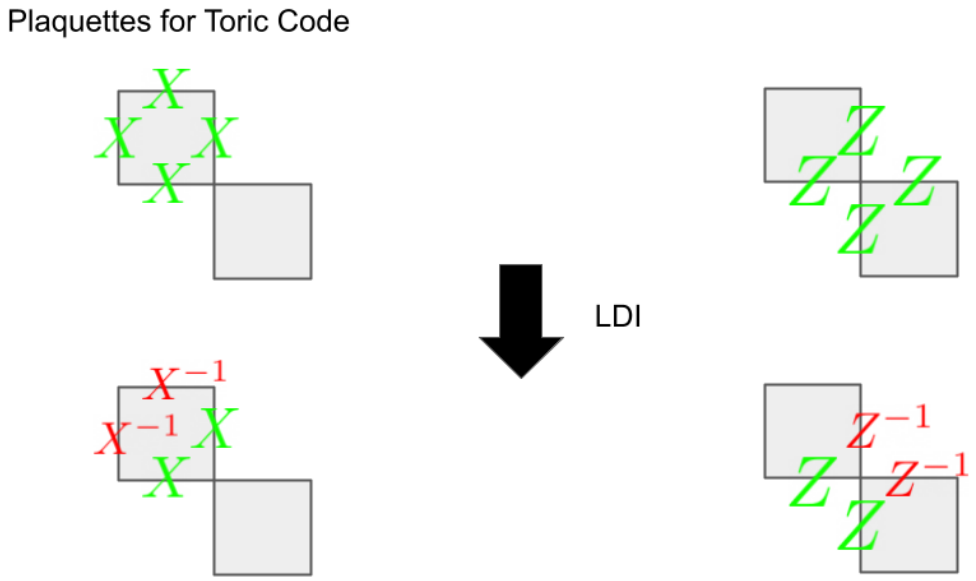

Figure 5.3: This figure shows the transformations on the stabilizing plaquettes for the qubit toric code to generate a toric code that works regardless of the local-dimension of the system. This transforms the code from a $[[2N^2, 2, N]]_2$ code into a $[[2N^2, 2, N]]_q$ code for any prime q.

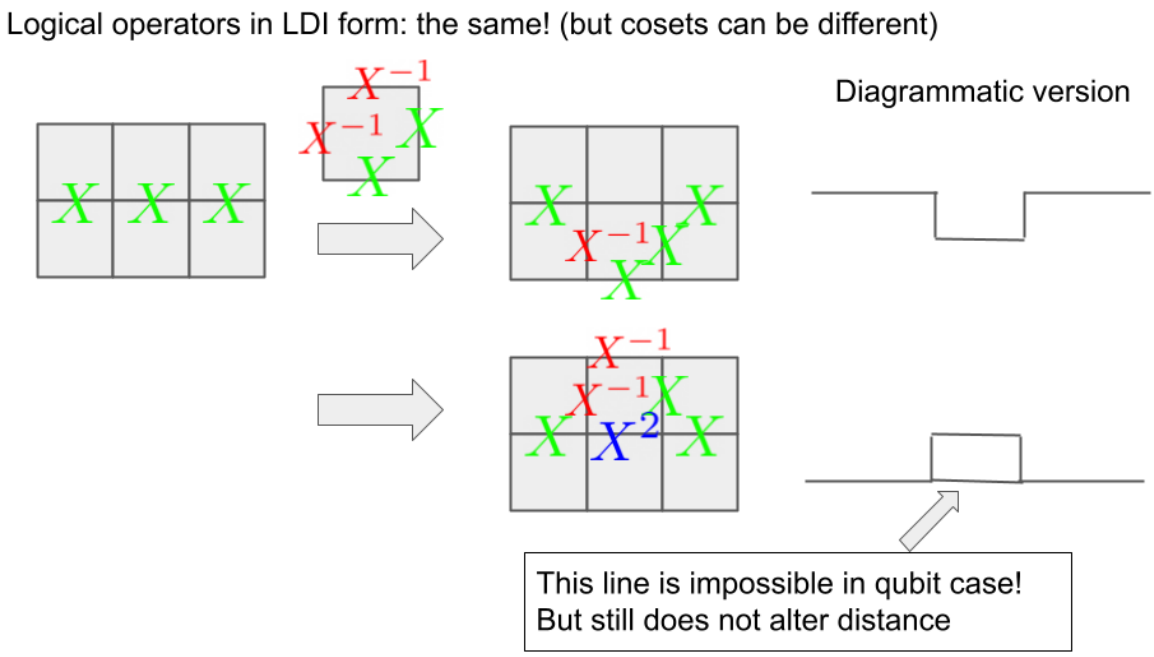

Figure 5.4: This figure illustrates the distance argument, showing that the distance of the code is preserved upon changing the local-dimension of the code. Notice that bridges are generated which are only existent in the non-qubit case.

5.10 Conclusion and Discussion

The local-dimension-invariant (LDI) representation of stabilizer codes allows these codes to be applied regardless of the local-dimension of the underlying system. LDI codes can have their distance promised to be at least preserved, once the system has sufficiently many levels. We have found two different bounds on the required local-dimension the second bound (5.27) suffers a severe dependency on the distance of the code, but it does provide a nearly quadratic improvement on the dependency of the largest entry in the LDI form of the code, given by B. So while this bound is less helpful in some cases than the first bound (5.25) it can be a tighter bound in others. Of particular note is the situation where one does not need to guarantee the same distance as the original code, but just some lower distance δ or larger. In this case the value for B does not change, however, everywhere that a d appears in the expressions for p^* may be replaced by δ. In these cases the quadratic improvement on the dependency on B shown here can become particularly advantageous.

While few qudit quantum computer prototypes are currently being built this provides another avenue for generating qudit quantum error-correcting codes. While currently the size of the local-dimension must be large to promise the distance of an arbitrary LDI code, we have provided a case, CSS codes, where this can be at least quadratically improved. Beyond this improvement we have also constructed a new qudit code family that is directly imported from a qubit code family. This is the first non-trivial family to be perfectly carried over via the LDI framework [113]. While there already exists qudit quantum Hamming families with paramters $[[n, n-2m, 3]]_q$ for $m \geq 2$ in the cases of $gcd(m, q^2-1) = 1$, $n = (q^{2m}-1)/(q^2-1)$ and $gcd(m, q-1) = 1$, $n = (q^m-1)/(q-1)$, this new code family fills in values of n which are not covered by these [6]. Additionally, while there exists $[[n, n-4, 3]]_q$ codes for odd prime power q values and $4 \leq n \leq q^2+1$, this provides options for n beyond q^2+1 [117]. Lastly, while arguably Maximally-Distance-Separable (MDS) codes are optimal, there are a number of values of n for which there are no known MDS codes for a given value of q [118]. While the family presented here is not MDS, perhaps the analysis used in this work can be applied to help fill in missing parameter choices.

Unfortunately, the utility of this method is somewhat limited as both bounds on the required local-dimension are quite large, as indicated in Table 5.1, but as seen in the examples this bound can often be significantly reduced through careful construction of the LDI form. In order to improve the practicality of this technique the value for p^* must be significantly decreased. One way to reduce these bounds is to reduce the expression for B, the maximal entry in the LDI representation. To do so, other analysis techniques will be needed beyond simple counting arguments. Since the LDI form for a code is not unique, one possible method may be to solve systems of homogeneous linear diophantine

equations, which given the surplus of variables (additions to entries) compared to variables (requirement of commutations to be zero) is likely to yield far smaller bounds on B. A starting point for this might include the following works: [119, 120].

Although in this work we find some critical value, p^*, above which all primes preserve the distance of the code, we believe that this result carries to all primes at least as large as the initial local-dimension if one uses other procedures to put the code into an LDI form. Proving this, or at least tightening the bound on the critical value, seems like an important extension of this result, since the current bound can be quite large.

Additionally, this work has only concerned itself with preserving the distance of codes in LDI representations, but investigating whether other desirable properties (such as transversality, cyclicity, or fault-tolerant properties of a given code) are able to be preserved is also an important direction.

Other directions that the work can be carried include knowing when it is possible to take codes already known over q levels, and not a perfect code, and preserve the distance while using the code over $p < q$ levels, or when a degenerate code can be used over a far smaller local-dimension value than it was initially designed for. Broadly speaking, if p^* can be reduced to q this would provide for a loose hierarchy of stabilizer codes whereby all 2-level codes could be used as 3-level, 5-level, and so forth codes, and all 3-level codes could be used for 5-level, 7-level, and so forth codes. While examples have seemingly indicated this, this is too much of a leap from current results.

Here we have shown at least the pedagogical utility of local-dimension-invariant stabilizer codes, and so naturally there are questions as to what other uses this technique will have. Is it possible to apply this technique to show some foundational aspect of quantum measurements?

Could the connection of these LDI codes to bosonic codes be made concrete? Or what are the possible applications of this work for the Gottesman-Kitaev-Preskill (GKP) coding scheme in continuous variable quantum computing [121, 122]? As a longer term goal, is it possible to go from using this work for bosonic codes fully to quantum convolutional codes [123, 124, 125, 126]? As that coding method in principle uses countably infinitely many bases, which suggests a possible correspondence or at least ability to intermix the interpretations between these seemingly disparate information protecting schemes.

Can this technique in some way be used for other varieties of stabilizer like codes, such as Entanglement-Assisted Quantum Error-Correcting Codes [127, 128]? If this method can be applied in this situation it is possible that it could remove the need for entanglement use in these codes, so long as the local-dimension is altered. However, even still, the local-dimension required would likely be quite large so the importance of decreasing the bounds

Code parameters	Bound from (5.25)	Bound from (5.27)
$[[9,1,3]]_2$	256	400
$[[13,7,3]]_2$	65536	6400
$[[21,13,3]]_2$	614656	19600
$[[29,19,4]]_2$	13824000000	1481544000
$[[13,7,3]]_3$	12960000	4161600
$[[27,22,3]]_3$	1049760000	37454400
$[[91,85,3]]_3$	218889236736	540841536
$[[25,22,3]]_5$	213813760000	31258240000

Table 5.1: This table compares the bounds on p^*, above which the distance of the code is known to be preserved, for a few example codes. The bound on B is used for the value of B. Examples taken from [5] for the qubit codes and [6] for qudit cases.

for p^* would become that much more. If, however, these prior points were addressed it could perhaps lead to far simpler low-density parity-check (LDPC) codes. Currently constructions utilize challenging homological structures of braiding groups, although have achieved the ideal parameters [129, 130, 131, 132]. We wonder whether, with these pieces, it would be possible to generate quantum LDPC codes directly from classical LDPC codes. This would permit far more direct importation of classical error-correcting codes with excellent properties, between LDPC codes to more general fault-tolerant schemes used classically.

References

[1] Lane G Gunderman, Andrew Stasiuk, Mohamed El Mandouh, Troy W Borneman, and David G Cory. Lamb shift statistics in mesoscopic quantum ensembles. *Quantum Information Processing*, 21(1):1–43, 2022.

[2] Lane G Gunderman. Local-dimension-invariant qudit stabilizer codes. *Physical Review A*, 101(5):052343, 2020.

[3] Lane G Gunderman. Degenerate local-dimension-invariant stabilizer codes and an alternative bound for the distance preservation condition. *Physical Review A*, 105(4):042424, 2022.

[4] Arun J Moorthy and Lane G Gunderman. Local-dimension-invariant calderbank-shor-steane codes with an improved distance promise. *arXiv preprint arXiv:2110.11510*, 2021.

[5] Markus Grassl. Bounds on the minimum distance of linear codes and quantum codes. Online available at http://www.codetables.de, 2007. Accessed on 2022-02-01.

[6] Avanti Ketkar, Andreas Klappenecker, Santosh Kumar, and Pradeep Kiran Sarvepalli. Nonbinary stabilizer codes over finite fields. *IEEE Transactions on Information Theory*, 52(11):4892–4914, 2006.

[7] Willis E Lamb Jr and Robert C Retherford. Fine structure of the hydrogen atom by a microwave method. *Physical Review*, 72(3):241, 1947.

[8] Serge Haroche and Jean-Michel Raimond. *Exploring the Quantum*. Oxford University Press, 2006.

[9] Alexandre Blais, Arne L. Grimsmo, S. M. Girvin, and Andreas Wallraff. Circuit quantum electrodynamics, 2020.

[10] JM Fink, R Bianchetti, Matthias Baur, M Göppl, Lars Steffen, Stefan Filipp, Peter J Leek, Alexandre Blais, and Andreas Wallraff. Dressed collective qubit states and the tavis-cummings model in circuit qed. *Physical review letters*, 103(8):083601, 2009.

[11] Ping Yang, Jan David Brehm, Juha Leppäkangas, Lingzhen Guo, Michael Marthaler, Isabella Boventer, Alexander Stehli, Tim Wolz, Alexey V Ustinov, and Martin Weides. Probing the tavis-cummings level splitting with intermediate-scale superconducting circuits. *Physical Review Applied*, 14(2):024025, 2020.

[12] LJ Zou, David Marcos, Sebastian Diehl, Stefan Putz, Jörg Schmiedmayer, Johannes Majer, and Peter Rabl. Implementation of the dicke lattice model in hybrid quantum system arrays. *Physical review letters*, 113(2):023603, 2014.

[13] Gershon Kurizki, Patrice Bertet, Yuimaru Kubo, Klaus Mølmer, David Petrosyan, Peter Rabl, and Jörg Schmiedmayer. Quantum technologies with hybrid systems. *Proceedings of the National Academy of Sciences*, 112(13):3866–3873, 2015.

[14] John JL Morton and Brendon W Lovett. Hybrid solid-state qubits: the powerful role of electron spins. *Annu. Rev. Condens. Matter Phys.*, 2(1):189–212, 2011.

[15] Ze-Liang Xiang, Sahel Ashhab, JQ You, and Franco Nori. Hybrid quantum circuits: Superconducting circuits interacting with other quantum systems. *Reviews of Modern Physics*, 85(2):623, 2013.

[16] Yuimaru Kubo, Cecile Grezes, Andreas Dewes, T Umeda, Junichi Isoya, H Sumiya, N Morishita, H Abe, S Onoda, T Ohshima, et al. Hybrid quantum circuit with a superconducting qubit coupled to a spin ensemble. *Physical review letters*, 107(22):220501, 2011.

[17] C Grezes, Brian Julsgaard, Y Kubo, M Stern, T Umeda, J Isoya, H Sumiya, H Abe, S Onoda, T Ohshima, et al. Multimode storage and retrieval of microwave fields in a spin ensemble. *Physical Review X*, 4(2):021049, 2014.

[18] Hua Wu, Richard E George, Janus H Wesenberg, Klaus Mølmer, David I Schuster, Robert J Schoelkopf, Kohei M Itoh, Arzhang Ardavan, John JL Morton, and G Andrew D Briggs. Storage of multiple coherent microwave excitations in an electron spin ensemble. *Physical review letters*, 105(14):140503, 2010.

[19] Xiaobo Zhu, Shiro Saito, Alexander Kemp, Kosuke Kakuyanagi, Shin-ichi Karimoto, Hayato Nakano, William J Munro, Yasuhiro Tokura, Mark S Everitt, Kae Nemoto,

et al. Coherent coupling of a superconducting flux qubit to an electron spin ensemble in diamond. *Nature*, 478(7368):221–224, 2011.

[20] Klemens Hammerer, Anders S Sørensen, and Eugene S Polzik. Quantum interface between light and atomic ensembles. *Reviews of Modern Physics*, 82(2):1041, 2010.

[21] Mikael Afzelius, N Sangouard, Göran Johansson, MU Staudt, and CM Wilson. Proposal for a coherent quantum memory for propagating microwave photons. *New Journal of Physics*, 15(6):065008, 2013.

[22] Valentina Caprara Vivoli, Nicolas Sangouard, Mikael Afzelius, and Nicolas Gisin. High-bandwidth quantum memory protocol for storing single photons in rare-earth doped crystals. *New Journal of Physics*, 15(9):095012, 2013.

[23] Christopher J Wood, Troy W Borneman, and David G Cory. Cavity cooling of an ensemble spin system. *Physical Review Letters*, 112(5):050501, 2014.

[24] Christopher J Wood and David G Cory. Cavity cooling to the ground state of an ensemble quantum system. *Physical Review A*, 93(2):023414, 2016.

[25] Audrey Bienfait, JJ Pla, Yuimaru Kubo, Xin Zhou, Michael Stern, CC Lo, CD Weis, Thomas Schenkel, Denis Vion, Daniel Esteve, et al. Controlling spin relaxation with a cavity. *Nature*, 531(7592):74–77, 2016.

[26] Bartolo Albanese, Sebastian Probst, Vishal Ranjan, Christoph W Zollitsch, Marek Pechal, Andreas Wallraff, John JL Morton, Denis Vion, Daniel Esteve, Emmanuel Flurin, et al. Radiative cooling of a spin ensemble. *Nature Physics*, pages 1–5, 2020.

[27] Vishal Ranjan, Sebastian Probst, Bartolo Albanese, Andrin Doll, Oscar Jacquot, Emmanuel Flurin, Reinier Heeres, Denis Vion, Daniel Esteve, JJL Morton, et al. Pulsed electron spin resonance spectroscopy in the purcell regime. *Journal of Magnetic Resonance*, 310:106662, 2020.

[28] T Holstein and Hl Primakoff. Field dependence of the intrinsic domain magnetization of a ferromagnet. *Physical Review*, 58(12):1098, 1940.

[29] Barry M Garraway. The dicke model in quantum optics: Dicke model revisited. *Philosophical Transactions of the Royal Society A: Mathematical, Physical and Engineering Sciences*, 369(1939):1137–1155, 2011.

[30] Ben Q Baragiola, Bradley A Chase, and JM Geremia. Collective uncertainty in partially polarized and partially decohered spin-1 2 systems. *Physical Review A*, 81(3):032104, 2010.

[31] Janus Wesenberg and Klaus Mølmer. Mixed collective states of many spins. *Physical Review A*, 65(6):062304, 2002.

[32] Edwin T Jaynes and Frederick W Cummings. Comparison of quantum and semiclassical radiation theories with application to the beam maser. *Proceedings of the IEEE*, 51(1):89–109, 1963.

[33] JM Fink, M Göppl, M Baur, R Bianchetti, PJ Leek, Alexandre Blais, and Andreas Wallraff. Climbing the jaynes–cummings ladder and observing its nonlinearity in a cavity qed system. *Nature*, 454(7202):315–318, 2008.

[34] Robert H Dicke. Coherence in spontaneous radiation processes. *Physical review*, 93(1):99, 1954.

[35] Janus H Wesenberg, Zoltan Kurucz, and Klaus Mølmer. Dynamics of the collective modes of an inhomogeneous spin ensemble in a cavity. *Physical Review A*, 83(2):023826, 2011.

[36] K Sandner, H Ritsch, R Amsüss, Ch Koller, T Nöbauer, S Putz, J Schmiedmayer, and J Majer. Strong magnetic coupling of an inhomogeneous nitrogen-vacancy ensemble to a cavity. *Physical Review A*, 85(5):053806, 2012.

[37] Z Kurucz, JH Wesenberg, and K Mølmer. Spectroscopic properties of inhomogeneously broadened spin ensembles in a cavity. *Physical Review A*, 83(5):053852, 2011.

[38] Michael Tavis and Frederick W Cummings. Exact solution for an n-molecule—radiation-field hamiltonian. *Physical Review*, 170(2):379, 1968.

[39] DI Schuster, AP Sears, E Ginossar, L DiCarlo, L Frunzio, JJL Morton, H Wu, GAD Briggs, BB Buckley, DD Awschalom, et al. High-cooperativity coupling of electron-spin ensembles to superconducting cavities. *Physical review letters*, 105(14):140501, 2010.

[40] OWB Benningshof, HR Mohebbi, IAJ Taminiau, GX Miao, and DG Cory. Superconducting microstrip resonator for pulsed esr of thin films. *Journal of Magnetic Resonance*, 230:84–87, 2013.

[41] Atac Imamoğlu. Cavity qed based on collective magnetic dipole coupling: spin ensembles as hybrid two-level systems. *Physical review letters*, 102(8):083602, 2009.

[42] Y Kubo, FR Ong, Patrice Bertet, Denis Vion, V Jacques, D Zheng, A Dréau, J-F Roch, Alexia Auffèves, Fedor Jelezko, et al. Strong coupling of a spin ensemble to a superconducting resonator. *Physical review letters*, 105(14):140502, 2010.

[43] E Ressayre and A Tallet. Holstein-primakoff transformation for the study of cooperative emission of radiation. *Physical Review A*, 11(3):981, 1975.

[44] Honghua Zhong, Qiongtao Xie, Murray T Batchelor, and Chaohong Lee. Analytical eigenstates for the quantum rabi model. *Journal of Physics A: Mathematical and Theoretical*, 46(41):415302, 2013.

[45] Andrzej J Maciejewski, Maria Przybylska, and Tomasz Stachowiak. Full spectrum of the rabi model. *Physics Letters A*, 378(1-2):16–20, 2014.

[46] BR Judd. Exact solutions to a class of jahn-teller systems. *Journal of Physics C: Solid State Physics*, 12(9):1685, 1979.

[47] Daniel Braak. Integrability of the rabi model. *Physical Review Letters*, 107(10):100401, 2011.

[48] Rodney J Baxter. *Exactly solved models in statistical mechanics*. Elsevier, 2016.

[49] NM Bogoliubov, RK Bullough, and J Timonen. Exact solution of generalized tavis-cummings models in quantum optics. *Journal of Physics A: Mathematical and General*, 29(19):6305, 1996.

[50] NM Bogolyubov. Algebraic bethe anzatz and the tavis-cummings model. *Journal of Mathematical Sciences*, 100(2):2051–2060, 2000.

[51] I Chiorescu, N Groll, Sylvain Bertaina, T Mori, and S Miyashita. Magnetic strong coupling in a spin-photon system and transition to classical regime. *Physical Review B*, 82(2):024413, 2010.

[52] Janus Wesenberg and Klaus Mølmer. Mixed collective states of many spins. *Physical Review A*, 65(6):062304, 2002.

[53] FT Arecchi, Eric Courtens, Robert Gilmore, and Harry Thomas. Atomic coherent states in quantum optics. *Physical Review A*, 6(6):2211, 1972.

[54] Robert Mann. *An introduction to particle physics and the standard model*. CRC press, 2011.

[55] Hermann Weyl. *The classical groups: their invariants and representations*, volume 45. Princeton university press, 1946.

[56] Ed S Coakley and Vladimir Rokhlin. A fast divide-and-conquer algorithm for computing the spectra of real symmetric tridiagonal matrices. *Applied and Computational Harmonic Analysis*, 34(3):379–414, 2013.

[57] Llewellyn Thomas. Elliptic problems in linear differential equations over a network: Watson scientific computing laboratory. *Columbia Univ., NY*, 1949.

[58] David S Watkins. Product eigenvalue problems. *SIAM review*, 47(1):3–40, 2005.

[59] W Barth, RS Martin, and JH Wilkinson. Calculation of the eigenvalues of a symmetric tridiagonal matrix by the method of bisection. *Numerische Mathematik*, 9(5):386–393, 1967.

[60] Bradley A Chase and JM Geremia. Collective processes of an ensemble of spin-1/ 2 particles. *Physical Review A*, 78(5):052101, 2008.

[61] Roger A Horn and Charles R Johnson. *Matrix analysis*. Cambridge university press, 2012.

[62] Rajendra Bhatia. *Matrix analysis*, volume 169. Springer Science & Business Media, 2013.

[63] BC Rose, AM Tyryshkin, H Riemann, NV Abrosimov, P Becker, H-J Pohl, MLW Thewalt, Kohei M Itoh, and SA Lyon. Coherent rabi dynamics of a superradiant spin ensemble in a microwave cavity. *Physical Review X*, 7(3):031002, 2017.

[64] Andreas Angerer, Kirill Streltsov, Thomas Astner, Stefan Putz, Hitoshi Sumiya, Shinobu Onoda, Junichi Isoya, William J Munro, Kae Nemoto, Jörg Schmiedmayer, et al. Superradiant emission from colour centres in diamond. *Nature Physics*, 14(12):1168–1172, 2018.

[65] Andreas Angerer, Stefan Putz, Dmitry O Krimer, Thomas Astner, Matthias Zens, Ralph Glattauer, Kirill Streltsov, William J Munro, Kae Nemoto, Stefan Rotter, et al. Ultralong relaxation times in bistable hybrid quantum systems. *Science advances*, 3(12):e1701626, 2017.

[66] Joel Spencer and Laura Florescu. Asymptopia, volume 71 of student mathematical library. *American Mathematical Society, Providence, RI*, page 66, 2014.

[67] JM Fink, R Bianchetti, Matthias Baur, M Göppl, Lars Steffen, Stefan Filipp, Peter J Leek, Alexandre Blais, and Andreas Wallraff. Dressed collective qubit states and the tavis-cummings model in circuit qed. *Physical review letters*, 103(8):083601, 2009.

[68] Michael J Hartmann, Fernando GSL Brandao, and Martin B Plenio. Quantum many-body phenomena in coupled cavity arrays. *Laser & Photonics Reviews*, 2(6):527–556, 2008.

[69] Felix Nissen, Sebastian Schmidt, Matteo Biondi, Gianni Blatter, Hakan E Türeci, and Jonathan Keeling. Nonequilibrium dynamics of coupled qubit-cavity arrays. *Physical review letters*, 108(23):233603, 2012.

[70] Andrea Tomadin and Rosario Fazio. Many-body phenomena in qed-cavity arrays. *JOSA B*, 27(6):A130–A136, 2010.

[71] Thomas Astner, Stefan Nevlacsil, Noomi Peterschofsky, Andreas Angerer, Stefan Rotter, Stefan Putz, Jörg Schmiedmayer, and Johannes Majer. Coherent coupling of remote spin ensembles via a cavity bus. *Physical review letters*, 118(14):140502, 2017.

[72] Matthew A Norcia, Robert J Lewis-Swan, Julia RK Cline, Bihui Zhu, Ana M Rey, and James K Thompson. Cavity-mediated collective spin-exchange interactions in a strontium superradiant laser. *Science*, 361(6399):259–262, 2018.

[73] Kangjun Seo and Lin Tian. Quantum phase transition in a multiconnected superconducting jaynes-cummings lattice. *Physical Review B*, 91(19):195439, 2015.

[74] Jian Xue, Kangjun Seo, Lin Tian, and Tao Xiang. Quantum phase transition in a multiconnected jaynes-cummings lattice. *Physical Review B*, 96(17):174502, 2017.

[75] Charles P Slichter. *Principles of magnetic resonance*, volume 1. Springer Science & Business Media, 2013.

[76] Shagnik Das. A brief note on estimates of binomial coefficients.

[77] Friedrich L Bauer and Charles T Fike. Norms and exclusion theorems. *Numerische Mathematik*, 2(1):137–141, 1960.

[78] Stanley C Eisenstat and Ilse CF Ipsen. Three absolute perturbation bounds for matrix eigenvalues imply relative bounds. *SIAM Journal on Matrix Analysis and Applications*, 20(1):149–158, 1998.

[79] Tosio Kato. *Perturbation theory for linear operators*, volume 132. Springer Science & Business Media, 2013.

[80] William K Wootters and Wojciech H Zurek. A single quantum cannot be cloned. *Nature*, 299(5886):802–803, 1982.

[81] Peter W Shor. Scheme for reducing decoherence in quantum computer memory. *Physical review A*, 52(4):R2493, 1995.

[82] Andrew Steane. Multiple-particle interference and quantum error correction. *Proceedings of the Royal Society of London. Series A: Mathematical, Physical and Engineering Sciences*, 452(1954):2551–2577, 1996.

[83] Alexei Ashikhmin and Emanuel Knill. Nonbinary quantum stabilizer codes. *IEEE Transactions on Information Theory*, 47(7):3065–3072, 2001.

[84] Daniel Gottesman. Stabilizer codes and quantum error correction. *arXiv preprint quant-ph/9705052*, 1997.

[85] Claude Elwood Shannon. A mathematical theory of communication. *Bell system technical journal*, 27(3):379–423, 1948.

[86] Raj Chandra Bose and Dwijendra K Ray-Chaudhuri. On a class of error correcting binary group codes. *Information and control*, 3(1):68–79, 1960.

[87] Erdal Arikan. Channel polarization: A method for constructing capacity-achieving codes for symmetric binary-input memoryless channels. *IEEE Transactions on information Theory*, 55(7):3051–3073, 2009.

[88] Claude Berrou, Alain Glavieux, and Punya Thitimajshima. Near shannon limit error-correcting coding and decoding: Turbo-codes. 1. In *Proceedings of ICC'93-IEEE International Conference on Communications*, volume 2, pages 1064–1070. IEEE, 1993.

[89] Daniel Gottesman. Stabilizer codes and quantum error correction. *arXiv preprint quant-ph/9705052*, 1997.

[90] A Robert Calderbank and Peter W Shor. Good quantum error-correcting codes exist. *Physical Review A*, 54(2):1098, 1996.

[91] Andrew M Steane. Error correcting codes in quantum theory. *Physical Review Letters*, 77(5):793, 1996.

[92] Daniel Gottesman and Isaac L Chuang. Demonstrating the viability of universal quantum computation using teleportation and single-qubit operations. *Nature*, 402(6760):390, 1999.

[93] Dorit Aharonov and Michael Ben-Or. Fault-tolerant quantum computation with constant error. In *Proceedings of the twenty-ninth annual ACM symposium on Theory of computing*, pages 176–188, 1997.

[94] Richard Cleve, Daniel Gottesman, and Hoi-Kwong Lo. How to share a quantum secret. *Physical Review Letters*, 83(3):648, 1999.

[95] Mark M Wilde and Joseph M Renes. Quantum polar codes for arbitrary channels. In *2012 IEEE International Symposium on Information Theory Proceedings*, pages 334–338. IEEE, 2012.

[96] David Poulin, Jean-Pierre Tillich, and Harold Ollivier. Quantum serial turbo codes. *IEEE Transactions on Information Theory*, 55(6):2776–2798, 2009.

[97] Mark M Wilde, Min-Hsiu Hsieh, and Zunaira Babar. Entanglement-assisted quantum turbo codes. *IEEE Transactions on Information Theory*, 60(2):1203–1222, 2013.

[98] Zhuo Li and Lijuan Xing. No more perfect codes: Classification of perfect quantum codes. *arXiv preprint arXiv:0907.0049*, 2009.

[99] Daniel A Lidar and Todd A Brun. *Quantum error correction*. Cambridge university press, 2013.

[100] A Robert Calderbank, Eric M Rains, PM Shor, and Neil JA Sloane. Quantum error correction via codes over gf (4). *IEEE Transactions on Information Theory*, 44(4):1369–1387, 1998.

[101] Yuchen Wang, Zixuan Hu, Barry C Sanders, and Sabre Kais. Qudits and high-dimensional quantum computing. *Frontiers in Physics*, 8:479, 2020.

[102] Pei Jiang Low, Brendan M White, Andrew A Cox, Matthew L Day, and Crystal Senko. Practical trapped-ion protocols for universal qudit-based quantum computing. *Physical Review Research*, 2(3):033128, 2020.

[103] Poolad Imany, Jose A Jaramillo-Villegas, Mohammed S Alshaykh, Joseph M Lukens, Ogaga D Odele, Alexandria J Moore, Daniel E Leaird, Minghao Qi, and Andrew M Weiner. High-dimensional optical quantum logic in large operational spaces. *npj Quantum Information*, 5(1):1–10, 2019.

[104] Rahul Sawant, Jacob A Blackmore, Philip D Gregory, Jordi Mur-Petit, Dieter Jaksch, Jesus Aldegunde, Jeremy M Hutson, MR Tarbutt, and Simon L Cornish. Ultracold polar molecules as qudits. *New Journal of Physics*, 22(1):013027, 2020.

[105] M Kononenko, MA Yurtalan, S Ren, J Shi, S Ashhab, and A Lupascu. Characterization of control in a superconducting qutrit using randomized benchmarking. *Physical Review Research*, 3(4):L042007, 2021.

[106] Muhammet Ali Yurtalan, Jiahao Shi, M Kononenko, A Lupascu, and S Ashhab. Implementation of a walsh-hadamard gate in a superconducting qutrit. *Physical Review Letters*, 125(18):180504, 2020.

[107] Avanti Ketkar, Andreas Klappenecker, Santosh Kumar, and Pradeep Kiran Sarvepalli. Nonbinary stabilizer codes over finite fields. *IEEE Transactions on Information Theory*, 52(11):4892–4914, 2006.

[108] Yang Liu, Ruihu Li, Guanmin Guo, and Junli Wang. Some nonprimitive bch codes and related quantum codes. *IEEE Transactions on Information Theory*, 65(12):7829–7839, 2019.

[109] Xiaoshan Kai, Shixin Zhu, and Ping Li. Constacyclic codes and some new quantum mds codes. *IEEE Transactions on Information Theory*, 60(4):2080–2086, 2014.

[110] HF Chau. Five quantum register error correction code for higher spin systems. *Physical Review A*, 56(1):R1, 1997.

[111] HF Chau. Correcting quantum errors in higher spin systems. *Physical Review A*, 55(2):R839, 1997.

[112] Daniel Gottesman. Fault-tolerant quantum computation with higher-dimensional systems. In *NASA International Conference on Quantum Computing and Quantum Communications*, pages 302–313. Springer, 1998.

[113] Lane G Gunderman. Degenerate local-dimension-invariant stabilizer codes and an alternative bound for the distance preservation condition. *arXiv preprint arXiv:2110.15274*, 2021.

[114] Michael A Nielsen and Isaac Chuang. Quantum computation and quantum information, 2002.

[115] Markus Grassl, Thomas Beth, and Martin Roetteler. On optimal quantum codes. *International Journal of Quantum Information*, 2(01):55–64, 2004.

[116] Pradeep Sarvepalli and Andreas Klappenecker. Degenerate quantum codes and the quantum hamming bound. *Physical Review A*, 81(3):032318, 2010.

[117] Ruihu Li and Zongben Xu. Construction of [[n, n- 4, 3]] q quantum codes for odd prime power q. *Physical Review A*, 82(5):052316, 2010.

[118] Xueying Shi, Qin Yue, and Yansheng Wu. New quantum mds codes with large minimum distance and short length from generalized reed–solomon codes. *Discrete Mathematics*, 342(7):1989–2001, 2019.

[119] LW Griffiths. A note on linear homogeneous diophantine equations. *Bulletin of the American Mathematical Society*, 52(8):734–736, 1946.

[120] Wallace Givens. Parametric solution of linear homogeneous diophantine equations. *Bulletin of the American Mathematical Society*, 53(8):780–783, 1947.

[121] Daniel Gottesman, Alexei Kitaev, and John Preskill. Encoding a qubit in an oscillator. *Physical Review A*, 64(1):012310, 2001.

[122] Kyungjoo Noh and Christopher Chamberland. Fault-tolerant bosonic quantum error correction with the surface–gottesman-kitaev-preskill code. *Physical Review A*, 101(1):012316, 2020.

[123] Mark M Wilde, Monireh Houshmand, and Saied Hosseini-Khayat. Examples of minimal-memory, non-catastrophic quantum convolutional encoders. In *2011 IEEE International Symposium on Information Theory Proceedings*, pages 450–454. IEEE, 2011.

[124] Monireh Houshmand, Saied Hosseini-Khayat, and Mark M Wilde. Minimal-memory, noncatastrophic, polynomial-depth quantum convolutional encoders. *IEEE transactions on information theory*, 59(2):1198–1210, 2012.

[125] Markus Grassl and Martin Rotteler. Quantum block and convolutional codes from self-orthogonal product codes. In *Proceedings. International Symposium on Information Theory, 2005. ISIT 2005.*, pages 1018–1022. IEEE, 2005.

[126] Markus Grassl and Martin Rotteler. Constructions of quantum convolutional codes. In *2007 IEEE International Symposium on Information Theory*, pages 816–820. IEEE, 2007.

[127] Todd Brun, Igor Devetak, and Min-Hsiu Hsieh. Correcting quantum errors with entanglement. *science*, 314(5798):436–439, 2006.

[128] Mark M Wilde and Todd A Brun. Optimal entanglement formulas for entanglement-assisted quantum coding. *Physical Review A*, 77(6):064302, 2008.

[129] Matthew B Hastings, Jeongwan Haah, and Ryan O'Donnell. Fiber bundle codes: breaking the n 1/2 polylog (n) barrier for quantum ldpc codes. In *Proceedings of the 53rd Annual ACM SIGACT Symposium on Theory of Computing*, pages 1276–1288, 2021.

[130] Nikolas P Breuckmann and Jens N Eberhardt. Balanced product quantum codes. *IEEE Transactions on Information Theory*, 67(10):6653–6674, 2021.

[131] Pavel Panteleev and Gleb Kalachev. Quantum ldpc codes with almost linear minimum distance. *IEEE Transactions on Information Theory*, 68(1):213–229, 2021.

[132] Pavel Panteleev and Gleb Kalachev. Asymptotically good quantum and locally testable classical ldpc codes. *arXiv preprint arXiv:2111.03654*, 2021.